Numerical Modeling of Heat Transport for Ground-Coupled Heat Pump (GCHP) Systems and Associated Life Cycle Assessments

By

Ayse Özdoğan-Dölçek

A dissertation submitted in partial fulfillment of the requirements for the degree of

Doctor of Philosophy

Department of Civil and Environmental Engineering

(Geological Engineering)

at the

UNIVERSITY OF WISCONSIN-MADISON

2015

Date of final oral examination: 12/07/2015

The dissertation is approved by the following members of the Final Oral Committee:

Tinjum, James M. (Advisor), Associate Professor, Civil and Environmental Engineering, Geological Engineering
Choi, Christopher Y. (Co-Advisor), Professor, Biological Systems Engineering
Hart, David, Professor, Geoscience
Wang, Herbert, Professor, Geoscience
Fratta, Dante, Associate Professor, Civil and Environmental Engineering, Geological Engineering

ABSTRACT

Numerical Modeling of Heat Transport for Ground Coupled Heat Pump Systems and Associated Life Cycle Assessments

Ayşe Özdoğan-Dölçek

Under the Supervision of Professors James Tinjum and Christopher Choi

at the University of Wisconsin-Madison

Space heating and cooling accounts for 48% of the total energy consumed worldwide. As part of the growing effort to mitigate the negative effects of greenhouse gases, increasing numbers of commercial enterprises and home owners are turning to ground-coupled heat pump (GCHP) systems as a more efficient and economical alternative. Understanding the heat transfer process between ground loop exchanger and surrounding ground that GCHP systems use and the sustainable utilization of a specific type of ground formation are crucial to any efforts made to optimize the efficiency of heat extraction and/or injection. Historically, studies of GCHPs have focused on the mechanical aspects of the system, but few have systematically accounted for the geological conditions with respect to questions of thermal sustainability and efficiency. Consequently, a significant majority of the current systems assume that both the temperature averages and the thermal conductivity of the surrounding ground remains constant over the entire vertical length of the borehole and throughout the operational life-span of the GCHP system. These assumptions neglect the variations in thermo-physical properties that actually may occur in the subsurface geology, variations that may well play a crucial role in the heat transfer process in the ground. Importantly, the ground temperature can decrease or increase depending on the respective lengths and energy balance of the heating and cooling cycles. Over a period of many years, this fluctuation can cause thermal imbalances, such as overheating due to a high amount of heat injected into the ground during a period when the system is being used to cool the interior of a building or home. Such an imbalance is especially likely to develop when the system relies on a large number of boreholes to cool sizeable commercial buildings.

In this study, a series of numerical models have been developed to evaluate the effects of a GCHP system on the thermal conditions of the ground into which the system's borehole(s) have been drilled. A three-dimensional (3D), time-dependent heat conduction process of a 300 m single borehole embedded in ground with varying lithologies was simulated using a finite-element software, ABAQUS. The monthly average surface temperature change and the natural geothermal gradients were considered as boundary conditions. More complex 3D, time-dependent, fluid-coupled models including all borehole components (e.g., fluid, pipe, and grout) were simulated using a finite-volume software, ANSYS computational fluid dynamic (CFD). This model was validated with previous experimental and analytical studies done by Erol and François (2014). Due to the increased computational burden of a 3D model, a 2D model equivalent to the 3D model of one meter depth and with adiabatic upper and lower surfaces was developed. The accuracy of enhanced 2D modeling was compared with 3D modeling results and the results have been validated with data collected from an actual GCHP system in Grand Marsh, WI.

The long-term ground thermal response is important for the design of district-scale GHXs and the sustainability of the GCHP's performance over time. To analyze the sustainability of a current borefield under operation in Wisconsin, 2D, non-linear, district-scale borefield was simulated using pre-designed heating and cooling loads (cooling-dominate). This model considers hydrogeological conditions (e.g., groundwater flow, porosity) to assess the advective heat transfer process, as well as the heat conduction occurring in their transmissive aquifer. This model was coupled with enhanced 2D model to simulate potential future mitigation strategies to resolve overheating problems, which often occur in cooling-dominant commercial operations.

Finally, to predict the CO_2 emissions from different GCHP systems (vertical, horizontal, and unconventionally deep single GHXs), a comprehensive "cradle-to-grave" life cycle analysis (LCA), which is implemented using SimaPro was conducted. Simulated results were compared with a conventional natural gas air conditioning unit for a case study in Wisconsin. The results show that a single unconventionally deep (300 m) GHX system emits 272 metric ton CO_2 equivalent emission over its 25-

year operation phase lifetime, which is 29% less CO_2 emissions than a conventional natural gas air conditioning system. For heat-pump systems, the highest emission contribution comes from the electricity used to operate it (93.3%). Therefore, CO_2 emissions could be decreased by reducing the use of fossil fuels, resulting in a cleaner grid. Our sensitivity analyses revealed that use of renewable energy sources at 50% could reduce CO_2 emissions of the GHX in our case study by 68%.

In summary, step by step a numerical model were developed for the best representative and computational affective model in terms of capability of simulating a dynamic thermal conditions that results in interaction between ground and ground heat exchangers inside the borehole as well as the surrounding ground. Each modeling step was validated according to their boundary conditions and complexity. Ultimate model, improved 2D model single geo-exchange model, aimed to account for geological and hydrogeological conditions as well as the building thermal conditions due to heating and cooling loads being applied by circulating fluid. The study's results show that, absent of appropriate mitigation strategies, overheating problems in the ground may occur even in the first few years of cooling-dominate GCHP operation due to building heating and cooling load imbalance. To balance the energy inputs/outputs to the ground, an operating scheme utilizing cold-water circulation during the off-season was evaluated. Under the simulated conditions, an energy imbalance was fully recovered, and thus the proposed mitigation strategy would seem a viable way to sustain the operating scheme of district-scale borefields in general. The positive impact, up to 50% less temperature rise in the ground was found by accounting groundwater flow at velocity of 1 m/d.

ACKNOWLEDGEMENTS

First and foremost, I would like to express my sincere gratitude to my advisor Professor James Tinjum for his invaluable support, guidance, and encouragement throughout my PhD life in Madison, WI. They will always be remembered. I would like to express my many thanks to Professor Christopher Choi for being my co-advisor and his guidance and experience I gained during last two years of my PhD study. I would also like to thank Professor Dave Hart, Professor Herb Wang and Professor Dante Fratta for serving as my committee members and their valuable contributions throughout my study.

I would like to thank the computational fluid dynamic (CFD) team in Prof. Choi's laboratory. Mario Mondaca Duarte, Jessica Drewry, Yifan Liang, Matt Harper for their excellent advice and assistance with software during my CFD training. Special thanks to undergraduate assistances, Ian Atkins and Rachel Woods-Robinson, for their help and outstanding efforts during my study. Without their support, I could not have finished my study.

I would like to thank all my fellow graduate students, undergraduate assistances and Post-docs in Civil and Geological engineering that in ways contributed to my academic life and for making my graduate study more fun. Lauren Meyer, Matthew Walker, Jeffrey Newgard, Abdullah Asbahan, Ali Soleimanbeigi, Jongwon Eun, Merve Gizem Bozkurt, Hulya Salihoglu, Jiannan Chen, Ben Warren, Idil Akin, Mehmet Yilmaz, Brigitte Brown, Kuo Tian. Many thanks to the Turkish Government- Turkish Ministry of National Education for providing fully financial support throughout my PhD education in US.

I am most grateful for my Mom's and Dad's love, encouragement and unconditional support during my graduate studies. To my husband, Tolga Dolcek, I extent my deepest thanks for his exceptional patience, moral support and for taking care of our little one, Emir Salih Dolcek throughout the time of all my graduate life. Thank you my dear husband.

TABLE OF CONTENTS

LIST OF FIGURES

LIST OF TABLES

CHAPTER 1 - INTRODUCTION

Ground-source heat pump (GCHP) systems (also referred to as geothermal heat pump systems or geo-exchange systems) are gaining popularity and are considered efficient technologies for space heating and cooling in residential and commercial buildings due to their economical and environmental benefits. GCHP system is the general term for three different categories based on the heat source/sink used: groundwater heat pump (GWHP), surface water heat pump (SWHP), and ground-coupled heat pump (GCHP) (ASHRAE 1995). Although they all utilize the earth as a "free-heat storage/reservoir," they vary in the way they deliver ground temperatures to the heat pump. A GCHP is distinct in that can be applied anywhere, even in areas with low geothermal gradients (ASHRAE 2007). Therefore, GCHP systems have seen increased interest in contrast to the other systems, which require the presence of specific geological conditions such as a proximity to a lake, pond, or flowing groundwater. In spite of the advantages of GCHP systems, the high initial cost, a limitation of design infrastructure, and the lack of improved design tools regarding to sustainability point of view for GCHP systems likely constraint and slow the implementation GCHP systems. In response to these concerns, this study seeks to develop a numerical model to estimate the in-service system performance, helping to ensure that future GCHP installations meet customer expectations.

GCHP systems rely on relatively constant subsurface temperature in a range extending from 6.1-m deep to about 45- m deep throughout the year (Hart and Couvillion 1986). This range has extended to 57 m deep according to the recent ground temperature profiles that have been specifically compiled for the State of Wisconsin by the Wisconsin Geological Natural History Survey (WGNHS 2012). This relatively constant temperature range within the near subsurface results from homeostatic heat flux from above (the sun and the atmosphere) and below (the earth's interior). In the shallow subsurface (i.e., less than 10 m deep), the subsurface temperature fluctuates due to the seasonal weather temperature averages. Below this range, greater than 57 m deep, the subsurface temperature approaches the natural geothermal gradient,

which increases with depth. At a global geothermal gradient of about (0.03 ^{o}C/m) (Grant et al., 1982) the subsurface temperature is higher than that of ambient air temperature in the winter and lower in the summer. The temperature of the ground is a function of the time of year and the depth below the surface and may be estimated by the following correlation (Kasuda 1965):

$$T = T_{mean} - T_{amp} * \exp\left[-Depth * \left(\frac{\pi}{365\text{K}}\right)^{0.5}\right] * \cos\left\{\frac{2\pi}{365} * \left[t_{now} - t_{shift} - \frac{Depth}{2} * \left(\frac{365}{\pi\text{K}}\right)^{0.5}\right]\right\}$$

Eq. 2.1

where T is temperature, T_{mean} is the average surface temperature, T_{amp} is the maximum air temperature minus minimum air temperature, Depth is the depth below the surface, κ is the thermal diffusivity of the ground, t_{now} is the current time, and t_{shift} is the day of the year on which the minimum surface temperature occurs.

Kasuda's equation results in the following distribution of temperature with respect to time (see Fig. 1.1) for different values of ground depth for Madison climatic conditions with a maximum temperature of 300 K (27 ^{o}C), a minimum temperature of 276.8 K (3.8 ^{o}C), and an average ground thermal diffusivity of 7.0×10^{-2} m^2/d. Given these assumptions, a constant ground temperature is reached after about 10-m depth when the freezing and thawing condition throughout the soil profile can be ignored.

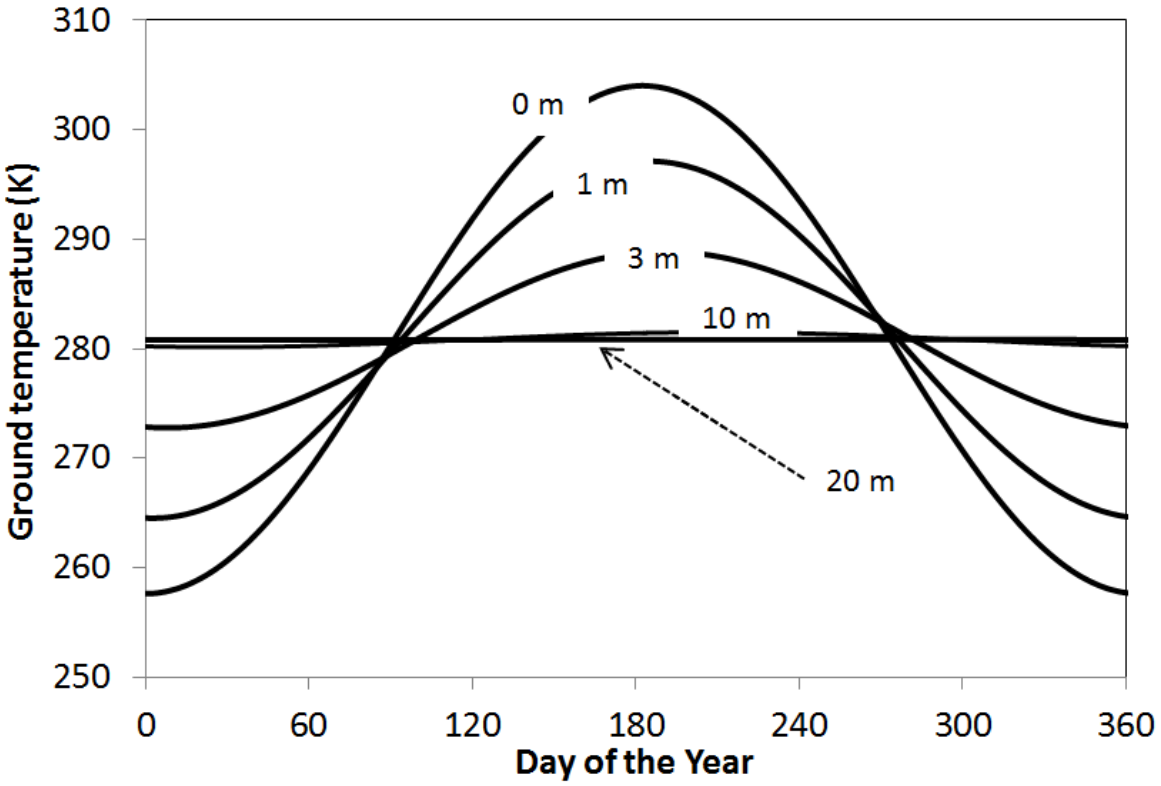

Figure 1.1 Temperature profile with depth for Madison, Wisconsin

GCHP systems typically include ground heat exchangers (GHXs) that have a sealed loop made of high-density polyethylene (HDPE) U-pipe that is buried in the ground and connected to a heat pump through which water/antifreeze is circulated. The GCHP systems have two types of GHXs, a vertical closed loop and a horizontal closed loop. When space is limited, as occurs with large systems or in urban areas, the vertical borehole configuration is usually preferred over a horizontal trench system because less area is required to provide the same heat transfer. A schematic of a GCHP system operating during a cooling cycle is shown in Fig. 1.2. In the case of winter, these heat flows are reversed. Space between the GHX and borehole is usually grouted to provide better thermal contact between the pipe and the surrounding soil/rock and also to prevent aquifer cross groundwater contamination. The typical depth of the borehole is usually between 40 m and 150 m with a diameter of 0.075 m to 0.15 m (Diao et al. 2004). Although multiple shallow boreholes are usually installed, a single but relatively deep borehole (e.g., 300 m) may be more

advantageous. These advantages can include higher temperatures at depth due to the natural geothermal gradient which may lead to a higher returning fluid temperature and thus a higher coefficient of performance (COP). COP is an important parameter, is defined as rejected/or extracted energy divided by the energy input, and characterizes the overall GCHP system's efficiency.

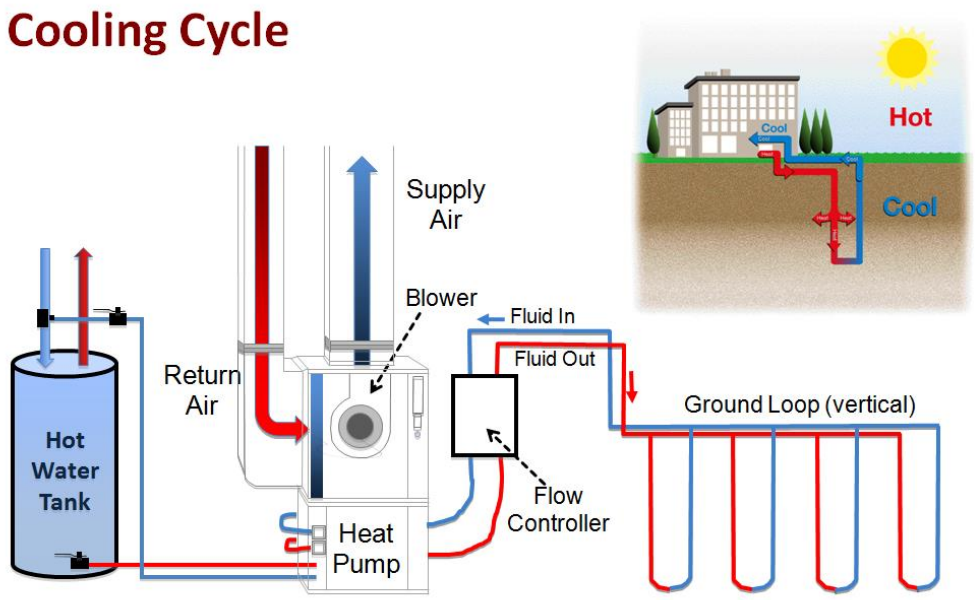

Figure 1.2 Typical ground coupled heat pump operation during cooling cycle

GCHP systems transfer heat rather than generate heat and can provide an equivalent temperature environment for as little as one quarter of the cost of operating a conventional heating, ventilating and air conditioning system (HVAC). GCHP systems use 25% to 50% less electricity than conventional resistive electrical heating systems, corresponding to about 300% system efficiency, while conventional systems can only provide up to 100% efficiency (U.S. Department of Energy 2013). Thus, the COP of properly designed and installed GCHP systems is three or above, meaning that for every unit of energy (1 $kWh_{electricity}$) put into the system, three or more units (3-4 kWh_{heat}) are harvested or rejected. The reason for the higher COP in a GCHP system is the roughly constant source/sink earth temperature compared to air temperature, which

varies. In addition, heat is efficiently transferred through water, which has a relatively high heat capacity that results in more efficient heat transfer ability than from air-source heat pumps.

Fossil fuels (including coal, petroleum, and natural gas) currently satisfy the majority of the world's energy needs; however, burning of fossil fuels directly contributes to global warming. Space heating and cooling accounts for 48% of the total world energy use (U.S. EIA 2013). Reduced energy consumption would result in less environmental impacts, such as less green-house gas (GHG) emissions. The Environmental Protection Agency (EPA) reported that the reduction in energy consumption with a GCHP system corresponds to a 44% reduction in GHG emissions in comparison to a conventional air-source heat pump and up to 72% in comparison to the electric resistance heating of a standard air-conditioning system. If fossil fuels remain the major energy sources, they would increase the GHG emissions by approximately 46% by 2040 (EIA 2013).

A GCHP system that is properly sized can achieve a savings of almost 40% in CO_2 emissions compared to a conventional gas boiler (Jenkins et al. 2009). However, despite the advantages offered by a GCHP system in terms of operating cost and environmental impact, these systems are still not widely used in comparison to conventional air conditioning systems for the following reasons: the comparably higher initial cost associated with installation (drilling), the limitations in the installation and business planning infrastructure, and possibly a lack of reliable system design and tools (Hughes 2008). Increased acceptance of GCHP systems in practice partially depends on the availability of reliable, fast and economical design-and-simulation methods. In addition, because a significant portion of the U.S. population wants minded more sustainable environment, there is a market for these systems and for such tools as the life-cycle assessment (LCA) and the life-cycle cost assessment (LCCA), which can more quickly provide an accurate estimation of cost-to-benefit metrics for geo-exchange systems.

A number of simulation tools can estimate the performance of a GCHP system based on analytical and numerical methods. Some noteworthy models are based on a combination of analytical and numerical solutions (Eskilson 1987, Yavuzturk 1999). For practical applications, commercial, whole-building-design

and energy-analysis programs are commonly used to evaluate the energy efficiency and sustainability of buildings. The U.S. Department of Energy (DOE) offers information on about 400 building software tools. Among these tools, the most well-known are the DOE-2.1e program, eQUEST, EnergyPlus, TRNSYS, and Energy Gauge. Analytical methods that use line-source or cylindrical source approaches are preferred for commercial applications because of their simplicity and computational efficiency, despite their being less accurate and less powerful in comparison to numerical methods (IGCHPA 1991, Kavanaugh 1985, ASHRAE 1999). However, with these analytical approaches, a number of assumptions must be made to allow for a solution in GHXs. The common assumptions can be summarized as follows:

1) Borehole units are assumed to be infinitely long, one-dimensional heat sources with pure conductive heat transfer to the ground in the radial axis (i.e., heat transfer in the U-pipe and grout are neglected)
2) Ground temperature along the borehole is assumed to be constant with depth
3) A single thermal conductivity value is estimated for the entire profile
4) Lithology around the borehole is homogeneous, and advective heat transfer by groundwater is neglected.

Although most commercial tools for designing GCHPs are based on analytical methods using the overarching assumptions above, they are preferred in practice because of their simplicity in applicability and time efficiency. However, true heat transfer occurs not only by conduction through the surrounding geological formation, but also by the convection resulting from fluid circulation along the U-pipe. Assuming the GHX as a line-heat source minimizes the heat transfer mechanism to the outside of the borehole by ignoring the convective heat transfer that occurs when the fluid flows through the U-pipe. Other borehole thermal resistors such as HDPE pipe and grout are also neglected. The true borehole heat load depends on these resistors and changes with time and depth in contrast to the methodology used in most design programs, which assume a single fixed load over a given time. In reality, the heat load is applied to the borehole by means of fluid and varies continuously due to changing building energy requirements. Even

over a short time period (e.g., a day), variation in heat load changes the return fluid temperature from 5.6 ^{o}C to 10 ^{o}C (Yavuzturk 1999). These variations have a direct impact on the COP of the heat pump units and thus influence the performance of the whole system's performance.

Estimation of the thermal conductivity values of the true lithology is important for sizing GHXs, yet in-situ thermal conductivity is very difficult to measure accurately. Determining the required borehole depth is highly dependent on the thermal properties of the ground. This also directly impacts the COP of the system. Estimating ground thermal conductivity and volumetric heat capacity using tabulated data is the traditional approach and is used in most design tools (Ingersoll 1954, Kavanaugh 1984, Eskilson 1987, IGCHPA 1991, Spitler et al. 1996). Although these estimates are integral to the design, they are difficult to achieve for many rock types for which there is a large range of possible thermal conductivity values (e.g., the conductivity for dolomite ranges from 1.6 to 6.2 W/m·K). Underestimating ground thermal conductivity can lead to an oversized GHX design, causing unnecessarily large capital outlays (Walker et al. 2015). Overestimating the thermal conductivity can result in an undersized system that will decrease heat pump performance, potentially causing operating temperatures that are outside of the system's norms. Laboratory testing of rock core samples from the site (albeit costly and difficult to obtain) can verify a rock's thermal conductivity and decrease the uncertainty of the thermal conductivity range. Meyer (2013) conducted an experimental study on a large variety of rock core samples collected from across Wisconsin, with measured values ranging from 2.30 W/m·K to 6.71 W/m·K. Specific heat capacities were also measured in the Meyer (2013) study and will be utilized in this study.

The objective of this research effort is to develop a numerical model to simulate the heat transfer process in and around the ground heat exchanger system. Each borehole components (e.g., pipe, fluid, grout) as well as the convective heat transfer through a geo-exchange pipe via the carrier fluid is considered. The impact of thermo-physical properties of the surrounding geological formation on heat conduction as well as the impact of hydrogeological conditions (such as groundwater flow on heat advection) are considered. The sustainability of ground temperature and the performance of the GCHPs are investigated

for a long-term (20 year) operation. Possible heat mitigation strategies for the overheating problem resulted from an imbalance of heating and cooling building loads from the simulated results are presented. Associated life-cycle assessment of the multiple types of GCHPs and its comparison with a conventional natural gas furnace- coupled with an electric central air unit for the environmental impact in terms of CO_2 emission are also conducted.

The results of this study are presented herein as series of papers. This study starts with Chapter 2 (Introduction to Heat Transfer and Existing Numerical Methods), which is the first part of the background and includes a discussion on methods which have been developed to estimate the heat transfer mechanism for designing geo-exchange systems. Chapter 2 (Geological Background) is the second part of the background and outlines the general geology of the study areas including the bedrock geology and rock thermal properties. The importance of heat transfer mechanisms is discussed.

Chapter 3 (Model Development) outlines the concepts of numerical methods developed during the course of this study. This section consists of four subsections. Chapter 3.1 presents a general introduction for the objective of model development. Chapter 3.2 is entitled "Numerical modeling of ground temperature response in a ground source heat pump system (GCHP)" and discusses the preliminary heat transfer process around the single but uncommonly deep (300 m) borehole embedded in varying ground lithology through a transient, three-dimensional (3-D) finite-element analysis using ABAQUS software. The modeling results shows that a deep geo-exchange system may be more thermally efficient by taking full advantage of the geothermal gradient and is less sensitive to seasonal impacts that shallow geo-exchange systems may experience. In contrast the most common assumption, which is the temperature profiles along the borehole and near surface are constant, this study shows thermal condition is varying when the lithology changes. The thermal conductivity values for each geological material should then be considered. This study has been published in *ASCE's Geotechnical special publication No.234*. Chapter 3.3 outlines the concept of computational fluid dynamics (CFD) and its applicability on a ground heat exchanger system. Steps for the transient, 3-D CFD simulation and its model validation for the geo-exchange system are presented. Model

justification from 3-D to 2-D model is also presented to increase the computational efficiency needed for long-term studies. Chapter 3.4 is entitled "Performance and sustainability of district-scale ground-coupled heat pump system" and ground temperature changes obtained from a real-world, district-scale geothermal borefield are simulated with transient 2-D finite-volume analysis using computational fluid dynamics (CFD). The impact of borehole components (e.g., pipe, fluid, grout) as well as the impact of groundwater flow on heat transfer are accounted for in this numerical modeling approach. Coefficient of performance (COP) of the heat pump based on simulated entering water temperature and the data found in the manufacturer heat pump manual are estimated. Results show that the cooling COP of the system dramatically decreases because the ground temperature increases over the 20-year operational period of the GCHP system due to imbalance of building loads. Thus, this results in an overheating problem in the ground even when incorporating the positive impact of advective heat transfer (i.e, due to groundwater flow). To overcome of ground overheating, some mitigation strategies are discussed and presented. This paper is in preparation for submission in the *Geothermics.*

Chapter 4 is entitled "Life-cycle assessment and comparison of various ground coupled heat pump systems based on a Wisconsin case study" and discussed the environmental impact of various configurations of GCHP systems in terms of CO_2 emissions. This study is in preparation for submission in the *Renewable and Sustainable Energy Reviews*. Chapter 5 contains conclusions and recommendations from this research effort, while Chapter 6 presents cited references. Supplementary material for he numerical modeling and some benchmarking problems are presented in Appendix A and B.

CHAPTER 2 - BACKGROUND ON HEAT TRANSFER MECHANISMS AND NUMERICAL METHODS

2.1 HEAT TRANSFER MECHANISMS

This section reviews the heat transport mechanisms and thermal processes taking place in a geologic unit and the relationship between physical properties and their thermal response. We will mainly

focus on thermal conductivity and specific heat, which are the two most important thermo-physical properties in heat transfer. Before one can determine the heat flux that occurs in any of a number of applications (such as extracting heat from a borehole, storing nuclear waste, or predicting the thermal evolution of igneous intrusions), one must have a thorough understanding thermal conductivity as well as other thermos-physical properties (Gueguen and Palciauskas 1994). In this Chapter, we will also present the study area in terms of its geological history and geothermal energy potential.

Transport of heat involves three mechanisms: conduction, convection, and radiation. Heat transport occurring in the Earth's lithosphere is dominated by conduction as opposed to the mechanisms of radiation and convection. Conduction is a crucial component when estimating spatiotemporal ground temperature changes.

2.1.1. Conductive Heat Transfer

Conduction is the mode of energy transfer in which energy moves from a region of high temperature to a region of low temperature without consideration of bulk fluid motion. The energy or heat transport in conduction occurs because of "lattice vibrations" (phonons), the interaction of molecules in the solid phase and collision of molecules in a liquid or gas phase, which have unbound molecules in random motion. Based on a "phenomenological" study of one-dimensional conductive heat transfer in a plane wall, the amount of heat energy transferred per unit time is proportional to the temperature gradient [dT/dx] and cross-sectional area [A] expressed as

$$Q = -\lambda A \frac{dT}{dx} \qquad \text{Eq. 2.2}$$

where Q is heat transfer rate [W], $\boldsymbol{\lambda}$ is the thermal conductivity of the medium [W/m·K], and dT/dx is temperature gradient in direction x (depth or length).

Eq. 2.2 is the formula of calculation of the rate of conductive heat transfer and is widely known as Fourier's law of heat conduction. The minus sign is necessary because heat is always transferred in the direction of

decreasing temperature. If the heat transfer rate, Q is divided by the cross-sectional area, A, then Fourier's law can be expressed as

$$q" = -\lambda \frac{dT}{dx} \quad \text{Eq. 2.3}$$

where q" is a local heat flux that refers to the heat flow rate per unit area [W/m^2]. Heat flux is a vector quantity, so we can write a more general form of the conduction rate equation as

$$q" = -\lambda \nabla T = -\lambda \left(\boldsymbol{i}\frac{dT}{dx} + \boldsymbol{j}\frac{dT}{dy} + \boldsymbol{k}\frac{dT}{dz}\right) \quad \text{Eq. 2.4}$$

where ∇ is the three-dimensional del operator and T (x, y, z) is the scalar temperature field.

Thermal Conductivity and Diffusivity

Thermal conductivity quantifies how rapidly temperature changes from one point in a medium to another point. Thermal conductivity tensor is the most important parameter appearing in Eq. 2.3, which describes the general conduction of heat. Therefore, the thermal conductivity of a geological unit wherein the heat extraction/ or rejection occurs and its dependence on temperature, pressure, and degree of saturation should be well characterized.

Most rocks are formed with minerals, which are anisotropic, such as quartz and calcite; thus, thermal conductivity is generally anisotropic. Thermal conductivity is actually defined as a tensor (k_{ijk}), as seen in Eq. 2.4 (Gueguen and Palciauskas 1994); but for a simpler case of an isotropic rock, is presented by Fourier's law of heat conduction (Eq. 2.3) for a temperature gradient in the x direction. For measuring the thermal conductivity of soil and rock, there are numerous laboratory testing methods such as guarded-hot-plate, heat flow meter and axial flow (ASTM C177 1985), and there is also an *in situ* test for measuring *in situ* gross conductivity—thermal response testing (TRT) (Gehlin 2002, Gehlin and Spitler 2002). Laboratory methods are used to measure the thermal conductivity of an isotropic medium (by measuring one-dimensional, steady-state heat flux using Eq. 2.3).

Other important thermal properties are necessary for full heat transfer analysis. These properties are generally known as thermo-physical properties and they include density (ρ) and specific heat (c_p). The specific heat of a medium is the energy required to raise the temperature of the unit mass by 1 K. When a material experiences a temperature increase, this heat will be stored in the material's molecules in the form of higher transitional, rotational, and vibrational energies (Waples and Waples 2004). As the material cools, the stored heat is released. Thermal diffusivity, κ, is the ability of a material to conduct thermal energy relative to its ability to store thermal energy. Higher thermal diffusivity allows the thermal condition to change more quickly, as

$$\kappa = \frac{\lambda}{\rho c_p} \qquad \text{Eq. 2.5}$$

Table 2.1 Thermal properties of rocks at 293.15 K (adapted from Kavanaugh et al. 1997)

Rock Type	% [1] Occurrence in Earth's Crust	λ^2 All [W m^{-1} K^{-1}]	λ^3 80% [W m^{-1} K^{-1}]	C_p [J kg^{-1} K^{-1}]	ρ [kg/m3]	D [m^2/s]
Igneous Rocks						
Granite (10% Quartz)	10.4	1.9 - 5.2	2.2 - 3.3	879.2	2643	9.7E-07 - 1.4E-06
Granite (25% Quartz)			2.6 - 3.6			1.1E-06 - 1.5E-06
Amphibolite	42.8	1.9 - 4.7	2.6 - 3.8		2803 - 3124	
Andesite		1.4 - 4.8	1.6 - 2.4	502.4	2563	1.2E-06 - 1.8E-06
Basalt		2.1 - 2.4		711.8 - 879.2	2883	7.5E-07 - 9.7E-07
Gabbro (Cen. Plains)		1.6 - 2.8		753.6	2963	7.0E-07 - 1.2E-06
Gabbro (Rocky Mtns.)		2.1 - 3.6				9.1E-07 - 1.6E-06
Diorites	11.2	2.1 - 3.3	2.1 - 2.9	921.1	2883	7.5E-07 - 1.1E-06
Granodiorites		2.1 - 3.5		879.2	2723	8.6E-07 - 1.4E-06
Sedimentary Rocks						
Claystone		1.9 - 2.9				
Dolomite		1.6 - 6.2	2.8 - 6.2	879.2	2723 - 2803	1.2E-06 - 2.5E-06
Limestone		1.4 - 4.5	2.4 - 2.8	921.1	2403 - 2803	1.1E-06 - 1.5E-06
Rock Salt		6.4		837.4	2082 - 2162	
Sandstone	1.7	2.1 - 3.5		1004.8	2563 - 2723	7.5E-07 - 1.3E-06
Siltstone		1.4 - 2.4				
Wet Shale (25% Qrtz.)	4.2	1.0 - 4.0	1.7 - 3.1	879.2	2082 - 2643	9.7E-07 - 1.3E-06
Wet Shale (No Qrtz.)			1.0 - 1.6			5.4E-07 - 6.5E-07
Dry Shale (25% Qrtz.)			1.4 - 2.4			7.5E-07 - 1.1E-06
Dry Shale (No Qrtz.)			0.9 - 1.4			4.8E-07 - 5.9E-07
Metamorphic Rocks						
Gneiss	21.4	1.7 - 5.7	2.2 - 3.5	921.1	2562 - 2803	9.7E-07 - 1.3E-06
Marble	0.9	2.1 - 5.5	2.1 - 3.3	921.1	2723	8.6E-07 - 1.3E-06
Quartzite		5.2 - 6.9		837.4	2563	2.4E-06 - 5.4E-06
Schist	5.1	2.1 - 4.5	2.4 - 3.8		2723 - 3204	
Slate		1.6 - 2.6		921.1	2723 - 2803	6.5E-07 - 9.7E-07

[1] Percentage of sedimentary rocks is higher near the surface

[2] "All" represents the conductivity range of all samples tested

[3] "80%" represents the mid-range for samples of rock

Variation in Thermal Conductivity with Temperature and Pressure

Several studies have indicated the pressure and temperature dependence of thermal conductivity. Cermak (1993) presented the temperature dependency of thermal conductivity as

$$\lambda = \lambda_o \, (1 + \mathrm{AT})^{-1} \qquad \text{Eq. 2.6}$$

where A is a coefficient (which differs with rock type). Thermal conductivity values of cored rock samples as a function of temperature and pressure are needed to calculate local heat flow and subsurface heat flux in the Earth, and to identify hot zones (heat flow anomalies) (Sass et al. 1971). The thermal conductivity of

various rock types and rock-forming minerals at high temperature and high pressure has been reported in many studies and shows a general decrease in thermal conductivity with an increase in temperature and increases with an increase in pressure. Jaupart and Mareschal (2011) also showed that thermal conductivity decreases with an increase in temperature, and increases by 20% with an increase in pressure when ground depth is increased from the surface to 200 km below ground.

Abdulagatov et al. (2006) studied the effect of pressure and temperature on the effective thermal conductivity ($\boldsymbol{\lambda}_{eff}$) of five different dry rocks (*sandstone, limestone, amphibolite, granulite, pyroxene-granulite)* with porosities ranging from 1% to 5%. By means of a steady-state parallel-plate apparatus, the $\boldsymbol{\lambda}_{eff}$ of those rocks with a temperature ranging from 273 K to 423 K and a pressure dependence of up to 350 MPa was measured. They found that the effect of pressure was less than the effect of temperature. The pressure effect on $\boldsymbol{\lambda}_{eff}$ depends strongly on the rock's nature (mineralogical composition, porosity and density) and increases with pressure increment (P = 0.1 MPa to 100 MPa). However, $\boldsymbol{\lambda}_{eff}$ was not affected significantly by the greater pressure increment because all of the cracks were assumed to be closed at high pressure (P > 100 MPa). The temperature dependence of the $\boldsymbol{\lambda}_{eff}$ also depends on the rock-type. Thermal conductivity varies inversely with temperature due to thermal expansion that has occurred in the rock media. Rocks that are rich in feldspar show a decrease in $\boldsymbol{\lambda}_{eff}$ of about 10%, while rocks that are poor in feldspar show a decrease of more than 40% (Clauser 1995). Proxene-granulite, which contains 34% plagioclase, shows an increase of $\boldsymbol{\lambda}_{eff}$ with T (see Fig. 2.1). The $\boldsymbol{\lambda}_{eff}$ of rocks decreases with temperature as porosity and the amorphous phase in rock increases. For example, the $\boldsymbol{\lambda}_{eff}$ of amorphous rock increases with each temperature increment, whereas the $\boldsymbol{\lambda}_{eff}$ of crystalline rock (sandstone, amphibolite with 1% porosity) decreases as temperature increases.

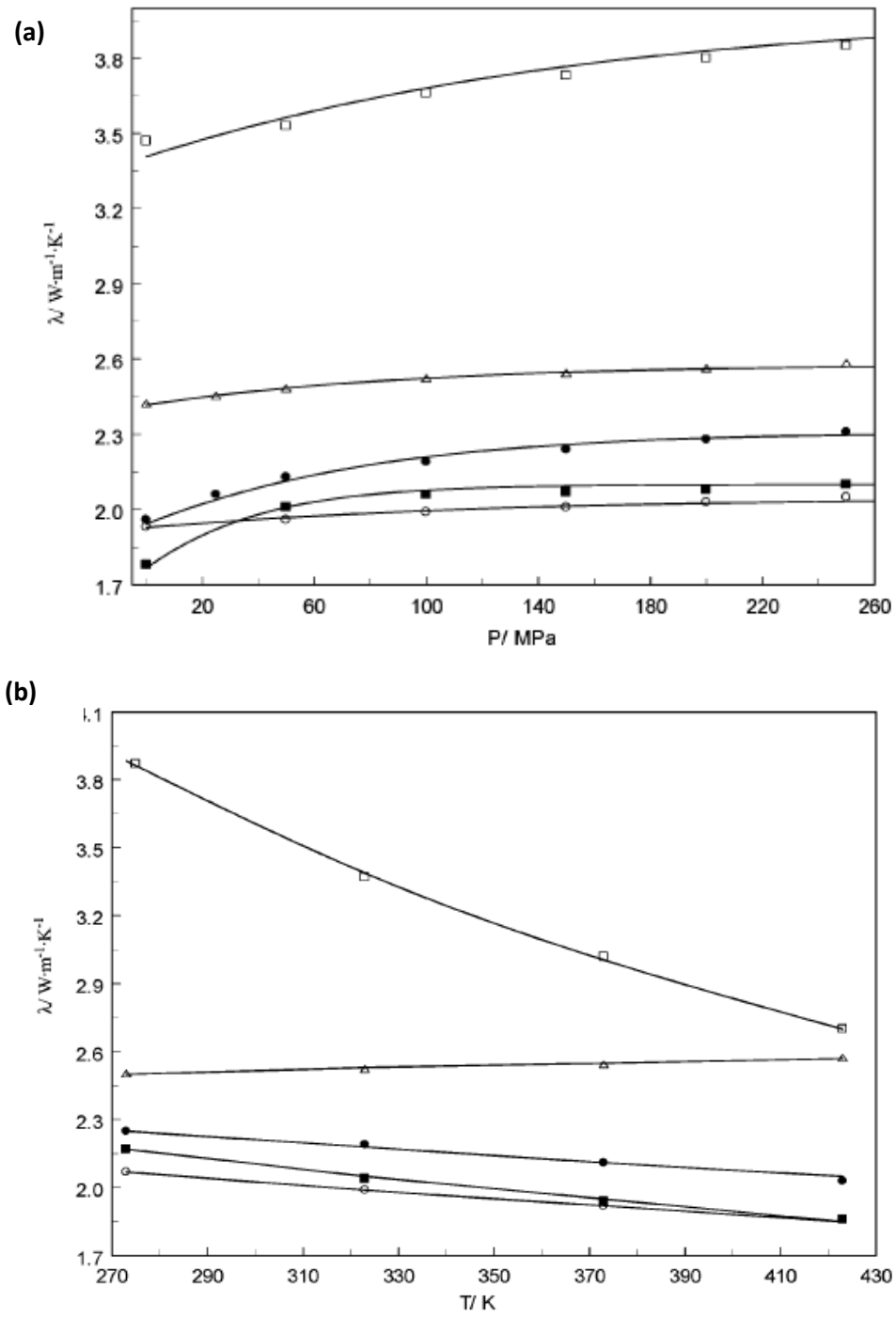

Figure 2.1 (a) Comparison of experimental pressure dependence of the thermal conductivity for various type of rocks at temperature of 323 K, and (b) comparison of experimental temperature dependence of the **λ**eff for various type rocks at pressure of 100 MPa (Abdulagatov et al. 2006)

(●, granulite (1 %); △, pyroxine−granulite (1.2 %); ○, sandstone (m = 5 %); □, amphibolite (m = 1 %); ■, limestone (m = 5 %); —, Theoretical solution)

Demirci et al. (2004) presented a variation in thermal conductivity under unaxial and triaxial stresses. They found that confining pressure on the rocks causes an additional heat flow to the surface because the thermal conductivity of the rock under confining pressure in tri-axial testing increases sufficiently compared with the thermal conductivity coefficient under uniaxial stress. They suggested that an estimation of thermal conductivity resulting from three-dimensional tests would more accurately calculate heat flow at depth. Vosteen et al. (2003) investigated an experimental solution in comparison to empirical solutions for the influence of temperature on three important rock thermo-physical properties—thermal conductivity ($\boldsymbol{\lambda}$), thermal capacity (ρc_p) and thermal diffusivity (κ)—for different types of water-saturated rock. From linear regression, they developed a general equation for temperature dependence of thermal conductivity for magmatic or metamorphic rock as follows:

$$\lambda\,(0) = 0.53\,\lambda(25) + \frac{1}{2}\sqrt{1.13\left(\lambda(25)\right)^2 - 0.42\lambda(25)}$$

$$\boldsymbol{\lambda(T)} = \frac{\boldsymbol{\lambda\,(0)}}{\boldsymbol{0.99+\frac{T\,(a-b)}{\lambda(0)}}} \qquad \text{Eq. 2.7}$$

where a and b are empirical constants and corresponding uncertainties a = 0.0030+/-0.0015 and b = 0.0042 +/- 0.0006 for crystalline rock and a = 0.0034 +/- 0.0006 and b = 0.0039 +/- 0.0014 for sedimentary rock. λ (0) is initial thermal conductivity and λ (T) is thermal conductivity at specified temperature. Vosteen et al. (2003) indicates no significantly different behavior among different types of rocks and found that the thermal conductivity decreased by 25% to 44% for the temperature interval of 1 ^{o}C to 300 ^{o}C, while thermal diffusivity decreased by 42% to 54%, respectively. The specific heat capacity of rock also increased with temperature to maximum values of around 1050 J/kg·K for sedimentary rock.

Mineral Composition and Porosity

The thermal conductivity of any rock type strongly depends on its mineralogy. Birch and Clark (1940) noted that feldspars, due to their lower conductivity, play an important role in determining the

conductivity of igneous rock, lower feldspars content implies higher thermal conductivity. An increase in quartz, which is one of the minerals with high conductivity, increases a rock's conductivity (Gueguen and Palciauskas 1994). The temperature dependence of the $\boldsymbol{\lambda}_{eff}$ of rocks is strongly dependent on the quartz content; a rock with high quartz content is strongly temperature dependent (thermal conductivity decreases with increasing temperature). Rocks containing low amounts of quartz showed much less temperature dependence (Ozbek 1976). Porosity is another important parameter that controls the value of thermal conductivity. A pore of about 10^{-6} μm causes a small temperature change ($\Delta T = 0.003$ K in advective heat transport); consequently, it is neglected in most studies. An increase in $\boldsymbol{\lambda}_{eff}$ was about 1.3% per 10 MPa for rock with small porosity, such as granite (10^{-3} μm) (Abdulagatov et al. 2006). High porosity can lead to a high soil/rock thermal resistance that may significantly impact geothermal performance.

Heat Diffusion Mechanism

One of the most important purposes of a conduction analysis is to define the temperature distribution in a medium resulting from conditions imposed on its boundary (Incropera et al. 2007). Once temperature distribution is known, heat transfer rate can be calculated from Fourier's law. Temperature distribution can be determined by applying the law of conservation of energy to a representative differential control volume to derive the following equation:

$$\frac{\partial}{\partial x}\left(\lambda\frac{\mathrm{dT}}{\mathrm{dx}}\right)+\frac{\partial}{\partial y}\left(\lambda\frac{\mathrm{dT}}{\mathrm{dy}}\right)+\frac{\partial}{\partial z}\left(\lambda\frac{\mathrm{dT}}{\mathrm{dz}}\right)+q'''=\ \rho c_p\frac{\partial T}{\partial t} \qquad \text{Eq. 2.8}$$

Where q''' is the internal heat source. Eq. 2.8 is the general form of the heat diffusion equation in Cartesian coordinates. This heat diffusion equation describes the process of general conductive heat transfer via mathematical expressions. When applying the heat diffusion equation to solve problems, Eq. 2.8 is often simplified in accordance with the requirements of the problem and the boundary conditions. The three common boundary conditions applied in heat transfer are shown in Fig. 2.2.

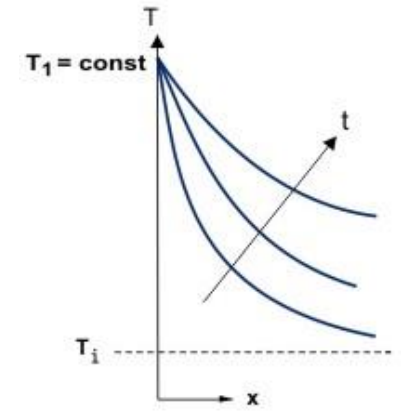

Constant surface temperature,
$T(0, t) = T_s$

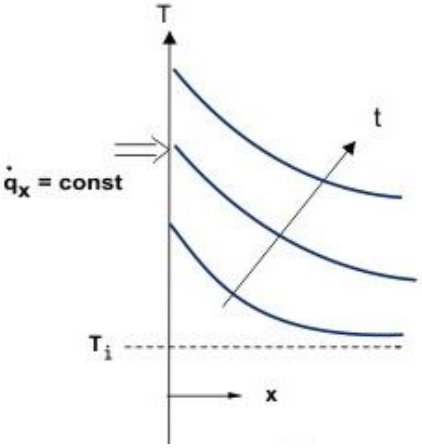

Constant surface heat flux,
$-\lambda \frac{dT}{dx}_{x=0} = q_s''$

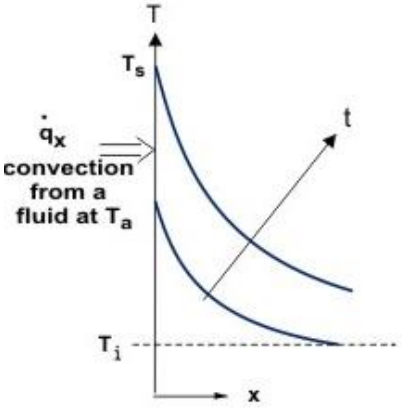

Convection surface condition $-\lambda \frac{dT}{dx}_{x=0}$
$= h [(T_\infty - T(0, t)]$

Figure 2.2 Boundary conditions for the heat transfer diffusion equation at the surface (x=0)

A constant temperature condition is the first kind of boundary condition to determine the temperature distribution in a medium. Because the heat equation is second order in the spatial coordinates, two boundary conditions must be expressed for each coordinate to describe the system's physical condition. A constant heat flux is the second kind of boundary used as corresponding to the existence of a fixed or constant heat flux q`` at the surface as most solutions heat transfer in GHX system are assumed. A special case of second kind condition corresponds to the perfectly insulated, or adiabatic, surface for which q"= 0 that are applied to the far-end distance from the borehole in numerical solution methods. The boundary condition of the third kind corresponds to the existence of convection heating (or cooling) at the surface and obtained from the surface energy balance. The third kind of boundary condition is usually neglected in analytical solutions for the borehole heat problem due to solution complexity.

2.1.2. Convective Heat Transfer

Convection refers to the transport of energy by matter through bulk fluid motion, in comparison to the microscopic delivery of heat between atoms involved with conduction. Convective heat transfer refers to the energy transfer within a fluid (it can also occur between a surface and a fluid passing over the surface). Energy is transferred by both bulk fluid motion (advection) and the random motion of fluid atoms (Incropera et al. 2007). Fluid movement can be caused by external forces or by buoyancy forces.

Newton's Law of Cooling

The basic formula for calculating convective heat transfer rate is Newton's law of cooling, which can be used to express the overall effect of convection:

$$Q = hA_c\Delta T \qquad \text{Eq. 2.9}$$

where Q is heat transfer rate [W], h is the convective heat transfer coefficient [W/m^2·K], A_c is cross-sectional area [m^2], and ΔT is the temperature difference between the surface and fluid [K]. The heat transfer coefficient defines the rate of heat transfer between a solid surface and a fluid surface per unit surface area per unit temperature difference. In most practical heat transfer applications, it is important to find heat

transfer coefficient due to convective heat transport. Once the heat transfer coefficient has been determined, the heat transfer rate can be calculated. Convective heat transfer between the circulating fluid and the pipe is an important mechanism in a GHX system.

Overview of Fluid Mechanics

A fluid can be classified based on the physical characteristics of flow fields. Fig. 2.3 presents one common classification of fluid flow.

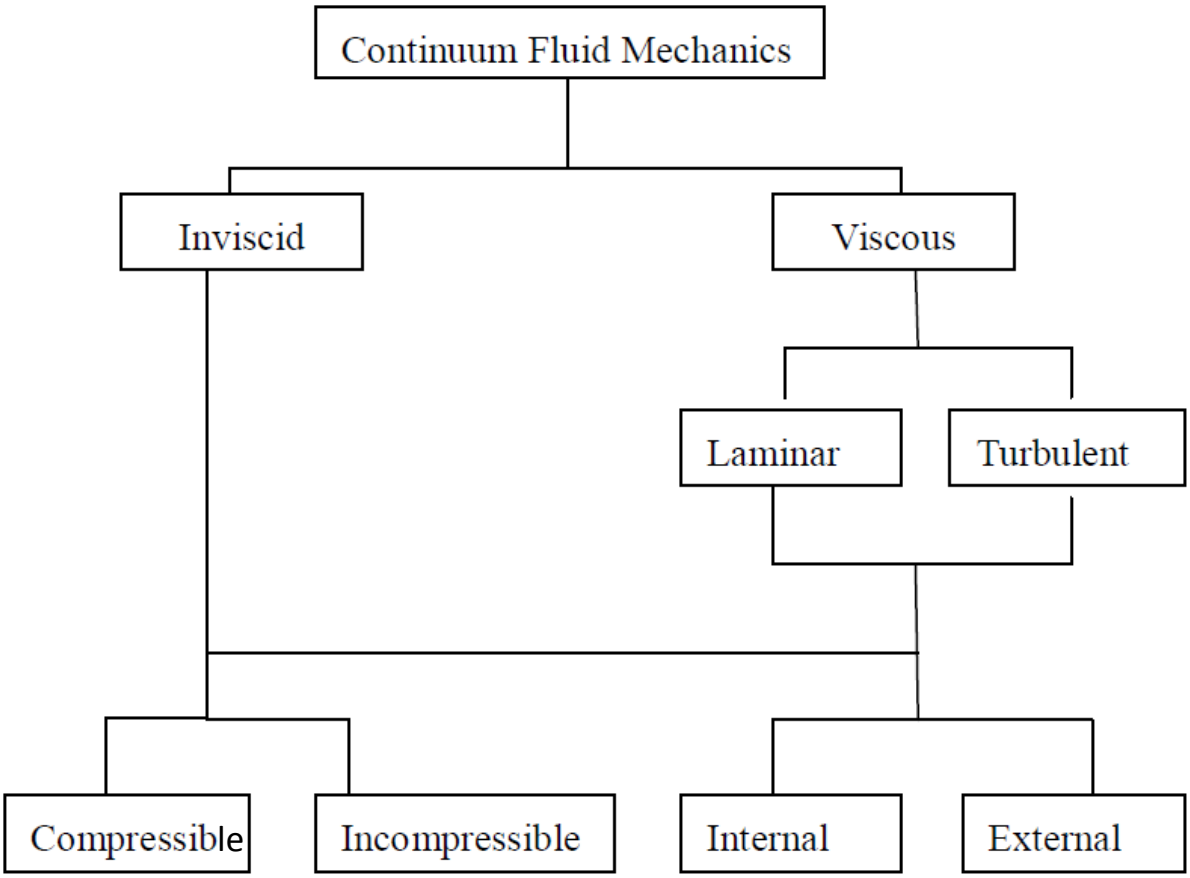

Figure 2.3 Classification of continuum fluid mechanic (Fox and McDonald 1994)

A Newtonian fluid has a surface shear stress that is directly proportional to its rate of deformation, which is expressed as

$$\tau_s = \mu \frac{\partial u}{\partial y}_{y=0} \quad \text{Eq. 2.10}$$

where τ_s is shear stress acting in planes that are parallel to fluid velocity, μ is a fluid property known as the dynamic viscosity, and u is the velocity. *Viscous flow and inviscid flow* are both applicable to a Newtonian fluid; the difference is that the viscosity of *inviscid flow* is neglected. Accordingly, the fluid viscosity is assumed to be zero. *Laminar* and *Turbulent* flow are classified based on flow structure. The structure of *laminar flow* is highly ordered and has readily identifiable streamlines along which fluid particles move. In contrast, the structure of *Turbulent flow* is random. The main difference between *Internal* and *External* flow is that the flow is completely bound by the solid surface for internal flow. *Compressible* and *incompressible* flows are defined on the basis of density variations. Incompressible flow occurs when density variations are negligible. In contrast, compressible flows occur where variations in density are not negligible. More details relating to a fluid's physical condition in terms of pipe flow are explained in Chapter 3 - Model Development.

The Continuity Equation

Conservation of mass is described as [Rate of mass flow into the control volume] + [Rate of mass flow out of the control volume] = 0. For mass conservation in a two-dimensional flow field, mass conservation is expressed as

$$\frac{\partial \rho u}{\partial x} + \frac{\partial \rho v}{\partial y} = 0 \quad \text{Eq. 2.11}$$

where ρ is density [kg/m^3] and u and v are velocities [m/s] in the x- and y-directions. Eq. 2.11 is the conservation of mass equation in differential form, which is also known as the continuity equation or mass balance for steady-state, two-dimensional fluid flow with constant density.

The Momentum Equation

The momentum balance for a control volume is given by [Rate of change of momentum inside the control volume] + [Net rate of flux of momentum out through the control surface] = [Forces acting on the control volume]. The momentum equation in a two-dimensional velocity profile is expressed as

$$\rho\left(u\frac{\partial u}{\partial x}+\upsilon\frac{\partial u}{\partial y}\right)=\mu\frac{\partial^2 u}{\partial y^2}-\frac{\partial p}{\partial x} \qquad \text{Eq. 2.12}$$

Eq. 2.12 results from the application of Newton's second law of motion in the x- direction in the dx.dy.1 differential control volume of the fluid. The left-hand side represents the net flow rate at which x-momentum leaves the control volume due to fluid motion across its boundary. The right-hand side shows the net force and net pressure force if there is a body force acting in the x-direction (Cengel 2007). Equation 2.12 is also called the Navier-Stokes equation.

Conservation of Energy Equation

Similar to the energy equation in Section 2.1.1 (Conduction mechanism), the energy equation is derived based on $E_{in} - E_{out} = \Delta T_{system}$ for two–dimensional flow of a fluid with constant properties and without shear stress and is expressed as

$$\rho c_p\left(u\frac{\partial u}{\partial x}+\upsilon\frac{\partial u}{\partial x}\right)=\lambda\left(\frac{\partial^2 T}{\partial x^2}+\frac{\partial^2 T}{\partial y^2}\right)+\ \mu\phi+q''' \qquad \text{Eq. 2.13}$$

where $\mu\phi$ is viscous dissipation and q''' is internal heat generation. When $u = \upsilon = 0$ for the non-moving fluid, the energy equation reduces to the steady two-dimensional heat conduction equation:

$$\frac{\partial^2 T}{\partial x^2}+\frac{\partial^2 T}{\partial y^2}=0 \qquad \text{Eq. 2.14}$$

Because the overall convective heat transfer equations from Eq. 2.11 to Eq. 2.14 involve partial differential equations that are difficult to solve when considering all terms, a simplified equation is derived by considering the boundary layer as incompressible, with constant properties and negligible body force, and

without energy generation. However, there are computational tools that can overcome those difficulties without applying too many simplifications that may reduce the accuracy of the results (Wang at al. 2013).

2.1.3. Radiation

Radiation is the transport of energy by electromagnetic waves (photons) and no medium is required for energy transfer to occur. While all three mechanisms play a role within the Earth's crust, heat transfer in the continental crust and lithosphere is governed mainly by conduction and convection mechanisms (Jaupart and Mareschal 2011). Heat transfer in the Earth's mantle is governed by the radiation mechanism due to high temperature (> 726 ^{o}C) (Gueguen and Palciauskas 1994). Since conduction and convection are dominate mechanisms for energy transport in the Earth's crust, more definition and equation development is warranted.

2.2 GEOTHERMAL POTENTIAL OF STUDY AREA

2.2.1 Geologic History of Study Area

Wisconsin's geologic timeline is divided into two major periods, the Precambrian (rocks older than 600 million years) and the Paleozoic (rocks younger than 600 million years. Precambrian strata consist mostly of crystalline rocks and are overlaid by Paleozoic strata that consist of sedimentary rocks that lie flat and are, in some cases, fossil-bearing. Precambrian strata exist as bedrock beneath glacial deposits in northern Wisconsin; however, to the south, Precambrian rock is located beneath Paleozoic rock. Wisconsin has been exposed to glacial ice flow across the state from Canada several times during the last several million years (Quaternary ice age). The last phase of glaciation, called the Wisconsin Glaciation (12,000 years ago), reached the Midwest and covered part of northern and eastern Wisconsin (Dott and Attig 2004). More recently, the State of Wisconsin was covered by unconsolidated surface deposits made by (1) the decay or weathering of older rocks; (2) river, wind, and wave deposition; and (3) the ice sheet of the last glacial period (Martin 1965). Fig. 2.4 shows the bedrock geology of Wisconsin, and the Glacial deposit map is shown in Fig. 2.5.

The study proposed here was carried out in two different geologic provinces of Wisconsin—Northern Highland (specifically Marathon country), and Eastern Upland (Columbia County). Marathon County is underlain by Precambrian volcanic rocks—basalt, gabbro, gneiss and rhyolite (early Proterozoic)—and intruded by a large granitic pluton (Archean-older than 2500 My). Meta-volcanic-plutonic rock is bounded on the north, west and south by gneiss, amphibolies, and migmatite. The eastern part of the Northern Highland is underlain by the Wolf River Batholith which is a large granitic pluton of Middle Proterozoic age. Paleozoic sandstones are exposed in southeastern Marathon County. In the last million years (i.e., Pleistocene), three separate till sheets (a compact, unsorted mix of clay, silt, sand, gravel and boulders) formed in Marathon County (LaBerge and Myers 1983). In similar fashion, Columbia County is underlain by Precambrian rock, mostly volcanic rholite, granite and quartzite. Cambrian and Ordovician sedimentary rocks, mostly sandstone and dolomite, are underlain by Precambrian rock and covered with glacial sediments (such as sand).

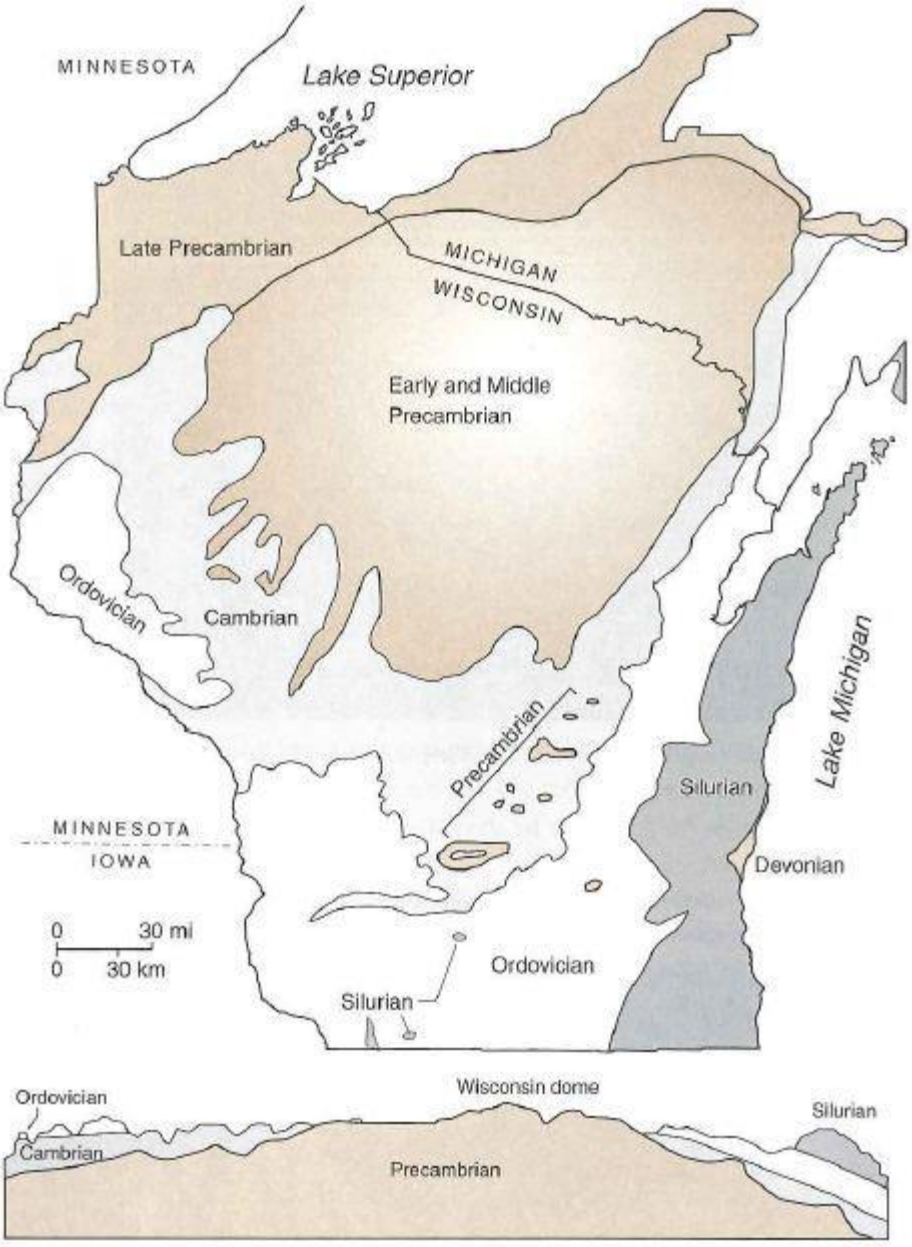

Figure 2.4 Generalized Bedrock Geology of Wisconsin: Precambrian Rocks in the North Form a Broad Dome with Paleozoic Strata Dipping Slightly away from It (Dott and Attig 2004)

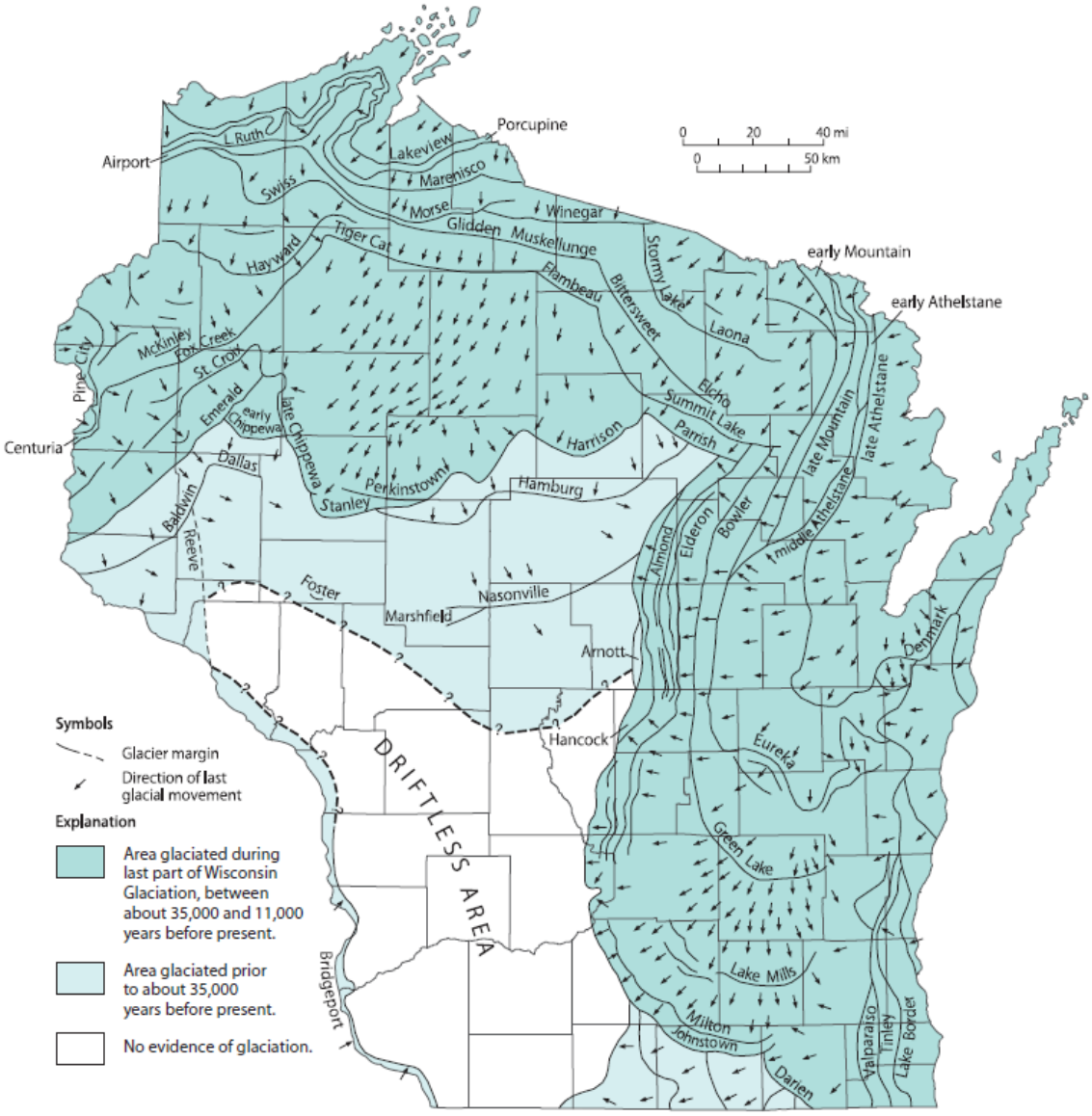

Figure 2.5 Distribution of Glaciation in Wisconsin, Glaciated Region and the Driftless Area (Attig et al., 2011)

2.2.2 Geothermal Potential of Study Area

Eight deep (~305 m) geothermal wells were recently drilled in Wisconsin by the Wisconsin Geological Natural History Survey (WGNHS). Three are located in northern Wisconsin and two in southern Wisconsin. Three more wells will be drilled in the future. Wells drilled in northern Wisconsin were comprised of igneous rock (granite) that dominates is relatively rich in radioactive elements—Uranium (U), Thoryum (Th) and Potasyum (K)—which generate heat through radioactive decay. The concentration of heat-producing elements in bedrock varies significantly. Turcotto and Schubert (1983) presented the typical concentration of heat-producing elements in several rocks (see Table 2.2). For granite, the concentration of U, Th and K is 4 ppm, 17 ppm and 3.2%, respectively. Compared to these typical values, the granite in the study area is significantly rich in U (8 ppm) and T (50 ppm). Fig. 2.6 shows a linear dependence between the surface heat flow [q_s] and the heat production rate of surface rock (q. H_s); thus, an increase in radioactive elements results in high conductivity and consequently results in high heat generation. We obtained data from geothermal wells drilled in southern Wisconsin where sedimentary rock covers the basement rock and perhaps insulates the underlying granites, thus resulting in higher temperature gradients.

Table 2.2 Typical concentration of heat-producing elements in several rock (From Turcotte and Schubert 1982)

Rock Type	Concentration		
	U	Th	K
	(ppm)	(ppm)	(%)
Reference undepleted mantle	0.026	0.103	0.026
"Depleted" peridotites	0.012	0.035	0.004
Tholeiitic basalt	0.1	0.35	0.2
Granite	4	17	3.2
Chondritic meteorites	0.013	0.04	0.078

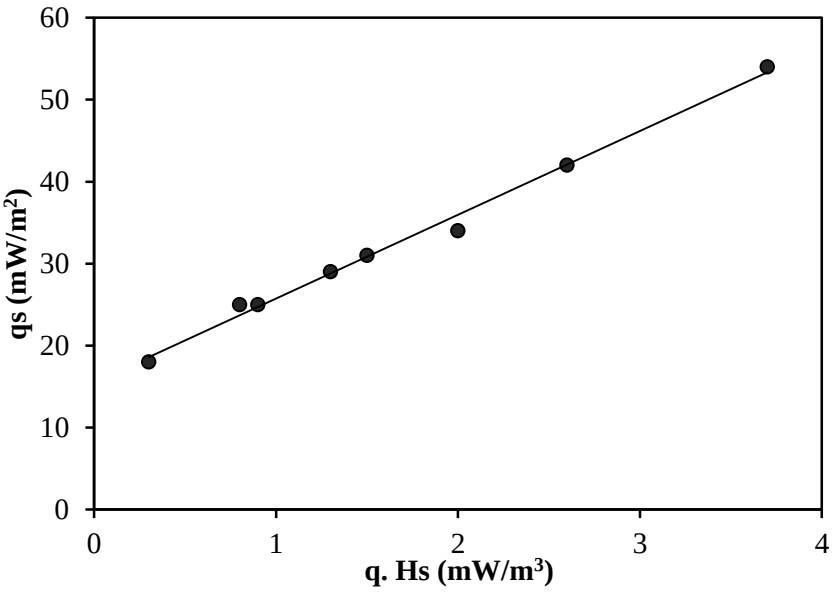

Figure 2.6 Surface heat flux in the eastern U.S. based on the radioactive heat content of surface rocks (Modified from Turcotte and Schubert 1983)

However, preliminary results from current geothermal wells showed a lower temperature gradient than expected. Worldwide, the average geothermal gradient is between 25 K/km and 30 K/km (Dickson and Fanelli 2004), whereas Wisconsin's geothermal gradient has been estimated to be at or below 20 K/km (Blackwell et al. 2007, Meyer 2013). As there is no significant topography (such as high Mountain, lowland etc.) in the study area, and hydraulic conductivities decrease with depth at about 2.1 x 10^{-4} cm/s at 20 m (Rayne et al. 1996), 3 x 10^{-14} cm/s -2 x 10^{-10} cm/s at 300 m due to impermeable granitic rock (Schwartz and Zhang, 2004), convective heat transfer probably does not play a significant role in the vertical temperature gradient and heat-flow variations. Therefore, the relatively low vertical gradient is most likely due to surface heat gain, possibly from recent (i.e., past 20,000 years) warming of the earth that occurred during the retreat of the Laurentide Ice Sheet. As mentioned, Wisconsin was exposed to several glaciations during the last several million years and the last phase, the Wisconsin Glaciation, retreated just 12,000 years ago. Therefore, granitic rock in our study area might still be responding to postglacial warming and consequently decreasing the apparent heat flux that has been calculated using the relatively shallow (<500 m) temperature logs available.

2.3. EXISTING MODELING TOOLS FOR GROUND-COUPLED HEAT EXCHANGER SYSTEMS

2.3.1 Analytical Methods

This section reviews two analytical methods commonly used to design ground heat exchanger (GHX) systems; one is Kelvin's line-source model, and the other is a cylinder-source model. Most design tools used in simulation programs are based on these two methods. Some noteworthy studies and their variations are discussed in this section. More advanced versions of these methods have been developed, and they are also discussed here. Table 2.3 provides a brief development history of the solution approach for GHX systems.

Table 2.3 Development of history of analytical solutions to GHXs

Analytical Solution to GHX Systems	**References**	**Model Specifications**
Kelvin's Line Source Theory (LS)	Kelvin (1882) Ingersoll et al. (1948-54) Hart and Cauvillon (1956)	• Infinite pipe and ground ($r = \infty$) • Infinite borehole and finite medium • $r_\infty = 4\sqrt{at}$
Cylindrical Source Theory (CS)	Carslaw and Jaeger (1947) Kavanaugh (1985)	• Temperature response factor, G-function (t, r) • Refined CS

Kelvin's Line-Source (LS) Solution

The first contribution to the modeling of GHXs came from Ingersoll et al. (1954), who used Kelvin's (1882) line-source equation that describes the continuous, time-dependent heat transfer occurring between a line source and the earth to obtain the temperature at any point in an infinite medium. The pipe in the borehole is assumed to be a line source of constant heat output or input and which is also infinitively long such that the heat source flows in one dimension (radially) through the infinite homogenous medium. The temperature profile in the medium is given by

$$T - T_o = \frac{q}{2\pi k}\int_n^{\infty} \frac{e^{-\beta^2}}{\beta} d\beta = \frac{q}{2\pi\lambda} I(n) \qquad \text{Eq. 2.15}$$

where n is a dimensionless parameter defined as $n = \frac{r}{2\sqrt{\kappa t}}$, T is the ground temperature at selected distance from the line source, T_o is the initial ground temperature [K], Q is the heat transfer rate per length over the source [W/m], r is far-field distance from the pipe center [m], λ is thermal conductivity of the ground formation [W/m·K], κ is thermal diffusivity of the ground formation defined as $\frac{k}{\rho c}$, ρ is density of the ground formation [kg/m^3], t is time since start of the operation [hr], and β is an integration variable equal to $\frac{r}{2\sqrt{\kappa(t-t')}}$. For values of n < 0.2 , the following approximation for the integral term is provided as

$$I(n) = 2.303 log10 \frac{1}{n} + \frac{n^2}{2} + \frac{n^4}{8} + 0.2886 \qquad \text{Eq. 2.16}$$

For n ≥ 2, I (n) is presented in tabulated form by Ingersoll et al. (1954), who suggested that if the radial heat flow from the source varies from month to month, the integral term in the equation should be discretized based on a monthly heat flow rate for a given time interval. The line-source method has been specifically used to predict the response of ground GHXs for a long-term performance, with an average monthly heat transfer rate. This model can only be applied to small pipe diameters (< 50.8 mm) for a few hours to months, due to the assumption of the infinite line source (Eskilson 1987). Ingersoll et al. (1954) stated that a noticeable error can be found when the dimensionless time-to-pipe ratio $\frac{\kappa t}{r^2}$ is less than 20. Therefore, the line-source solution by Ingersoll et al. (1954) has been used mostly for *in situ* thermal conductivity testing because that test requires only a short time period (48 h to 72 h).

Kelvin's line-source equation was used by Hart and Couvillion (1986) to estimate continuous time-dependent temperature variations between the line-source and the finite ground. They introduced the far-field radius (r_∞) for the surrounding ground, which would be influenced by the amount of heat transfer from the line source. In Kelvin's theory, the temperature distribution in the surrounding ground formation is

incorrectly predicted because of the infinite ground assumption at all radii any time after the line source is started. Therefore, the only correct value for (r_∞) is that $r_\infty = \infty$. Hart and Couvillion assumed an arbitrary far-field radius as

$$r_\infty = 4\sqrt{\kappa t} \qquad \text{Eq. 2.17}$$

The change of ground temperature beyond this far-field radius is assumed to be negligible. Similar to the Ingersoll approach, the line-source equation was formed as

$$T - T_0 = \frac{q}{4\pi\lambda}\int_x^\infty \frac{e^{-l}}{l} dl = \frac{q}{4\pi\lambda} Ei\left(-\frac{r^2}{4\kappa t}\right) \qquad \text{Eq. 2.18}$$

where $x = \frac{r^2}{4at}$, and Ei is the exponential integral function. The integral part of the equation is simplified as the sum of a power series of N terms; thus, the final line source equations for the temperature distribution around a line source are

$$T - T_o = \frac{q}{4\pi\lambda}\left[ln\frac{r_\infty}{r} - 0.9818 + \frac{4r^2}{2r^2{}_\infty} - \frac{1}{4x(2!)}\left(\frac{4r^2}{r_\infty}\right)^2 + \cdots + \frac{(-1)^{N+1}}{2Nx(N!)}\left(\frac{4r^2}{r_\infty{}^2}\right)^N\right] \qquad \text{Eq. 2.19}$$

where r is the radial distance from the line source whenever the desired temperature value is reached. This equation is applicable for pipes with a ratio of $\frac{r}{r_p} \geq 15$, where r_p is the pipe radius. For the ratio of $\frac{r}{r_p} \geq 3$, two N-power terms are recommended, while the suggested terms are increased for a ratio less than 3.

There are studies that develop a more advanced solution, starting with the analytical solution discussed above. For instance, Zeng et al. (2003) and Dieo et al. (2004) introduced a convection term for the solution to the heat transfer process in GHXs by using the finite line-source model developed by Hart and Cauvillion (1986). The temperature response of the borehole over a long-term period is described, and temperature rise in the ground is then estimated to determine the borehole wall temperature for a specified operational period (Zeng et. al 2002). They developed a new "quasi-three-dimensional," explicit analytical solution by taking into account the fluid axial convective heat transfer and thermal "short-circuiting"

occurring among U-tubes. Different configurations of single and double U-tube boreholes were compared with regard to their borehole resistance. The inlet and outlet fluid temperatures were then defined based on the borehole wall temperature, borehole resistance, and heating rate of the GHXs. Results showed that equipping boreholes with a double U-tube reduces the borehole resistance by 30% to 90% compared to a single U-tube.

Cylindrical Source (CS) Solution

The cylindrical source (CS) solution method is based on one-dimensional radial heat conduction occurring in a cylinder surrounded by an infinite homogenous medium by Carslaw and Jaeger (1946). The cylinder represents the borehole's outer boundary with either a constant heat transfer rate or a constant pipe surface temperature and ground properties. Heat transfer between a borehole and the surrounding ground that are assumed to be in perfect contact. The cylindrical source equation is given as

$$T - T_o = \frac{q}{\lambda} \mathrm{G}\ (\mathrm{z}, \mathrm{p}) \qquad \text{Eq. 2.20}$$

where $z = \frac{\kappa t}{r_{b^2}}$ is known as Fourier's number, $\mathrm{p} = \frac{r}{r_b}$, and r and r_b are the far-field and outer pipe radius [m], respectively. The expression G (z, p) is a function of time and the distance from the borehole center and is often referred to as the "Geometry-function." However, it also contains an integral (from zero to infinity) of a complicated function that includes Bessel functions (Yang et al. 2010). The G-function is usually estimated using tabular and algebraic expressions and can be found in the literature (Kavanaugh1985, Hellstrom 1991, Liu et al. 2001). The CS solution method was used by Kavanaugh (1985) to estimate the temperature distribution or heat transfer rate around a pipe buried in the borehole through refinements in the CS equation. Kavanaugh (1985) assumed that the pipe was surrounded by an infinite, solid medium with constant properties and in perfect contact with the ground. Graphical results for G (z, p) function when p = 1, which represents the surface of the pipe, were defined (Kavanaugh 1985). The thermal resistance of the ground per unit length was calculated as a function of time. The coefficient of heat

transferred from the fluid inside the pipe to the outer pipe wall was also considered in the heat transfer process as

$$h_{eq} = \left[\frac{r_0}{r_i h_i} + \frac{r_0}{\lambda} ln\left(\frac{r_0}{r_i}\right)\right]^{-1} \quad \text{Eq. 2.21}$$

where r_i is the inside pipe radius and r_o is the outer pipe diameter. The convective heat transfer coefficient for turbulent flow in a circular pipe was defined as

$$h_i = Nu_{Di}\frac{k_f}{D_i} \quad \text{Eq. 2.22}$$

The Dittus-Boelter relationship was used to calculate the Nusselt number according to the following equation:

$$Nu = 0.023 Re_{Di}^{0.8} Pr^n \quad \text{Eq. 2.23}$$

where Nu is the Nusselt number, Re is the Reynolds number, Pr is the Prandtl number, k_f is the fluid thermal conductivity, D_i is the inside diameter of the pipe, and n = 0.3 for cooling of fluid and n = 0.4 for heating of fluid.

The two main analytical-solution methods—line-source and cylindrical-source modeling—are discussed in this section. Most simulation programs are typically based on these two analytical methods. Both methods make a number of assumptions to solve complicated mathematical algorithms. In the line-source method developed by Ingersoll (1954), for example, the physical sizes of the U-pipe in the borehole are simplified and assumed to be a line. In the cylindrical-source model, one pipe, co-axial with the borehole, is assumed. The axial heat flux through the borehole is neglected, and the heat conduction process in the ground is reduced to a one-dimensional problem. In actual GHX systems, the heat flow rate is coupled to the ground and the fluid temperatures. Both LS and CS methods neglect the thermal capacities of the fluid and the grout in the GHXs; both assume the ground as an infinite homogenous medium. Therefore, the analytical models can only provide a rough approximation of the actual heat transfer process when

simulating a ground source heat pump system (GCHP). However, due to the fact that the analytical-solution methods require less computation time and can be easily integrated into a design program, most design programmers prefer to use classical LS and CS methods. For example, one of the most common modeling institutions, the American Society of Heating, Refrigerating and Air Conditioning Engineers (ASHRAE) (1997), uses Ingersoll's modified method for analyzing short-term variations in ground temperature. This method basically transforms the simple, steady-state, heat transfer equation into

$$q = \frac{L(T_g - T_f)}{R} \qquad \text{Eq. 2.24}$$

where T_g is ground temperature and T_f is fluid temperature in the pipe and R is the thermal resistance. Rearranging Eq. 2.24 above for L, which is the required vertical bore length, in an equation in the form of the CS method in cases where the LS method may error when calculating long-term variation (> 6 h) for cooling and heating as follows:

$$L_{cooling} = \frac{q_a R_{ga} + (q_{lc} - 3.14 W_c)(R_p + PLF_{gm} R_{gm} R_{gd} F_{sc})}{T_g - \frac{T_{wi} + T_{wo}}{2} - T_p} \qquad \text{Eq. 2.25}$$

$$L_{heating} = \frac{q_a R_{ga} + (q_{lh} - 314 W_h)(R_p + PLF_{gm} R_{gm} R_{gd} F_{sc})}{T_g - \frac{T_{wi} + T_{wo}}{2} - T_p} \qquad \text{Eq. 2.26}$$

where F_{sc} is the short-circuit heat-loss factor, L_c is required borehole length for cooling (ft), PLF_{gm} is partial load factor during the design month, q_a is net annular average heat transferred to the ground [Btu/h], q_{cl} is building design cooling block load [Btu/ft], R_{ga} is effective thermal resistance of the ground-annual pulse [h.ft.F/Btu], R_{gd} is effective thermal resistance of the ground-daily pulse [h.ft.F/Btu], R_g is effective thermal resistance of pipe [h.ft.F /Btu], T_g is undisturbed ground temp [F], T_p is a temperature penalty for interference of adjacent boreholes [F], T_{wi} is fluid temp at the heat pump inlet [F], T_{wo} is fluid temp at the heat pump outlet [F], W_c is power input at design cooling load [W], and W_h is power input at design heating load [W]. This method is commonly used when accounting for the thermal resistance of the pipe wall and the resistance between the pipe and the fluid and the pipe and the ground. The thermal interference between

boreholes after 1 year and after 10 years can be described and applied to the entire loop field to correct for the number of boreholes surrounded by one, two, and three adjacent boreholes.

The International Ground-Source Heat Pump Association (IGSHPA) provides another conventional modeling method that uses the LS method (Ingersoll 1957, Kavanaugh 1997) for GHX design. This method computes the borehole depth based on the hottest and coldest month of the year and the coefficient of performance (COP) using the following equations:

$$L_{heating} = \frac{q_{d,heat}\left[\left(\frac{COP_h - 1}{COP_h}\right)R_p + R_g F_h\right]}{T_{g,min} - T_{ewt,min}} \quad \text{Eq. 2.27}$$

$$L_{cooling} = \frac{q_{d,cool}\left[\left(\frac{COP_c - 1}{COP_c}\right)R_p + R_g F_c\right]}{T_{ewt,min} - T_{g,min}} \quad \text{Eq. 2.28}$$

where $q_{d,heating}$ is the design heating load, COP_h is the design heating coefficient of performance of the heat pump, R_p is the pipe thermal resistance, R_g is the soil/ground thermal resistance, F_h is the ground heat exchanger partial load factor for heating, $T_{g,min}$ is the minimum undisturbed ground temperature, and $T_{ewt,min}$ is the minimum design entering water temperature at the heat pump. This method uses an equivalent pipe diameter as defined by Bose (1984):

$$D_{eq} = \sqrt{n}\,(D_o)$$

where n is the number of U-tube legs in a borehole and D_o = the outside diameter of pipe. The ground resistance for multiple vertical GHXs is defined by superimposing the thermal resistivity effects of adjacent GHXs and adding the total effect to the ground thermal resistance of a single pipe of an equivalent radius. Kusuda's (1965) theoretical model is used to estimate the undisturbed ground temperatures. The minimum entering fluid temperature T_{min} of 30 °F to 40 °F (-1.1 °C to 4.4 °C) that is above the coldest outdoor air temperature at a given location, and the maximum entering fluid temperature, T_{max} of 100 °F (37.8 °C), are assumed. The ground (R_s) and pipe resistance (R_p) for a vertical U-tube are given as

$$R_s(X) = \frac{I(X_{r_o})}{2\pi k_s} \; with \; X_{r_o} = \frac{r_o}{2\sqrt{\kappa_s t}} \qquad \text{Eq. 2.29}$$

$$R_p = \frac{1}{2\pi k_p} ln \frac{D_{eq}}{D_{eq}-(OD-ID)} \qquad \text{Eq. 2.30}$$

where I (X_{ro}) is the exponential integral, r_o is the outer pipe radius [ft], κ_s is the ground thermal diffusivity [ft^2/h], k_s is the thermal conductivity of the ground formation [Btu.ft.F/h], and t is the time [h]. OD and ID are the pipe outer and inside diameters, respectively.

Unlike the ASHRAE method, IGSHPA's method does not consider the long-term variation that could cause a thermal imbalance over a period of many years due to significant differences between the annual heat extracted from the ground and the heat rejected to the ground during the cooling season. However, this simplified equation has been considered acceptable at the preliminary feasibility stage of system design. These two conventional methods provide a method for estimating the length of the borehole, and both require entering fluid temperature and leaving temperature at the heat pump to be specified for the long-term performance of both the heating and cooling modes. The details relating to, and a comparison of these two conventional methods can be found in the literature (ASHRAE 1995, IGSHPA 1991, Yavuzturk1999). Recent studies have developed calculation tools for minimizing the number of assumptions required of the CS and LS methods (Bernier 2004, Nagano 2006). A noteworthy study by Sanaye and Niroomand (2009) modifies IGSHPA's method for optimizing the design parameters that affect system performance and initial capital and operational costs.

Another important limitation in CS and LS theory is the time function used during GCHP operation. LS and CS methods are used for continuous long-term (monthly or yearly) operation and ignore the effect of the short-time response of the GHX. In reality, short-term variation has significant effects on the performance of the heat pump and the overall system (Yavuzturk, 1999), but the short-term response of the GHX requires the actual geometry of the borehole components (i.e., pipe, grout, fluid) to define the transient and spatial variation appropriately. The importance of short-term operation in GCHP systems provides the

motivation to develop tools that include the thermal effects of the borehole parameters on the heat transfer process. Tools that allow more comprehensive detail are discussed in the following section.

2.3.2 Numerical Methods

Analytical solutions are restricted to simple geometry and boundary conditions even though some analytical approaches can be used to solve simple two- and three-dimensional heat transport problems in GHXs. However, in many cases, complicated geometry or boundary conditions prevent the use of simple analytical methods. For example, as discussed previously, both LS and CS models simplify the actual borehole geometry and neglect axial heat flow along the borehole depth, but numerical methods are more likely to account for axial heat transfer by considering a borehole with finite length. Numerical methods use discretization techniques, which approximate the differential equations through a system for algebraic equations at a set of discrete locations in space and time, and then these equations can be solved using a computer program. After defining the applicable mathematical equation based on the specific problem, the suitable discretization method is chosen. A number of numerical methods for GHX systems are increasingly available due to an increasing computer efficiency that can overcome complicated non-linear heat transfer problems. Unlike most analytical methods, numerical methods consider the full heat transfer process inside the borehole as well as around the borehole. Depending on the problem's complexity, widely used numerical methods for solving heat transfer problems are the finite difference, finite element and finite volume methods. These numerical methods are discussed separately in the next section, each with an example application for modeling GHX system.

Finite Difference Method (FDM)

The FDM is the numerical method for solving the partial differential equation (PDE), having been introduced by Euler in the 18th century, and it is the easiest method for solving simple geometries. The FDM discretizes the problem into grids, and the differential equations at the each grid point are approximated by replacing the partial derivatives using Taylor series expansions. Figure 2.7 shows an example of a grid scheme for the ground around a borehole. Each grid is connected by temperature nodes

that are defined by a set of indices, which are the indices of the grid lines that intersect at (i, j, m) in 3D. The neighbor nodes are defined by increasing or reducing one of the indices by unity. Even though FDM is restricted to simple grids and does not conserve momentum, mass, or energy on a coarse grid, this method is popular for the modeling of GHXs due to ease of implementation.

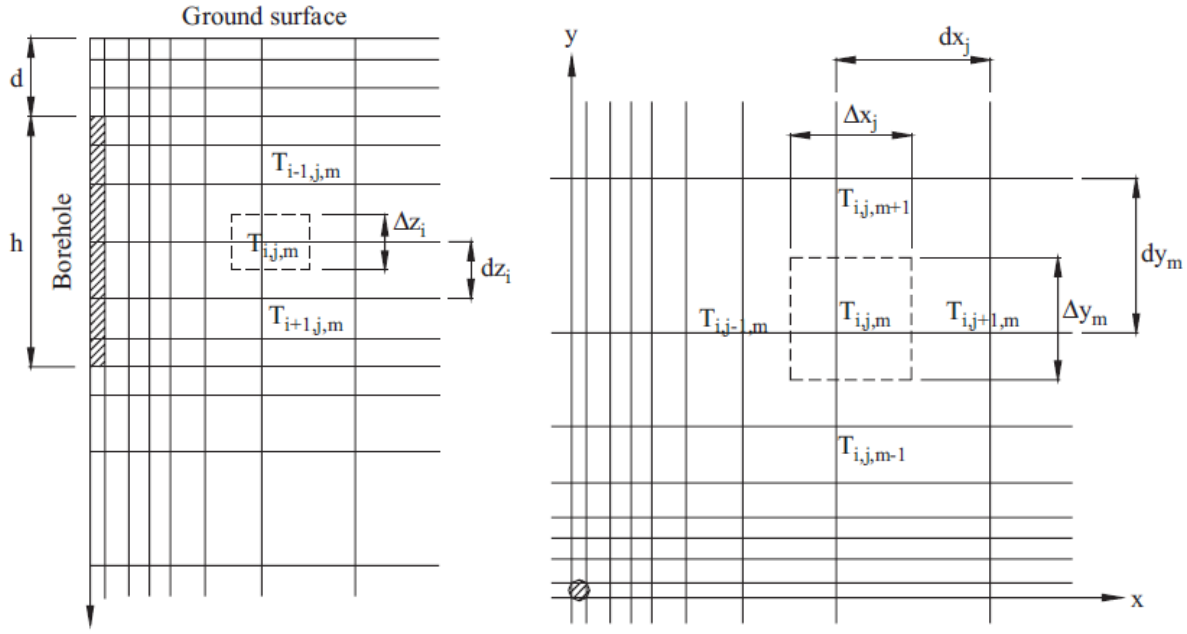

Figure 2.7 Finite difference grid for three-dimensional conductive heat transfer in the ground (Lee and Lam 2008).

The first numerical method used to model borehole temperature response in a GHX was a 2D finite difference model that was built on the finite-line source assumptions to account for the finite length of the borehole in a radial-axial coordinate system (Eskilson 1987). This method describes the dimensionless temperature response factors (known as G-function) of a single borehole. The ground is assumed to be homogenous with constant initial and boundary conditions, and the thermal resistant of the borehole elements (grout, pipe and fluid flow) is neglected. The response of a single borehole to each stepped heat pulse is described and superimposed to calculate overall borehole response. This model was mainly used to estimate the performance of ground to heat extraction/rejection over a longer time period (up to 25 years); however, as this numerical method does not include exact information about borehole geometry, it cannot

be used for the short-term (an hour to a week) application. The temperature T (r, z, t) response of the ground for any constant heat extraction must be calculated using the heat conduction equation in cylindrical coordinates, as given by

$$\frac{1}{\kappa}\frac{\partial T}{\partial t} = \frac{\partial^2 T}{\partial r^2} + \frac{1}{r}\frac{\partial T}{\partial r} + \frac{\partial^2 T}{\partial z^2} \qquad \text{Eq. 2.31}$$

The effective undisturbed ground temperature, T_m, is assumed at the mid-depth of the borehole and applied to the equation as follows:

$$T(r, z, 0) = T_m \text{ (initial condition)}$$

$$T(r, 0, t) = T_m \text{ (boundary condition at the finite difference ground surface)}$$

This method uses simplified initial and boundary conditions in contrast to more precise methods that consider a geothermal gradient and air temperature variations at z = 0; however, the error in heat extraction is less than 1% (Claesson 1985). This model is limited because it requires a lot of time to merge to a solution and is only valid for times greater than 3 h to 6 h for typical boreholes (Yavuzturk 1999). However, Eskilson's g-function approach was considered state-of-the-art and was integrated into many building-energy simulation tools including TRANSYS, Energy Plus, and GLEHEPRO (Javed and Claesson 1999).

Eskilson's next study included the condition of circulating fluid through the GHX system in addition to refining the assumptions in the first model. The long-term thermal performance of various borehole configurations was analyzed by considering the thermal process in the ground and in the borehole, including hydraulic coupling, pumping rate, and loading conditions (Claesson and Eskilson 1987). Assuming an average borehole temperature and mean fluid temperature, they demonstrated that the efficiency of the GHX system is a function of the amount of heat extracted from or injected into the ground. They showed that minimum and maximum temperatures may take several years to manifest, especially in a borefield that consists of multiple boreholes in close proximity to each other. For example, the worse

design-case condition might occur more than 10 years after installation. Therefore, an extended time period should be considered to efficiently evaluate the system's performance (Kavanaugh 1995).

Another model that included coupling fluid conditions was developed using an explicit (Euler) FD method for estimating the transient conductive heat transfer in the ground (Rottmayer et al. 1997). A thermal resistant network at the soil-grout interface was included, and 2D finite difference equations on a polar grid were used to calculate the radial heat transfer over a 3-m-deep vertical borehole. Conduction in the axial direction was neglected, and each vertical section was coupled with flow along the U-pipe. The circular leg of the U-pipe was approximated by a "pie-sector shape" and by matching the perimeter of the modeled non-circular tube to the actual circular pipe perimeter. Rottmayer et al. (1997) found that this method under-predicts the heat transferred from the U-pipe by 5% compared to an analytical model due to simplified pipe geometry.

Unlike the previous studies, Lee and Lam (2008) coupled the numerical and analytical solutions by considering both heat transfer processes around the borehole and in the GHXs. A 3D, implicit FD method with a rectangular coordinate system was developed based on the prescribed borehole temperature profile under quasi-steady-state conditions to determine the ground temperature and the borehole temperature profile. The geometry of a 110-m-deep borehole was approximated as a square column. The temperature rise at the different far-field distances, defined using $r_{max} = 3\sqrt{\kappa t_{max}}$, where t_{max} is the maximum operational time, was also evaluated. The model was validated using two conventional, analytical finite-line-source and cylindrical-line-source solution methods with good agreement. Lee and Lam (2008) found that neither temperature nor heat load were constant along the borehole, in contrast to the constant temperate or heat flux assumptions made in both analytical approaches. This method was also used to estimate the performance of various borehole fields (borehole spacing taken as 5 m). The results showed that the percentage of deviation from the finite line-source model was no more than 2.1 for a small borefield (up to 3x3 boreholes), but the deviation rose to 5% when the size of the borefield was larger (for 5x5 boreholes)

due to the thermal interference of adjacent boreholes, which occurs because of the higher borefield thermal resistance variation of a larger borefield.

Finite Element Method (FEM)

The FE method has been used by engineers for modeling the mechanistic response of a complex system and for structural mechanics problems under loadings (Keene 2012). The FE method is also used for solving fluid flow and heat transfer problems. The problem domain is divided into a set of finite elements that are generally unstructured (triangles or quadrilaterals in 2D, and tetrahedra or hexahedra in 3D). The distinguishing feature of the FE method is that equations are multiplied by a weight function before they are integrated over the entire domain. The finite-difference form of partial differential equations is conceptually straight forward, while finite-element methods require application of some principals that are more conceptually difficult and require more attempts to create algebraic equations. However, elements rather than nodes allow more convenient treatment with respect to the variability of nodal spacing, thermal conductivity, and heat production (Wang 1984). An important advantage of the FE method is its capability to deal with complex or irregular geometries (e.g., circular U-tubes in a rectangular domain). The FE method is excellent for diffusion-dominated (conduction, etc.) problems. The grids are easily refined, and each element is simply subdivided, giving higher accuracy for coarse grids. Experience has shown the FEM to be generally superior to FDM in terms of solution stability (Wang and Anderson 1982, Ferziger and Peric 2002). The disadvantage of this method is that it is poorly suited for determining flow conditions, particularly those problems involving turbulent flow.

Taking advantage of the geometrical flexibility of the FEM, the first FEM was developed to show that transport phenomena occurred between the legs of the U-tube and the effect that the backfill had on the thermal process in the borehole (Muraya et al. 1996). Muraya et al. (1996) attempted to quantify this interference by defining heat exchanger effectiveness based on ground formation and grout properties, U-pipe configuration, far-field and loop temperatures, and heat-dissipation rates. The model's validation was conducted against two different applications of the analytical cylinder source solution using constant

temperature and constant flux approaches. A cooling-dominated area was selected to conduct tests of the performance degradation of the GHX system due to moisture migration, which is the major influence on thermal conductivity ($\boldsymbol{\lambda}$ = 5 - 10 W/m·K), for a particular soil that contains a mixture of solid minerals, air ($\boldsymbol{\lambda}$ = 0.0022 W/m·K), and water ($\boldsymbol{\lambda}$ = 0.61 W/m·K). The impact of moisture was neglected in this study because the unsaturated soil section is minimal (up to 10 m) compared to the saturated section of soil (~300 m). The parametric study showed that the overall thermal effectiveness and backfill effectiveness were strongly dependent on borehole geometry.

Another example of a FE solution was introduced by Zheng et al. (2011). Physical and mathematical models were developed for a vertical U-tube heat exchanger based on an FE technique including both convective and conductive heat transfer over a 115-m-deep borehole. Mathematical equations were established based on mass and energy conservation equations for heat transfer in the pipe wall, soil and grout, and between the fluid and pipe wall. U-tubes were presented with one equivalent tube as $r_e = \sqrt{2}r$ (r is a single pipe radius in the U-tube). This model assumed 1D convective heat transfer along the tube and 2D conductive heat transfer in three different types of media (sand, clay, and sandstone) and in the grout. A constant, undisturbed temperature of 9.62 ^{o}C was set as the initial condition for the entire model domain. The boundary of the soil surface temperature was estimated as

$$\mathrm{T}(0,\mathrm{t}) = \mathrm{T_m}\cos\left(\frac{2\pi \mathrm{t}}{\mathrm{t_o}}\right) + \mathrm{T_o} \qquad \text{Eq. 2.32a}$$

The far-field boundary at 5 m from the borehole wall and the bottom side of the borehole was taken as the adiabatic-boundary condition

$$-\lambda_{\mathrm{g}}\frac{\partial \mathrm{T}}{\partial \mathrm{r}} = 0 \qquad \text{Eq. 2.32b}$$

The wall boundary of the equivalent pipe was taken as the constant flux when the pump is on and adiabatic when the pump is off:

$$-\lambda_g \frac{\partial T}{\partial r} = q'' \qquad \text{Eq. 2.32c}$$

Zheng et al. (2011) found that the soil temperature remained constant at a 3-m distance from the pipe center in both the short term (1 d) and the long term (10 d). The main factor that controls the heat transfer between the GHXs and the soil is the thermal diffusivity of the soil. Depending on the soil's heat diffusion capability, the space between the U-pipes in the borefield can be larger or smaller based on the radial magnitude of the thermal impact from the pipe center. The results with regard to different soil type suggested that 5 m should be considered as the best spacing to overcome the thermal interference between U-pipes.

A comprehensive study by Al-Khoury et al. (2010) developed a 3D FE method for estimating the time-dependent temperature variation in a 100-m-deep, double U-pipe, vertical GHX by considering thermal interactions between the borehole components (pipe, fluid, grout) and between the borehole and surrounding soil. The borehole heat exchanger was discretized using the Petrow-Galerking method and implemented in the finite-element package FEFLOW. Initial and boundary conditions are set based on experimental data that included varying entering-fluid temperature during the operation period. Al-Khoury et al. (2010) found that the calculated inlet and outlet temperature obtained from the numerical method agreed with the experimental data with an error of less than 1%. From an energy-consumption point of view, however, the measured power of the system and the calculated power gave an error of 15%, which is much greater than that obtained from the temperature differences.

Finite Volume Method (FVM)

The FVM uses the integral form of the conservation equations as its starting point. The problem domain is subdivided into a finite number of connected control volumes, and the conservation equation is applied to each control volume. One advantage of the FVM over finite-difference methods is that FVM does not require a structured (regular) mesh (although a structured mesh can be used). The FVM is preferable to other methods because it can accommodate any type of grid that is suitable for complex

geometries, and boundary conditions can be correctly applied. Mass, momentum, and energy are conserved, so the variables are resistant to shocks and discontinuities. This is true because the values of the conserved variables are located within the volume element, and not at nodes or surfaces. However, FVMs use a higher method of order than the second order developed in 3D because the FVM requires three levels of approximation: interpolation, differentiation, and integration (Ferziger and Peric 2002). More details of FVM are discussed in Section 3.

Yavuzturk and Spitler (1999) developed a 2D fully implicit, finite-volume solution for the modeling of a vertical GHX system. In this study, Eskilson's dimensionless, temperature-function (G-function) model was extended by introducing the effect of a short-time period (as small as 3 min) into the transient thermal process. This is only possible when the borehole elements (grout, pipe, and fluid) are fully considered in the model. This enhanced G-function model was expressed in terms of a short-time step function model and assumed the cross section of the two legs of U-pipe to be "pie-sectors" with constant heat flux entering the numerical domain for each time step. To account for the variation in temperature between upward flow and downward flow in the U-tube, 60% of the total heat flux was assumed to go to one leg and 40% to the adjacent leg. This method utilizes an automated, parametric grid-generation algorithm for a variety of borehole geometries, pipe diameters, and pipe shank spacing. This model is applicable for time frames of between 2.5 min and 200 h, while Eskilson's g-functions are applicable for longer times (> 200 h). Yavuzturk's short-term G-function is regarded as state-of-the-art in determining short-term response of a GHX and has been implemented in energy building simulations by TRNSYS and Energy Plus.

A 3D, unstructured, finite-volume model was developed by Li and Zheng (2009) for vertical GHX systems. A "Delaunay triangulation" method was used to mesh the borehole cross- section of the borehole, including both outside the borehole and inside the borehole (Fig. 2.8). With this method, the actual geometry of the borehole is protected, and no assumptions are required for the geometry correction. The vertical section of 47-m-deep borehole was discretized using structured grids due to the relatively simple

geometric structure. They treated the heat transfer process around and in the borehole as transient and conjugated processes, terms that refer to a thermally interacting process occurring between the convective heat transfer of the fluid in the pipe and the conductive heat transfer of the surrounding medium. An undisturbed ground temperature of 8.5 ^{o}C was assumed over the entire borehole for the initial condition, and the constant, far-field temperature condition was applied at the outer side of the model domain. The surrounding soil was divided into layers in the vertical direction to account for the impact that the fluid temperature as it changed with depth had on the thermal process in the borehole. They also simulated the thermal process during the off-time period of the GHX, which requires consideration of the free convection heat transfer coefficient, as suggested by Kavanaugh (1985), to be 136 $Wm^{-2}C^{-1}$. The results of the numerical model were validated with an in-service cooling system and using the hourly entering-fluid temperature as the input variable for model simulations. A comparison of the predicted exiting-fluid temperature of GHXs and the measured temperature resulted in good agreement.

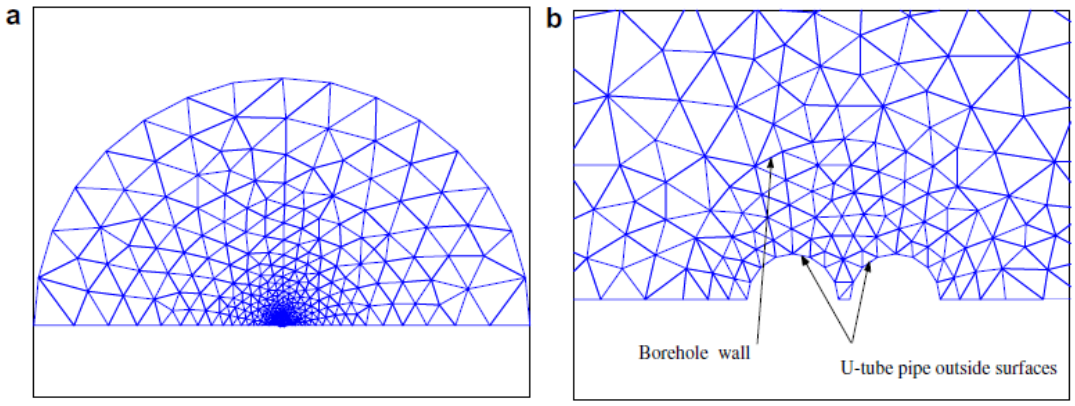

Figure 2.8 (a) The cross-section domain of the borehole (Delaunay triangulation) and (b) local mesh of near the borehole (Li and Zheng 2009).

Computational Fluid Dynamics (CFD)

CFD is well known as a powerful technique for solving heat and mass transport (Bansal et al. 2010). CFD codes are structured around those numerical algorithms that can tackle fluid-flow problems which are

governed by the Navier-Stokes equation, which is basically a vector equation obtained by applying Newton's Law of motion to a fluid element called the momentum equation. The Navier-Stokes equation is also supplemented by the continuity equation and the energy equation. These equations are expressed in terms of partial differential equations, which are generally discretized using a finite-volume based method. The CFD solution technique has become more preferred in recent years because it considers the interaction of fluids and surfaces. As axial fluid behavior in the GHX system is one of major factors controlling heat transfer mechanisms in the entire GCHP system, an accurate solution technique is preferable to simulate the real condition. Therefore, CFD methods are proposed for this study to predict complex heat transfer processes, including the dynamic fluid condition in the pipe legs as well as the groundwater flow.

A noteworthy study of CFD simulations, conducted by Khalajzadeh et al. (2011), considered a full 3D transient with heat transfer, and it can be used to define the effect of simultaneous variation that design parameters—inlet fluid temperature, borehole diameter, pipe diameter, borehole depth, and Reynold's number—have on the efficiency of GHXs. Unlike most previous research, a variable ground temperate profile in the shallow region (10 m in depth) was considered to eliminate the inaccurate temperature prediction of the shallow region of GHXs, which is produced by other methods that assume that the ground temperature is constant with depth. The radius of the cylindrical model's domain was carefully estimated to ensure that the soil boundary was not affected by the GHXs during the simulation time period. As discussed in the Analytical Method Section 2.3.1, Hart and Cavillion (1986) introduced the correct r_∞ as infinity. However, the computational model should be restricted in the numerical simulation. In this case, the following equation is suggested:

$$r_\infty = 4\sqrt{\alpha t} \qquad \text{Eq. 2.33}$$

Two functions—the total heat transfer efficiency and the heat exchanger efficiency—were defined with the aid of CFD results using the following equations, respectively:

$$\text{Total heat transfer rate, } Q = \frac{mc(T_{in} - T_{out})}{H} \qquad \text{Eq. 2.34}$$

$$\text{Heat exchanger efficiency, } \theta = \frac{T_{in} - T_{out}}{T_{in} - T_g} \qquad \text{Eq. 2.35}$$

where Q is the total heat transfer rate [W/m], m is the fluid mass flow rate [kg/s], c is the fluid specific heat [J/kg·K], H is the borehole depth [m], and $\boldsymbol{\theta}$, heat transfer efficiency, is a function of dimensionless parameters (length of pipe and borehole, entering-fluid temperature and Reynold's number). CFD results were verified with experimental data collected from 67-m deep vertical, ground heat exchangers. Based on the outlet-fluid temperature at the GHXs, the maximum difference between the CFD and experimental data was in the range of 3.5%. Khalajzadeh et al. (2011) also optimized the numerical methods using the second-order response surface model (RSM). The results showed that the dimensionless entering-fluid temperature and the dimensionless pipe diameter significantly affect the response variables, while these variables are less affected by dimensionless depth. However, the heat exchanger's efficiency increased with borehole depth, whereas total heat transfer efficiency decreased. Maximum efficiency was provided by a combination of these dimensionless design variables: a borehole depth of 278.83, a fluid inlet temperature of 1.91, a pipe diameter of 0.33 and a Re of 3200. CFD simulation was again performed using this combination of design variables, and the results showed good agreement with predicted values from RSM optimization.

Another CFD effort was conducted by Gustafsson et al. (2010) to study how the borehole thermal resistance might be influenced by natural convective heat flow. In some countries in a region of Scandinavia, boreholes are usually not grouted but filled with groundwater. A 3D steady-state model for simulating the different heat transfer rates and borehole water temperatures of a 3-m-long vertical borehole was developed. Because low thermal resistance in the borehole and ground are desirable to increase heat transfer between of the U-pipe and surrounding rock, a constant temperature was set at the outside of the U-pipe and at the outer bedrock wall. For the bottom and the top boundaries, adiabatic surfaces were set. This model showed that natural convective heat flow induced by fluid density differences due to a temperature gradient decreased the thermal resistance by three times compared to stagnant water in the

borehole. Model verification showed good agreement between theoretical and experimental studies, and this method was suggested as a way to account for thermal resistance in a groundwater filled borehole.

Congedo et al. (2012) presented 3D, transient CFD simulation to find the most important parameter of those that influence the performance of horizontal GHX systems. This study applied real air-temperature data and its impact at the underground as a boundary condition in order to simulate the system's operation in both winter and summer. This boundary condition was verified with experimentally measured data before the simulation proceeded. Entering-fluid temperature was also applied to the pipe inlet as a boundary condition. This model showed that ground thermal conductivity is the most important parameter influencing system performance in any type of configuration (Wu et al. 2013). An increase in thermal conductivity from 1 [W/m·K] to 3 [W/m·K] can increase the thermal energy transferred from the ground in winter by 75% to 133%, depending on the pipe configuration. The mass flow rate in the pipe is also key to heat transfer performance for all arrangements. Buried depth did not show any impact on heat transfer performance for the geometries evaluated.

As summarized from the literature, the complexity of modeling a GHX system increases as the computational tools are improved. Earlier numerical studies apply a number of assumptions, either for geometrical simplification or boundary conditions. For instance, FDMs are redistricted to simple borehole and pipe geometries, which are assumed to be rectangular in shape, rather than circular. This geometric limitation might cause error when transient convective heat transfer is considered, especially for a short-term operation. However, recent numerical methods simulate the exact model geometry including the U-pipe, fluid, grout, and soil parts, to simulate a full heat-transfer process in the GHX system. Most of these studies largely focus on the impacts that the short-time scale and on/off cycling may have on the thermal performance of GHX system due to computational cost. Also, one study compared the impact that continuous (long-term) and discontinuous (short-term) operational periods have on the performance of heat transfer in GHX system. The heat exchanger rate of the GHX, both operation types, showed that the short-time discontinuous operation (two hours operation with constant interval of off-time) increases the

performance of a GCHP system by 53.1% for a double tube, 33.3% for a single U-tube, and 29.1% for multi-tubes, as compared to continuous operation (Jalaleddun et al. 2010). From this point of view, it is important to consider on/off cycling when attempting to achieve an accurate estimation of GCHP performance.

The most complex numerical levels are three-dimensional modeling and coupled heat and mass transfer, such as those included in the CFD method. However, none of the methods discussed here consider the dynamic boundary condition in their simulations; they usually assume constant temperature or adiabatic conditions for the solid part of the model domain. This boundary condition might be reasonable for the short-time period, but for the long-term operation period of GHXs, the temperature or the heat flux at the boundary of the borehole elements (pipe, grout and soil) will tend to change, especially at the far-field distance. This change will inherently result in inaccurate soil temperature estimation. This issue might also be more important in cases where the soil around the GHXs is of low conductance, a condition that can result in heat accumulation around the borehole, one that significantly decreases GCHP performance, particularly during the cooling period. A recent study by Wang et al. (2013) developed a 3D transient simulation based on the dynamic boundary condition rather than on the constant temperature or heat flux boundary. The mass, momentum, turbulence, and energy conservation of the fluid flow were considered for the borehole elements-fluid conjugated heat transfer of the GHXs. The goal of this study was to develop dynamic boundary conditions in the borehole elements based on the energy conservation of the fluid, pipe, grout, and soil as follows:

$$Q_{in} + Q_{sink} + Q_{top} + Q_{bottom} + Q_{far-end} = 0 \qquad \text{Eq. 2.36}$$

$$Q_{top} = q"_{top} A_{top}$$

$$Q_{bottom} = q"_{bottom} A_{bottom}$$

$$Q_{far-end} = q"_{far-end} A_{far-end}$$

where Q_{in} is the pipe heat transfer rate, Q_{sink} is the heat consumption or release in the solid zone, Q_{top} is the boundary heat transfer rate at the top surface, Q_{bottom} is the bottom surface, $Q_{far\text{-}end}$ is the far-end surface, q" is the heat flux, and A is the area for corresponding positions. Dynamic boundary conditions were achieved by dividing the critical time (t_c), which refers to when the impact of GHXs reaches the bottom and far-end surface of the ground into two stage. If the operation time (t) of the GHX was less than the critical time, the bottom surface of the ground and the far-end surface of the ground were assumed to be adiabatic. Heat fluxes at the bottom and far-end were calculated when $t > t_c$, using a formula that was based on energy conservation equations in Eq. 2.36. Numerical outlet fluid temperature at the GHX was compared with experimental data. A reasonable percentage error of less than 5% was defined. The simulation results derived from the thermal boundary conditions of constant temperature, adiabatic, and dynamic thermal boundary conditions showed that the constant temperature boundary results in an underestimation, while the adiabatic boundary results in an overestimation of the influence that the GHX's operation has on the solid-zone temperature. In addition, during a long-term operation or a large-scale application of the GHX, these impacts become more obvious. A reasonable estimation of solid-zone temperature was obtained using the dynamic boundary conditions, which can overcome the limitations imposed by using constant temperature and adiabatic boundary conditions.

CHAPTER 3 - MODEL DEVELOPMENT

3.1 INTRODUCTION

Various methods for designing and simulating ground-coupled heat pump systems were discussed in the literature review (Chapter 2). There are advantages and disadvantages to each of the currently available solution methods, and each method should be evaluated for its individual merit depending on the given, specific limitations or on the desired application (see Table 3.1). However, most studies focus on the mechanical behavior of the GCHP system— none systematically, accurately, or reliably accounts for the ground's geological conditions in terms of the efficiency of GCHPs. A significant majority of the current methods assume an average uniform ground temperature and thermal conductivity for the entire length of borehole during the operation of the GCHP. These assumptions limit the possibility of accounting for variations in the thermal conductivity of the subsurface geology over the operation period, variations that may play a crucial role in the heat transfer process along with fluid circulation through the U-pipe. Furthermore, during operation, the undisturbed (also known as far-field) ground temperature will increase/or decrease depending on the heating and cooling cycle, which could cause a thermal imbalance over a period of many years. To evaluate annular heat extraction and heat rejection to the ground during operation, a solution for the analysis of heat flow occurring between the geological formation and the GHX loop for long-term operation (+10 years) is desirable, including the short-time, operational on-and-off cycles. This energy balance would then allow for quantification of the impacts of GCHPs operations on the surrounding ground temperature.

A typical modeling effort first analyzes how the ground responds when a certain amount of heat is applied along the borehole wall. Models based on a cylindrical heat source simulate basic heat conduction around the borehole without considering the borehole elements (grout, pipe and heat exchanger fluid) and heat transfer occurring between them. The long-term response of ground in these models typically describes the performance of a particular borehole field configuration over a period of a year. Theoretical approaches and corresponding formulas, which were presented in the literature review section, are applied. More

powerful models analyze the heat transfer process, including the convective heat transfer occurring between a moving fluid and the pipe surface in addition to conduction through the grout and the surrounding ground, with computational fluid dynamic (CFD) analyses, which are derived from first principle of thermodynamics. The section covering the steps and objectives of model development are summarized in Fig. 3.1.

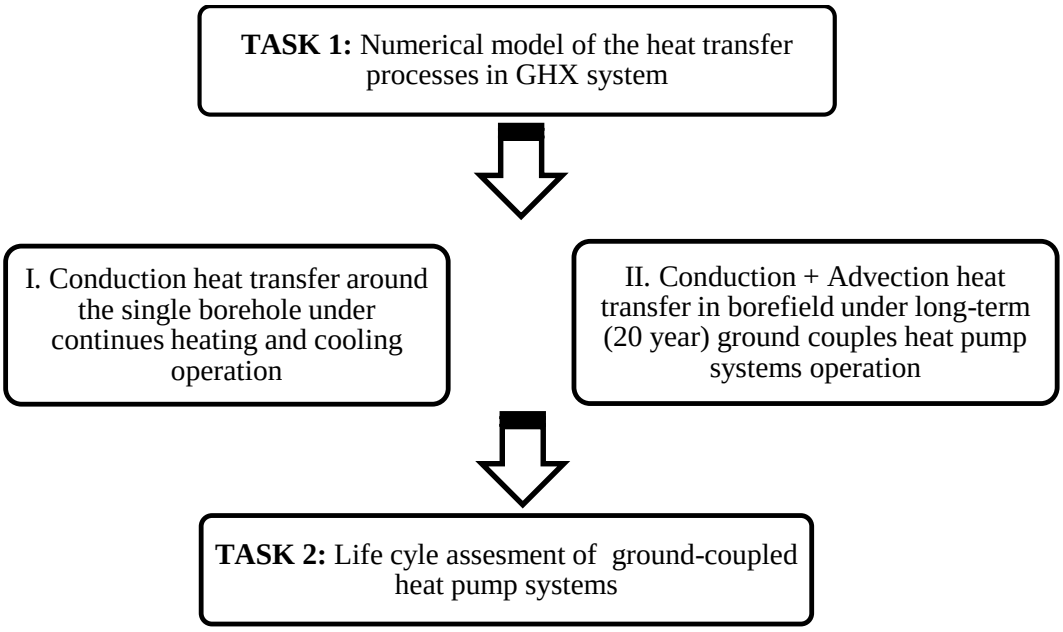

Figure 3.1 Steps and objectives of model development

Table 3.1 Existing numerical models of GHX system based on different solution approaches, chronologically

Numerical Solution To GHX Systems	References	Model Specifications	Model Limitations
Finite Difference Method	Eskilson (1987) Claesson and Eskilson (1987) Rottmayer et al. (1997) Lee and Lam (2008)	• the dimensionless temperature response (G-function) of single borehole • the G-function of multiple boreholes include hydraulic coupling, pumping rate • 2D, explicit (Euler) FDM on a polar grid • Transient conductive heat transfer-consider fluid-soil interface • 3D, implicit FDM on a rectangular system • Consider borehole elements (fluid, pipe, grout)	• applicable for long-term simulation (+25 yr) and no fluid conditions considered • assume average borehole temperature • no axial heat flow-only radial • soil is homogenous
Finite Element Method	Muraya (1996) Zheng et al. (2011) Al-Khoury et al. (2005)	• 2D, transient FEM • Heat exchanger effectiveness based on grout,pipe spacing, moisture migration impact • Consider U-pipe and grout thermal interface • Model for conductive + convective heat transfer • Include axial heat transfer by fluid flow • Consider daily surface temp variation • 3D, transient FEM of GHX with borehole elements • Consider a soil temperature variation in simulation	• constant heat flux along the borehole wall
Finite Volume Method	Yavuzturk and Spitler (1999)	• 2D, implicit FVM (extension of Eskilson 1987) • Short-time (- 3min) response of the ground temperature-include borehole elements	• no temperature variation along the borehole wall • applicable for short-time steps (2.5 min to 200 h)
Computational Fluid Dynamic	Congedo et al. (2010) Khalajzadeh et al. (2011) Wang et al. (2013)	• 3D, transient CFD model • Define the most important design parameters in GHXs as a thermal conductivity of the soil • 3D, transient CFD model • Impact of simultaneous change of design parameters (T_i, D_b,D_p, Re_D)*on GHX performance • Consider a variable ground temp due to seasonal change • 3D, transient CFD model of GHXs –consider fluid-solid thermal interface • Simulate dynamic boundary condition and compare with constant temp and adiabatic boundary conditions	• applicable for short-term (≤ 4 h) simulation • applicable for shallow applications (≤ 2 m)

*T_i inlet fluid temperature at the GHX, D_b is the diameter of borehole, D_p is the diameter of the pipe and Re_D is the Reynold's number

3.2 NUMERICAL MODELING OF GROUND TEMPERATURE RESPONSE IN A GROUND COUPLED HEAT PUMP SYSTEMS (GCHP)

This subsection consists of a paper that was prepared, submitted and accepted for publication and an interactive poster presented at the 2014 American Society of Civil Engineers-Geo-Congress: Geo-Characterization and Modeling for Sustainability. This paper is hereby included as a subpart of the model development section in this study. The paper's introduction is not given herein to avoid repeating content that was described in Chapter 2.

Abstract: The paper describes the long-term, cumulative thermal response of the ground around a vertical ground heat exchanger (GHX) operating in both heating and cooling modes, with the dominant GCHP mode being cooling. An actual 300-m-deep borehole through varying lithology has been modeled with fully three-dimensional finite element analysis using ABAQUS software. The monthly average surface temperature and temperature at depth were used as boundary conditions, and the monthly heating and cooling loads were applied as constant heat-load with depth along the borehole. The modeling results show that a deep GHX system may be more efficient because it takes advantage of the geothermal gradient and is less sensitive to seasonal impacts than are shallow GHX systems. Based on the modeling results, the temperature profiles along the borehole and near surface are not constant and vary significantly when the lithology changes. Therefore, the actual thermal conductivity values for each geological material should be considered.

3.2.1 Theory

Governing Equation

A three-dimensional (3D) finite element model by ABAQUS solver was used to quantify the ground temperature responses through the borehole where the heating and cooling loads were applied. The model considers transient and fully 3D heat transfer in multi-layer ground. Heat transfer by groundwater advection in the ground was neglected. Heat transfer in the borehole was solely controlled by conduction. The ground properties were assumed to be constant over the period of the computer simulation.

The governing equation for pure heat conduction can be stated in 3D space by Fourier's law as

$$\frac{1}{\kappa}\frac{\partial T}{\partial t} = \left(\frac{\partial^2 T}{\partial x^2} + \frac{\partial^2 T}{\partial y^2} + \frac{\partial^2 T}{\partial z^2}\right) \quad \text{where } \kappa = \frac{k}{\rho c} \qquad \text{Eq. 3.1}$$

where κ is the thermal diffusivity [m^2/s], ρ is the density [kg/m^3], c is the specific heat capacity [J/ kg· K], k is the thermal conductivity [W/m·K], T is the temperature [K], and t is the time [s].

Spatial Discretization

The problem domain *V* is discretized into finite elements connected at the nodes. The global equation for the domain can be assembled from finite element equations using information gathered at the connected node. Temperature inside a finite element is estimated via interpolation using a shape factor, *Ni*.

$$\begin{aligned} \mathrm{T} &= [\mathrm{N}]\{\mathrm{T}\}, \\ [\mathrm{N}] &= [\mathrm{N}_1, \mathrm{N}_2 \ldots.], \\ \{\mathrm{T}\} &= \{\mathrm{T}_1, \mathrm{T}_2 \ldots.\} \end{aligned} \qquad \text{Eq. 3.2a}$$

Differentiation of the temperature-interpolation equation gives the following interpolation relation for temperature gradients:

$$\begin{Bmatrix} \frac{\partial T}{\partial x} \\ \frac{\partial T}{\partial y} \\ \frac{\partial T}{\partial z} \end{Bmatrix} = \begin{bmatrix} \frac{\partial N_1}{\partial x} & \frac{\partial N_2}{\partial x} \dots \\ \frac{\partial N_1}{\partial y} & \frac{\partial N_2}{\partial y} \dots \\ \frac{\partial N_1}{\partial z} & \frac{\partial N_2}{\partial z} \dots \end{bmatrix} \{T\} = [B]\{T\} \qquad \text{Eq. 3.2b}$$

where, {T} is a vector of temperatures at nodes, [N] is a matrix of shape functions, and [B] is a matrix for temperature-gradient interpolation. Using the Galerkin approach, the heat transfer equation can be written in the following form:

$$\int \left(\frac{\partial q_x}{\partial x} + \frac{\partial q_y}{\partial y} + \frac{\partial q_z}{\partial z} + \rho c \frac{\partial T}{\partial t} \right) N_i \, dV = 0 \qquad \text{Eq. 3.3}$$

After applying the divergence theorem to the first three terms, the following boundary conditions can be added to the equation:

1. Specified Temperature,

   $T_s = T_1 (x, y, z, t)$ on S_1

2. Specified heat flow,

   $q_x a_x + q_y a_y + q_z a_z = -q_s$ on S_2

where S is the surface where boundary is being applied, T_s is the unknown surface temperature, q is Fourier's heat rate, and a is an outer normal the surface of body. Hence, the discretized equations will be

$$\int \rho c [N]^T [N] dV T(t) + \int k [B]^T [B] dV = \int q_s [N]^T dS \qquad \text{Eq. 3.4}$$

where {T (t)} is a nodal vector of temperature derivatives with respect to time, n is the outer normal to the surface of the body.

Time Integration

The transient term is approximated by employing the unconditionally stable Euler-implicit scheme (also called the modified Crank-Nicolson operator) in the pure conduction element in ABAQUS. The time term $\{T(t)\}$ is

$$\frac{dT}{dt} = f(t, T) \quad \text{with initial value } T(t_o) = T_o \qquad \text{Eq. 3.5}$$

where the function f and the initial values t_o and T_o are known; the function T depends on the real variable time, and t is unknown. A numerical method produces the sequence T_o, T_1, T_2,….such that T_n approximates $T(t_o + n\Delta l)$, where n is discrete time points, and Δl is the step size as shown below.

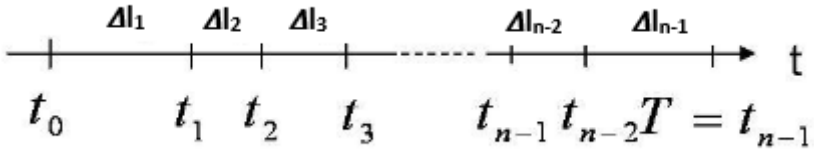

The backward Euler implicit method computes the approximation as

$$T_{n+1} - T_n = \Delta l f(t_{n+1}, T_{n+1}) \qquad \text{Eq. 3.6}$$

Integrating the differential equation (Eq. 3.5) from t_n to $t_{n+1} = t_n + \Delta l$ yields

$$T(t_{n+1}) - T(t_n) = \int_{t_n}^{t_{n+1}} f\big(t, T(t)\big)\, dt \qquad \text{Eq. 3.7}$$

Approximating the integral on the right-hand side with the one-rectangle method as

$$T(t_{n+1}) - T(t_n) \approx \Delta l f(t_{n+1}, T(t_{n+1})) \qquad \text{Eq. 3.8}$$

Finally, T_n should approximate $T(t_n)$, and the formula for the Euler implicit method follows. More details can be found in the ABAQUS 6.12 theory manual.

3.2.2 Model Geometry and Meshing

The model domain is assumed as a circular geometry, 50 m in radius and 335 m in depth (see Fig. 3.2). The radius selected for the cylinder had to be large enough to ensure that the ground at the edge was not affected by the thermal influence of the borehole at the center (which is referred to as the far-field). The 300-m-deep borehole is embedded in a multi-layer geological formation. Layer 1 is termed the upper layer (from 0 m to 20 m), layer 2 the middle layer of sandstone (from 20 m to 265 m) and the layer 3 the bottom layer of granite (from 265 to 335 m). The different layers were assembled according to their depth, and the "surface-to-surface" contact was used to provide heat transfer between the two different geological formations. To perform the finite element analysis, the model had to be discretized into tetrahedron (DC3D4) 3D heat transfer elements. The area of the borehole was meshed more finely to ensure calculation accuracy (Fig. 3.2). The matrix contains 491139 total elements, 33565 for the upper overburden of soil, 405292 for the middle sandstone, and 52282 for the lower granite.

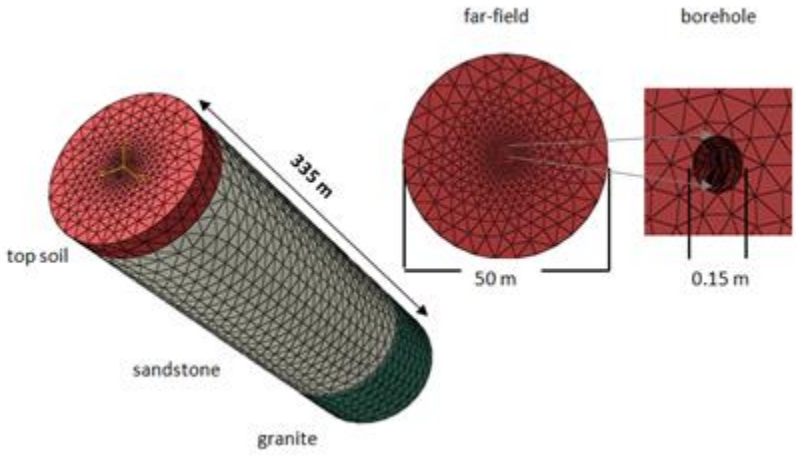

Figure 3.2 Model geometry with numerical mesh

3.2.3 Boundary Conditions and Material Properties

Monthly variations between the air temperature and the ground surface at the top and the undisturbed measured bottom hole temperature (T_g = 285 K) at the site were applied as boundary conditions

(Fig. 3.3a). The outer edge of the model was assumed to be adiabatic (i.e., no heat flow). Surface heat flux was applied to the entire GHX borehole as a boundary condition for each monthly heating and cooling period. Each month requires a different amount of heat for heating and cooling purposes; thus, surface heat flux was calculated based on the GHX's typical values of heat rate extracted from the ground (35 W/m during heating) and heat rate rejected to the ground (90 W/m during cooling) (Kavanaugh 1997) (Fig. 3.3b). The values from Fig. 3.3b were distributed evenly along the entire borehole without regard to layering and based on the heating and cooling period. Thermal conductivity, specific heat capacity, and the density of the soil and rock were used as physical parameters for the transient heat-transfer analysis. Those parameters were experimentally measured using guarded-comparative-longitudinal heat-flow experiments (ASTM-E1225) on rock cores that were sampled from the Wisconsin Geological Natural History Survey (WGNHS) and that were representative of the layers. The physical and thermal properties of the ground used for the simulation are presented in Table 3.2 (Meyer 2013).

Table 3.2 Properties of the multilayer ground

Layer	**Density [kg·m^{-3}]**	**Specific heat [J·kg^{-1} · K^{-1}]**	**Thermal Conductivity [W·m^{-1}·K^{-1}]**	**Thermal diffusivity [m^{2}·s^{-1}]**
Layer 1: Unconsolidated Soil	1300	800	1.5	1.4x10^{-6}
Layer 2: Sandstone	1800	900	2	1.3 x10^{-6}
Layer 3: Granite	2800	800	4	1.8 x10^{-6}

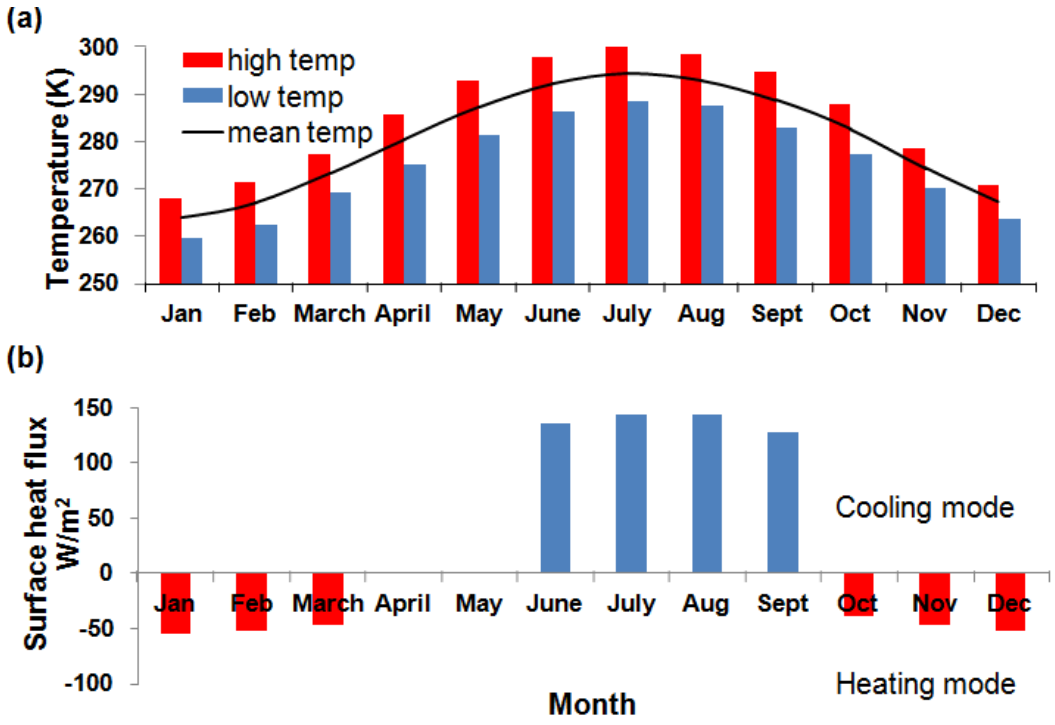

Figure 3.3 (a) Arlington (WI) air temperature variation (U.S. climate data) and (b) calculated based on typical estimated heating load capacity of GHX system

3.2.4 Results and Discussions

Ground Temperature Distribution before the Heating-Cooling Operation

The ground temperature profiles over 12 months (with varying air temperatures) were simulated to assess the ground-temperature distribution along multi-layer ground. The model started with undisturbed heat and temperatures. Twelve time-steps, each of a one-month period, were applied, starting with January. The monthly average air temperatures varied from 267 K (-9 ^{o}C) to 294 K (21 ^{o}C), as shown in Fig. 3.3a. The simulation results for January, August, and December are shown on the left-hand side of Fig. 3.4, while the temperature profiles with depth along the borehole at the center are shown to the right. As can be seen in both results, ground temperatures at up to 20 m in depth were strongly influenced by variances in air temperature occurring between summer and winter then at greater depth reached the natural thermal gradient. This shows that a deep GHX system may be more efficient for heating dominate GCHP application because it takes advantage of the thermal gradient and is less sensitive to seasonal impacts than are shallow GHX systems.

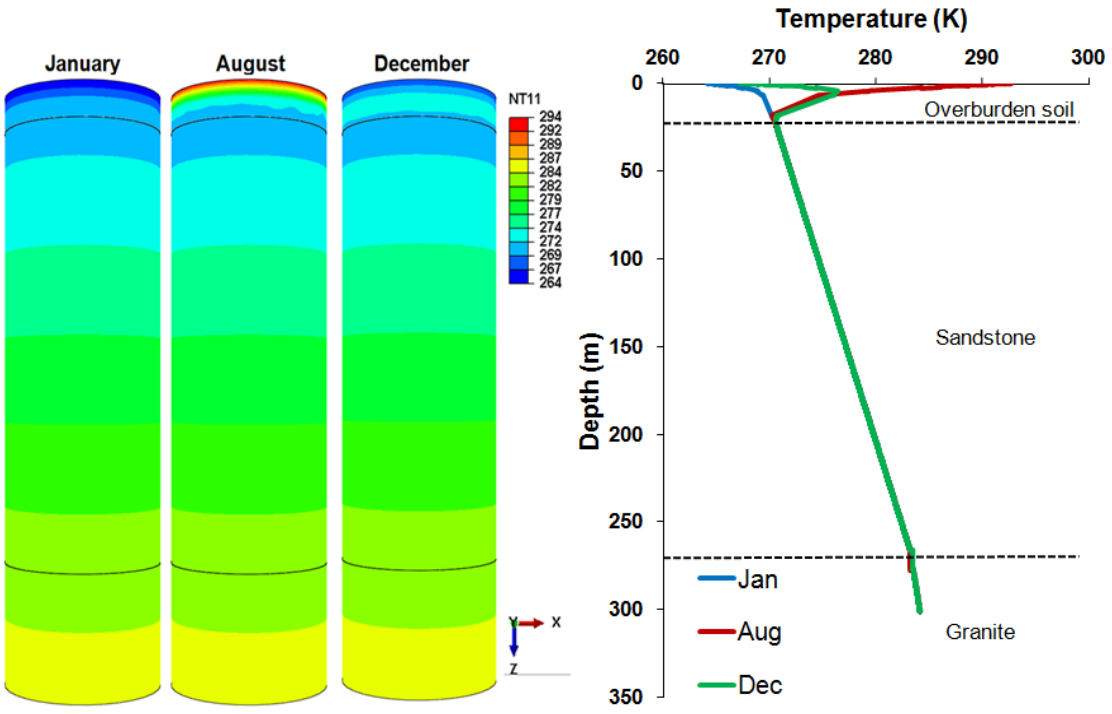

Figure 3.4 Temperature profile at far-field ground (on left) and along the borehole (on right) under the monthly mean air temperature variation

Ground Temperature Distribution under Continuous Heating-Cooling Operation

The GCHP system was assumed to operate continuously each month as the borehole was subjected to monthly variations of surface heat flux, as presented in Fig. 3.3b. The simulation results of the temperature variation in the ground and around the borehole for January, May and August are shown in Fig. 3.5. The temperature profiles along the horizontal distance from the borehole are plotted from the mid layer of each geologic unit in Fig. 3.6. The ground temperature around the borehole decreased during the heating mode (from Oct to March), while the temperature increased during the cooling mode (from June to Sept) for each geological unit. The ground temperature began recovering during the non-operational time period (April and May) (Fig. 3.5). In August, the temperature rise around the borehole was high, up to 305 K at the top, 300 K at the middle, and 295 K at the bottom. The cooling cycle created a greater impact because the heat rate rejected to the ground was much higher than the amount of heat extracted from the

ground in this simulation (see Fig. 3.3). The cumulative heat impact from the borehole extended radially to about 8 m, 6 m, and 12 m at the top, middle and bottom layers, respectively (Fig. 3.6). This difference was caused by the variations in the thermal diffusivity of the different layers. The thermal conductivity and thermal diffusivity of the granitic rock (bottom layer) is higher than that of the overburden soil and sandstone, and this resulted in a higher radial thermal impact and less temperature rise in the ground around the borehole. This variation is important for the evaluation of long-term system efficiency because a long-term operation of a GCHP system might cause heat to build up around the borehole, resulting in an imbalance in ground temperature. Zeng et al. (2011) showed that the temperature rise that occurred in clay was two times greater than that occurring in sand and sandstone as a result of more heat accumulation in clay due to its low thermal diffusivity. The radius of thermal impact for 10 d of continuous operation reached up to 2.5 m, 2.0 m, and 3.2 m in sand ($\boldsymbol{\lambda}$ = 1.13 W/m·K), clay (1.62 W/m·K), and sandstone (2.84 W/m·K), respectively. This can lead to a substantial deviation in estimating the performance of multi-boreholes when considering the thermal interference effects occurring between buried pipes. This is especially important for a practical engineering design operating under the long-term conditions. Temperature response in the overburden soil was highly affected by seasonal air temperature; this layer exhibited a temperature change of between 270 K and 275 K at the far-field, extending out approximately 18 m from the borehole. The ground temperature at the far-field changed slightly in layer 2 and layer 3, reaching ambient temperatures of 275 K and 284 K, respectively.

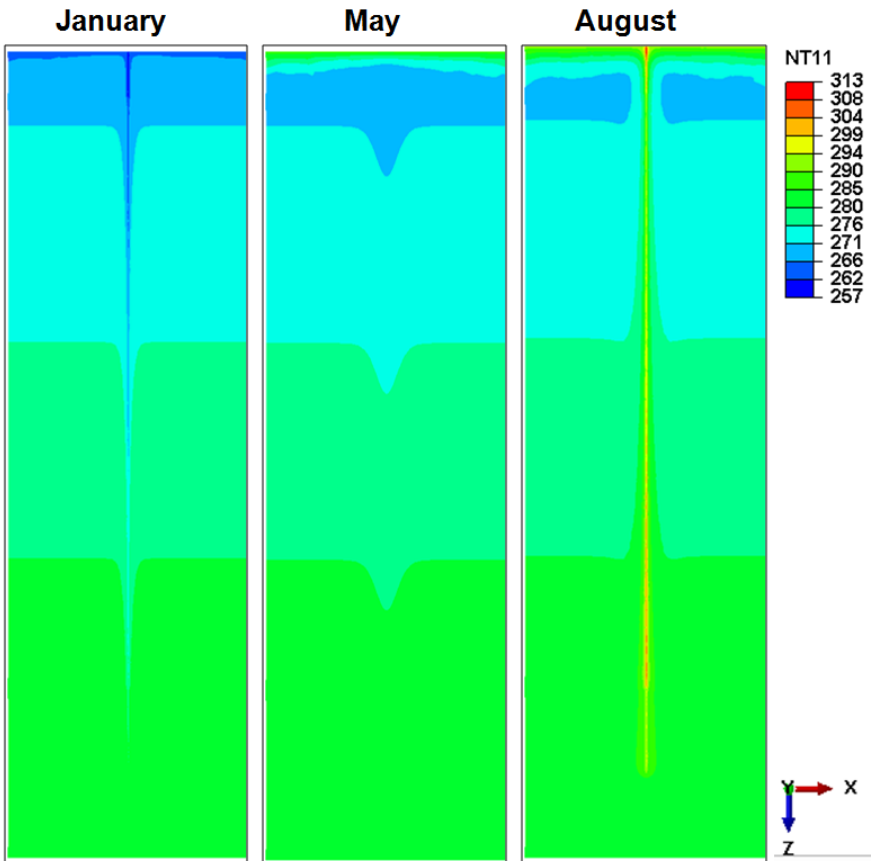

Figure 3.5 Cross-section view of temperature distribution in and around the borehole after one month heating (January), non-operational (May), and cooling (August) period

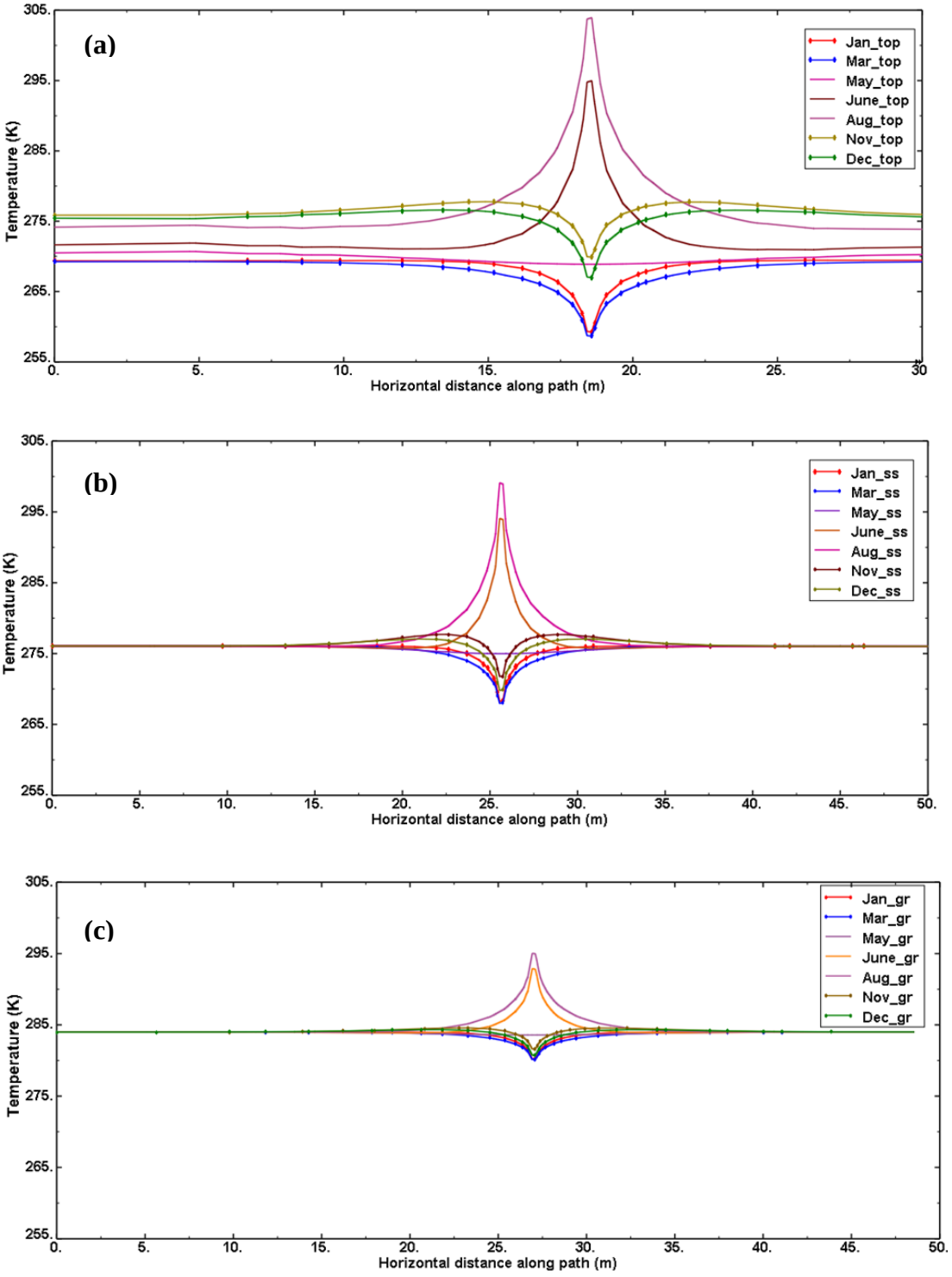

Figure 3.6 Temperature profile (after 1 year) at depth of 10 m in top overburden layer (a), at 125 m in mid layer (b), at 280 m in bottom layer (c)

3.3 COMPUTATIONAL FLUID DYNAMICS (CFD)

ANSYS Fluent 14.5 (a popular CFD software package) provides numerical solutions for the fluid flow and heat transfer processes involved in heat exchanger. Fluent 14.5 packages include sophisticated user interfaces for inputting problem parameters and examining the results (Bansal et al. 2010). There are three main elements in CFD codes in Fluent: (i) a pre-processor, (ii) a solver, and (iii) a post-processor. Pre-processing consists of entering the inputs of a flow problem into a CFD program by defining the geometry of the region of interest: the computational domain, grid generation—the subdivision of the domain into a number of smaller, non-overlapping, sub-domains: a grid (or mesh) of cells (or control volumes or elements) —selection of the physical and chemical phenomena to be modeled, definition of fluid properties, and specification of boundary conditions at cells which coincide with or touch the domain boundary. The Fluent solver is based on a finite-volume method for discretizing the governing equations into solvable algebraic equations. A post-processor is used for the analysis and visualization of the resulting solution.

3.3.1 Discretization Method Using Finite Volume Method (FVM)

The finite volume method (FVM) is commonly used in CFD codes as the FVM guaranties the conservation of variables for incompressible flow, with an advantage in memory usage and solution speed, especially for complex problems such as those involving turbulent flow (i.e., high Re) (Bakker 2002). The solution domain is subdivided into a finite number of small control volumes (cells) by grids (see Fig. 3.7), and conservation equations are applied to each control volume to obtain an algebraic equation for each control volume. The FVM is not limited by grid type (structured or unstructured, Cartesian or body-fitted) as is the FD method, so FVM is suitable for complex geometries such as inside the borehole (fluid, pipe, grout etc.). The grids define the boundaries of the control volumes while the computational nodes imply the center of the control volumes. These control volumes are called "cells" P, and for which the fluid-

property values are regarded as representative of the whole cell. The cell is surrounded by neighboring nodes, which are designated by N, S, E, W, B and T.

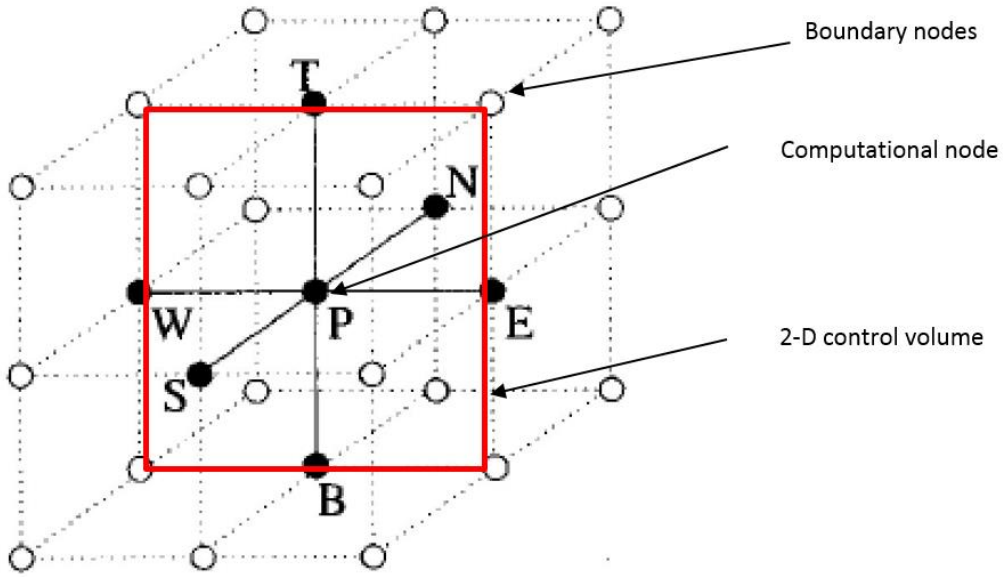

Figure 3.7 3-D Representation of a control volume (modified from Mohammadi and Jazayeri 2012)

Finite volume equations are derived via the integration of the governing equations (typically the Navier-Stokes equations (Eq. 2.12), the mass and energy conservation equations (Eq. 2.13), and the turbulence equations) over finite control volumes that, when taken together, fully cover the domain of interest (Fig. 3.7). The finite volume equation yields a governing equation in the form of

$$\frac{\partial}{\partial t}\iiint \mathrm{QdV} + \iint \mathrm{FdA} = 0 \qquad \text{Eq. 3.9}$$

where Q is the vector of conserved variables, V is the volume of the control volume element, and A is the surface area of the control volume element. F is the vector of fluxes (such as those from the Navier-Stokes equations that describe the Newtonian fluid flow (Ferziger and Peric 2002) as

$$\rho\left(\frac{\partial v}{\partial t} + v.\nabla v\right) = \mu\nabla^2 v - \nabla p + f \qquad \text{Eq. 3.10}$$

where f represents "other" body forces (forces per unit volume), such as gravity or centrifugal force. The shear stress term is $\mu\nabla^2 v$ (∇^2 is the Laplacian term) when a fluid is assumed to be incompressible, homogeneous, and Newtonian, where μ is the (constant) dynamic viscosity. The net flux through the control volume boundary is the sum of integrals over the six control-volume faces (four in 2D).

3.3.2 Three-Dimensional Ground Heat Exchanger Model for Short Term Application

The objective of this section is to model dynamic fluid conditions in the GHX system using CFD to define the impact of fluid circulating through geothermal heat exchange pipes on the heat transfer in the nearby composite layer (e.g., pipe, grout) within the borehole and the surrounding ground. We replicated a recent study done by Erol and Francois (2014) due to the fact that the study presented a strong agreement in both numerical and analytical method predictions, and they were experimentally validated as well. Here, the results from CFD were validated with reference study. Applicability of CFD to heat transfer process within GHX and surrounding medium were evaluated in terms of CFD's computational time and effort.

Model development

A 3D model for the small scale thermal response test (TRT) sandbox experiment conducted by Erol and Francois (2014) was computationally replicated using CFD-Fluent. In the sandbox experiment, a borehole with a diameter of 0.135 m was operated with two heat pumps to circulate water with a constant temperature of 12 ^{o}C for the inlet flow and 15 ^{o}C for the outlet flow. However, in a real TRT, the water circulates through a 100- to 200-m-long geothermal heat exchange pipe to have a temperature difference (ΔT) between the inlet and outlet flows. Since our experimental set up had a 1-m pipe in 1-m^3 soil, the fluid temperatures in the two pipes were controlled separately to have the desirable temperature difference (ΔT = 2 K). The numerical model domain was set according to the sandbox size (interior dimensions 1 m x 1 m x 1 m). The borehole, grout, pipe and fluid were also modeled explicitly with the same dimensions as the experimental setup. The model domain was discretized into tetrahedron finite-volume cells and fine cells

were placed where greater temperature gradients were expected, e.g. close to the borehole wall, and less cells where temperature gradients are smaller, e.g. far from the borehole (Fig. 3.8). A constant temperature of 20 ^{o}C was applied to each side of the box. Inlet (12 ^{o}C) and outlet (15 ^{o}C) flow temperatures were set according to the sandbox experiment as well. The thermal properties of the model domains and the boundary conditions used in this simulation are listed in Table 3.3. The soil was assumed to be an isotropic-homogenous medium where all thermo-physical properties are the same throughout and the fluid flowing through the ground heat exchanger pipe was incompressible that the density of fluid does not change with temperature. The outer size of the pipe was 0.032 m, and the mass flow rate was set to $3.66e10^{-4}$ m^3/s, which allows for turbulent flow using the Reynolds number (1.1×10^4).

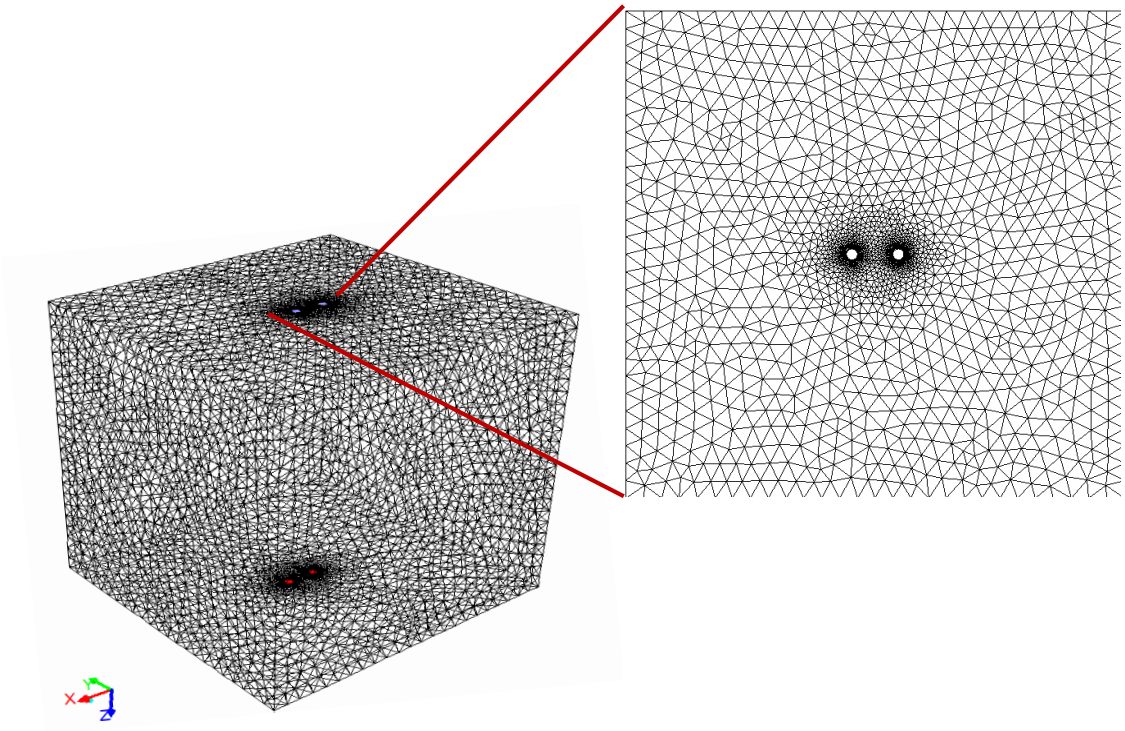

Figure 3. 8 3-D model geometry with tetrahedron mesh

Table 3.3 Model parameters and boundary conditions used in simulation.

Thermo-physical properties			
Borehole components	λ [$W \cdot m^{-1} \cdot K^{-1}$]	c_p [$J \cdot kg^{-1} \cdot K^{-1}$]	ρ [$kg \cdot m^3$]
Pipe	0.42	2170	960
Fluid	0.59	4185	1000
Grout (silica sand)	2.3	820	1800
Dry sand	0.35	830	1500
Boundary Conditions			
Fluid inlet temperature, T_{in}		283 K	
Fluid outlet temperature, T_{out}		288 K	
Model side temperature, T_{wall}		293 K	
Time step, Δt		1800 s	
Total time, t		50 h	
Mass flow rate, $\dot{m}$		0.366 $kg \cdot s^{-1}$	
Reynolds number		~11900	

Results and Discussions

Model validation

A minimum suggested time period of a TRT, 50 hours (Austin et al. 2000, Gehlin 2002), was used to estimate the temperature distribution over time at the borehole wall (x = 0 m, y = 0.135 m and z = 0.5 m). After a number of sensitivity analyses in terms of mesh and time-steps, were performed, we determined that 20 min (1800 s) was the time step (Δt) at which the temperature response no longer changed. The simulation results from our 3D model strongly agree with the experimental and numerical values from Erol and Francois (2014; Fig. 3.9). On the other hand, the numerical and analytical results somewhat varied from their experimental results. One potential reason for this difference might be the limitation of boundary

conditions that we could not factor in, such as the influence of varying room temperatures, ranging from 19.8 ^{o}C to 21.6 ^{o}C, as measured in the study (Erol and Francois 2014). Fig. 3.10 shows the cross section temperature contours around the heat exchange pipes and in the surrounding soil at the end of total simulation time (50 h). As expected, the temperature distributions directly around the borehole were unevenly spread due to the thermal interaction among the pipe legs, while the temperature contours more distant from the borehole had an even circular distribution. (Fig. 3.10a). Temperature distribution along the fluid flow inside the pipes did not change as expected (Fig. 3.10b), likely due to the small length (1 m) between the pipe inlet and outlet flows and high Reynold's number. However, the thermal impact in nearby layers (pipe, grout and ground) was well-defined and had consistent temperature decay through the ground (Fig. 3.10c).

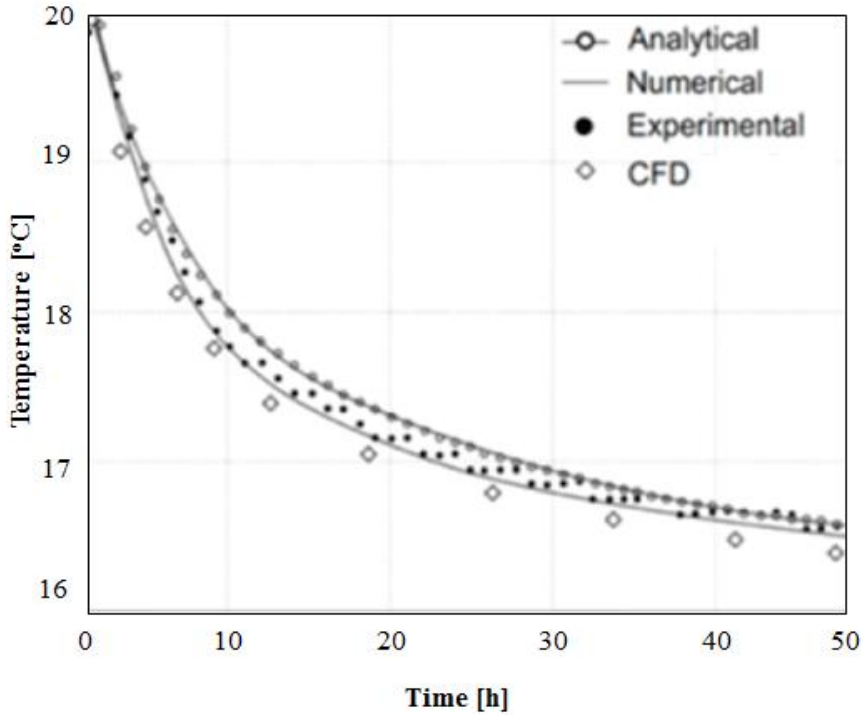

Figure 3.9 (a) Comparison of temperature profile between the results obtained with the CFD 3D model and previous work (Erol and Francois 2014)

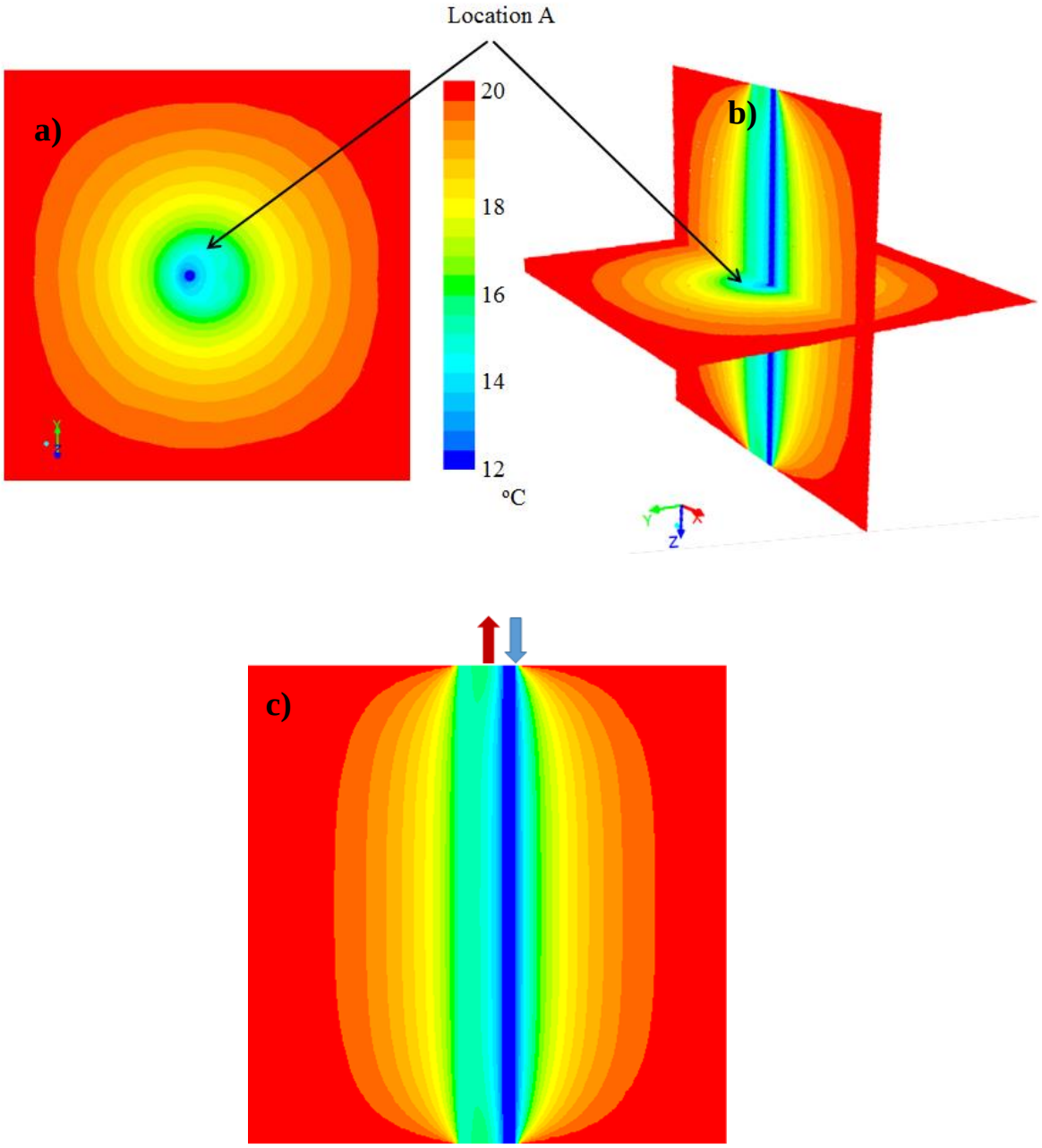

Figure 3.10 Temperature contours around the GHXs. (a) Plane view of temperature contours around the borehole, (b) Vertical and horizontal plane view of temperature contours, and (c) close vertical plane view of b

Simplification of 3D Model into 2D Model

We found that our model of 3D-transient, fluid-coupled heat transfer GHXs with turbulent flow required high computational effort (> 72 h with a 4 GB Intel Core2 6400 @ 2.13 GHz PC), even for short-term (50 h) operation. This shows that modeling for exact GHXs (~length of 100 m or >) may not be feasible in terms of computational time and high aspect ratio between the borehole and surrounding ground.

We developed a 2D model equivalent to the 3D model of one meter depth and adiabatic top and bottom surfaces to compare the differences between model predictions due to 3D effects and dynamic fluid transport. Although 2D simulation necessitates more simplifications as opposed to existing 3D numerical and analytical solution methods, 2D modeling can provide more comparable results with highly accurate analytical solutions, using various borehole configurations and thermal properties along with less computational time and mesh efforts. One important assumption in modeling 2D geometry is the boundary condition that the fluid flow is not explicitly modeled; rather, the fluid in the pipe is set as a constant temperature boundary at inner side of the pipe at the inlet and at the outlet. The modelling input parameters, geometry and boundary conditions were similar to those used in the previous section (Table 3.3). Temperature responses predicted by both 2D and 3D modeling in the y direction from the center of the borehole to edge of sandbox (x = 0 m, y = 0.5 m) reveal a strong agreement between both models (Fig. 3.11). A sudden change occurred at 0.07 m due to a change of thermal condition from the grout to the surrounding ground. After that point, the temperature started increasing faster due to high thermal conductivity of the ground. Between the 2D and 3D models, the temperature gradients inside the borehole were slightly different due to dynamic fluid condition in the 3D model (Fig. 3.12). This discrepancy might be an issue for short term-GHX cycles when monitoring fluid temperature; however, in most cases, that detail can be negligible for long term GHX operation. Nevertheless, the temperature gradients outside the borehole, where most questions arise, were identical between 2D and 3D modeling (Fig. 3.12).

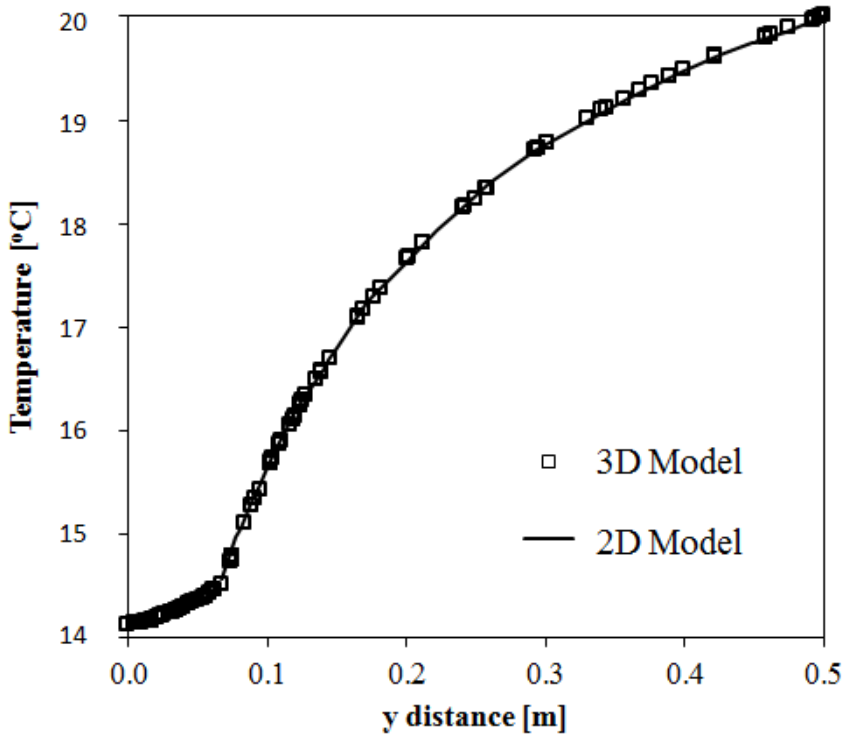

Figure 3.11 Comparison of the results obtained from 2D model (x = 0, y = 1) and 3D model (x = 0, y = 1, z = 0).

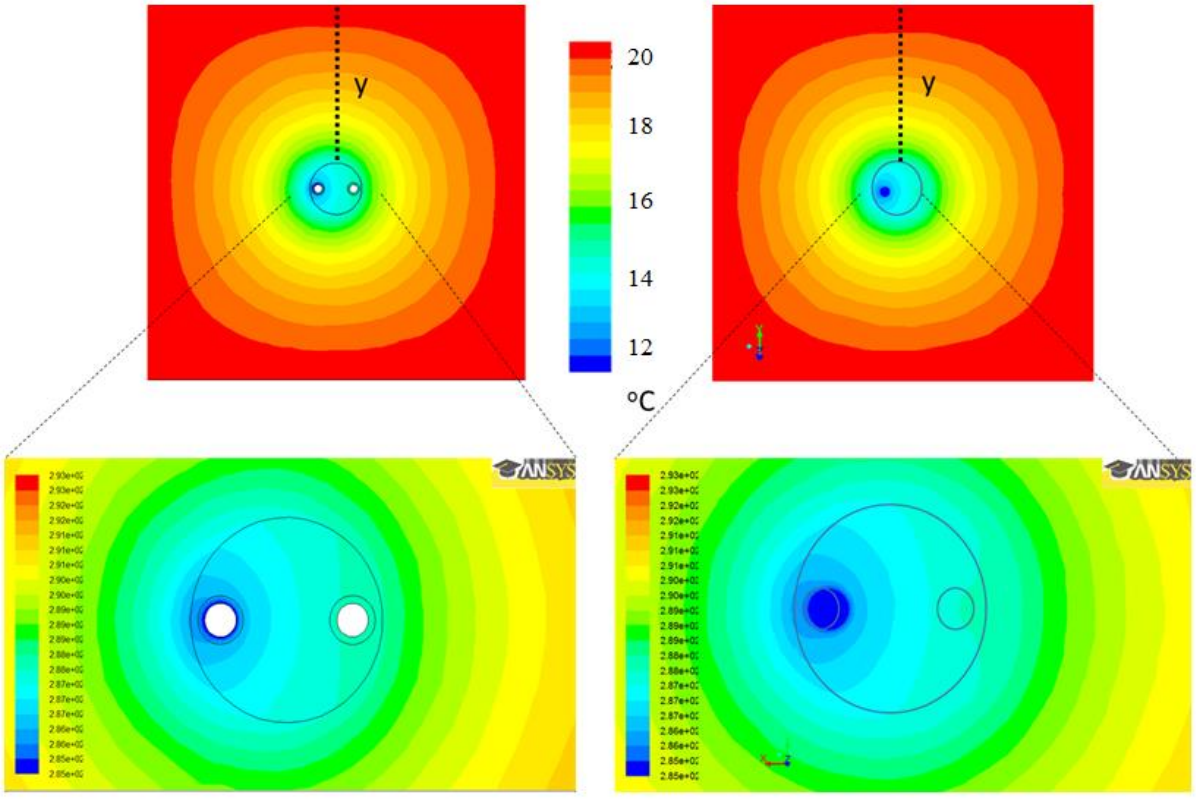

Figure 3.12 Temperature contours around the boreholes in 2D model (left) and 3D model (right)

Thermal Impact of Grout on Heat Transfer

Several recent studies have sought to solicit the most important resistant parameter in GHXs. Zeng et al. (2003) showed that the most important factor affecting borehole thermal resistance is the thermal properties of grout. Grout material with poor thermal conductivity increases the borehole thermal resistance significantly (Hellstrom 1998), and improving the grouting material with addition of graphite powder results in remarkable increases of heat exchange rate (Delaleux et al. 2012). However, several mechanical and thermo-physical tests to evaluate two widely used commercial grouting materials revealed that the thermal conductivity of grout does not significantly impact the heat exchange rate when the thermo-physical properties of the surrounding ground is low (ʎ= 0.35 W/m·K; Erol and Francois 2014). The objective here is to determine how the grouting materials drive the heat exchange rate in the borehole with various soil conductivities and how grout materials may change the duration of recovery period after 50 h TRT tests. Finally, to address whether different soil types can alter heat transfer in a borefield, we investigated the effect of various thermal ground conductivities and their impact on the heat transfer rate of the borehole.

First, to test how different grouting materials can alter the heat exchange rate in the borehole, we examined the effect of two different commercial products that have been commonly used as backfilling material (Erol and Francois 2014) in our 2D model. The first grout material was bentonite based (0.95 W/m·K) and the other was thermally enhanced with synthetic graphite (W/m·K). Those two grout materials were chosen for their relatively high difference in thermal conductivity. For the boundary conditions, entering and leaving fluid temperatures 52 ^{o}C (325 K) and 50 ^{o}C (323 K) based on a cooling- dominate system were used. Furthermore, the model used a typical Wisconsin GHX borehole (0.15 m diameter) and pipe size (OD 0.61 cm, ID 0.51). The underground temperature was initialized to 283 K, as typical for Wisconsin ground (WGNHS 2013). The boundary of the surrounding ground was carefully defined as x = y = 10 m to avoid boundary effects at the edge of the model domain. The time step for the simulation was selected as $\Delta t = 1200$ s for a total simulation time of 50 h and the thermo-physical properties of the borehole components used in this simulation are shown in Table 3.4.

Table 3.4 Model parameters and boundary conditions used in this simulation.

Borehole Components	**Thermal C. [$W \cdot m^{-1} \cdot K^{-1}$]**	**Specific heat [$J \cdot kg^{-1} \cdot K^{-1}$]**	**Density [$kg \cdot m^{-3}$]**
fluid	0.63	4182	1000
pipe	0.42	950	2300
grout	0.95 to 2.5	820	1750
ground	**1 to 4**	800	2630

When we applied our 2D model to examine the two common commercial grout types, we found that a borehole with low thermal grout has a steeper temperature gradient than the one which uses a high thermal grout, which implies the magnitude of heat exchange rate as seen in Fig. 3.13 and Fig. 3.14. In both cases, thermal interaction between the pipe legs was observed. The temperature profile and the integrated heat flux (W/m^2) at the borehole wall (x = 0 m, y = 0.075 m) over time are shown in Fig. 3.15. During the operation cycle, a borehole filled with thermally enhanced grout had a 20% temperature rise and a corresponding 36% increase in heat flux in comparison to borehole with low-conductive grout. The differences are enhanced in the first hours of operation due to high temperature differences between the fluid and surrounding layers and the heat transfer was controlled by the thermal properties of the fluid, pipe, and grout. As the operation continues, the temperature rise and the corresponding heat flux stabilized. The temperature recovery at the borehole wall was faster with high-conductive grout than with low conductive grout directly after the operation was turned off. Some temperature deficiency (1 K) continued after the first 10 h of recovery time. Principally, the recovery period equals the operation period (Rybach and Eugster 2010). However, our simulation results show the ground temperature is not simply recovered he

initial ground temperature for 50 h after turning off the system. This temperature rise/or drop, depending on the cycle of GCHP operation, is termed a “temperature penalty” (Kavanaugh 1997, Berner 2008). Details about the ground temperature penalty and the ground temperature change over long-time operations are discussed in Chapter 3.3.3.

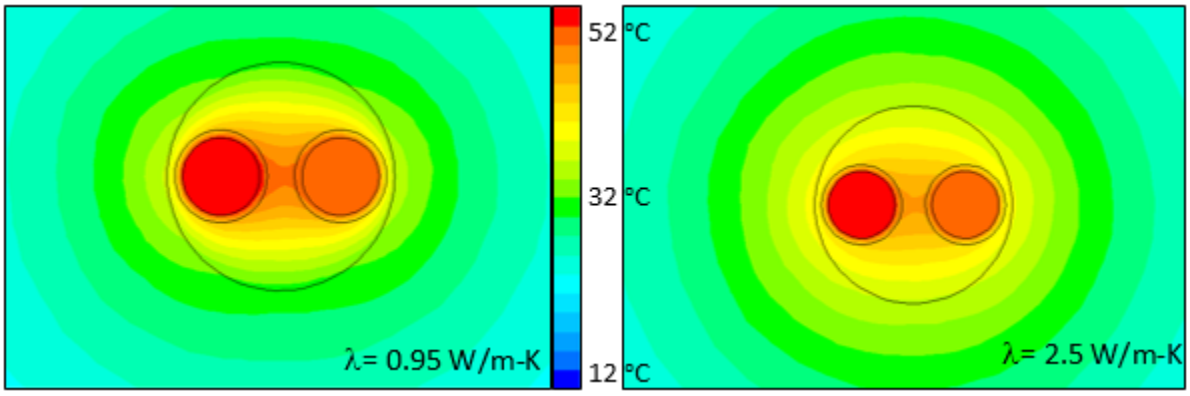

Figure 3.13 Temperature contours in borehole and surrounding geological unit during 50 h operation.

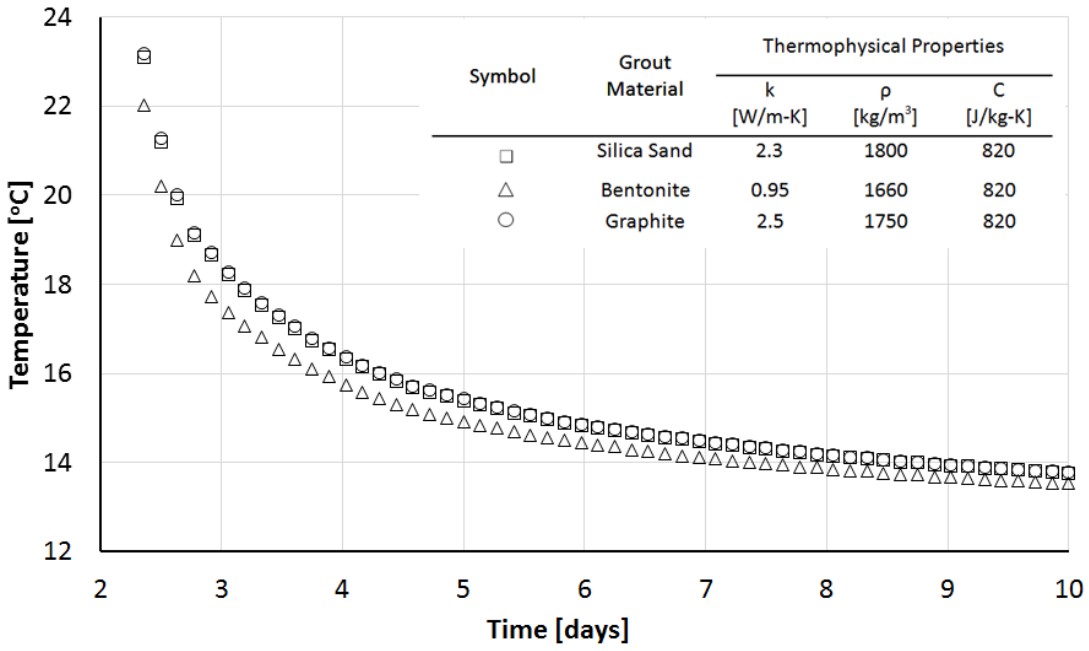

Figure 3.14 Comparison of temperature at the center of circulating fluid with various grouts

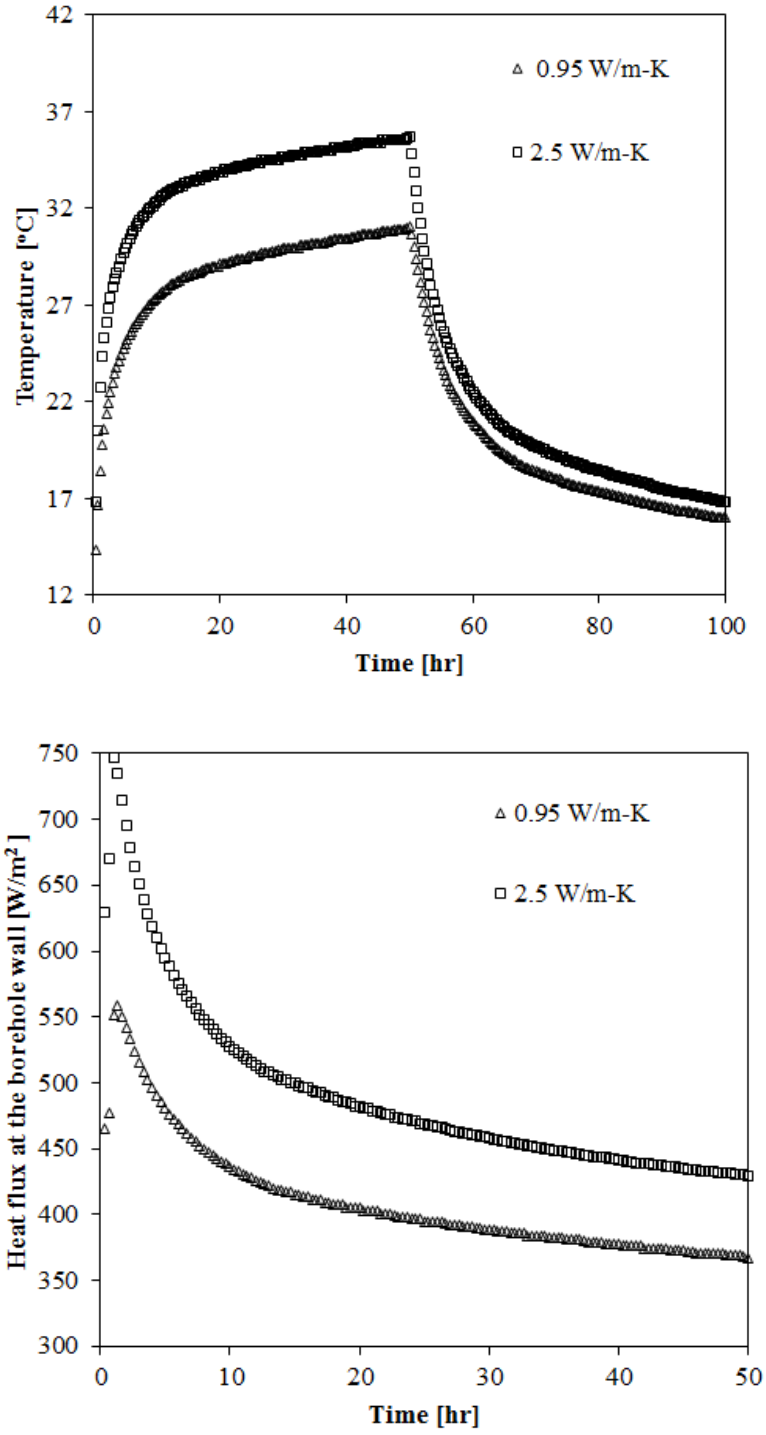

Figure 3.15 Temperature at the borehole wall (x = 0, y = 0.075) during operation (first 50 h) and nonoperation period (+50 h) (upper panel) and integrated heat flux at the borehole wall as a function of time and for various values of grout thermal conductivity (bottom panel)

Thermal Impact of Ground on Heat Transfer

The ground is normally assumed to be homogenous in TRT analyses and with energy building design tools. However, the ground is actually stratified along the borehole depth with layers of different geological materials and hydrogeological conditions such as unconsolidated soils (sand, gravel, clay) and rock. The effect of the ground heterogeneity on the GHXs and the TRT has been understudied by most modelers and remains unclear. To determine whether different soil/ground types (from 1 W/m·K to 4 W/m·K) can alter temperature dynamics of a borefield, we modeled the temperature contours around the borehole with a thermally enhanced grout t (2.5 W/m·K; Fig. 3.16). We found that with increased thermal conductivity, temperature from the fluid spreads more, resulting in much cooler temperatures (Fig. 3.17). Conversely, when the borehole was surrounded by low-conductivity, grout temperatures would build-up inside the borehole. Likewise, a highly conductive ground (4 W/m·K) had 30% less temperature build-up than the borehole with a low-conductive ground (1 W/m·K) over time at the borehole wall, indicating a more efficient heat transport rate (W/m) between the fluid and the surrounding ground.

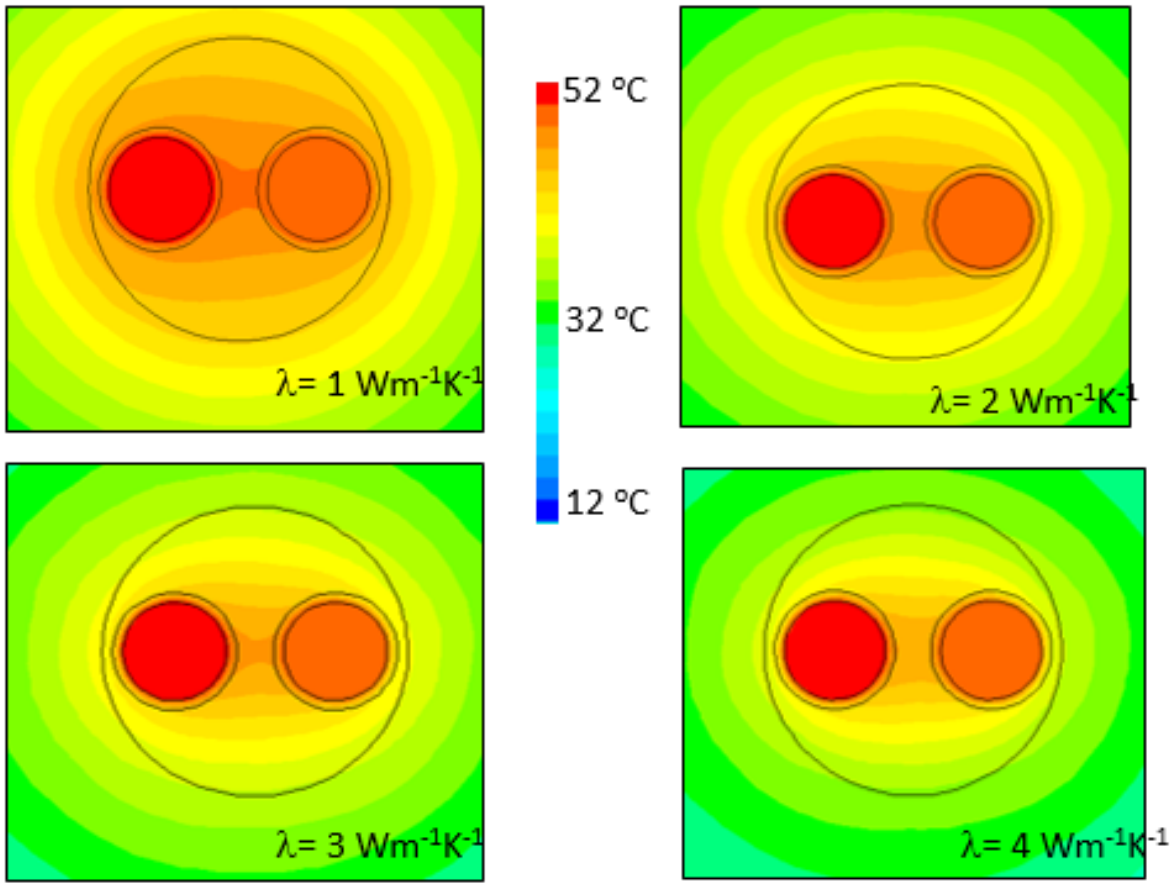

Figure 3.16 Temperature contours in borehole and surrounding geological unit during 50 h operation for different surrounding ground with thermal conductivity values of 1 to 4 W/m·K

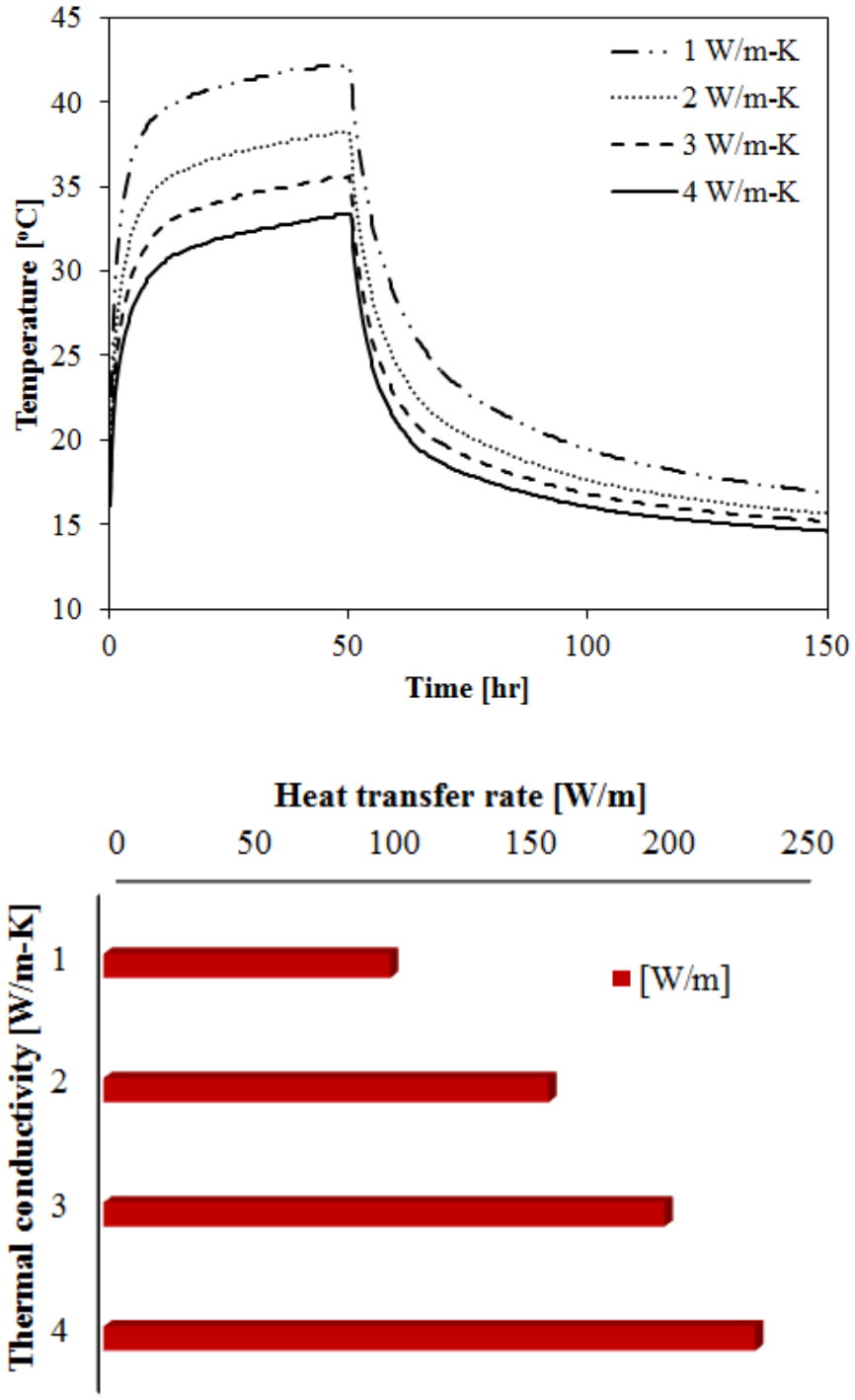

Figure 3.17 Temperature profile at the borehole wall during operation (first 50 h) and non-operation (+ 50 h, upper panel), and total heat transfer rate for various value of ground thermal conductivity (lower panel)

3.4 EVALUATION OF PERFORMANCE AND SUSTAINABILITY OF DISTRICT-SCALE GROUND COUPLED HEAT PUMP SYSTEMS

This paper is submitted to *Geothermics* in December 2015.

Abstract: Ground heat exchangers (GHXs) are used to condition (heating and cooling) interior spaces and work best in the long-term if they achieve a balance between the heat extracted from the ground and the heat rejected into the ground. Such a balance becomes especially important to sustaining the long-term efficiency of district-scale, ground-coupled heat pump systems (GCHPs). Computer simulations can facilitate the process of designing these systems and analyzing their long-term sustainability. Most of the studies undertaken and assumptions used to develop these tools have ignored the dynamic changes in ground temperature resulting from heating and cooling cycles; rather, these models generally assume a constant ambient ground temperature throughout the years of operation. This assumption ignores the effective temperature increases and decreases that occur in the ground over the course of each heating and cooling cycle, regardless of the system's purpose (cooling-dominant or heating-dominant). This study examines the efficacy of an ongoing, district-scale geothermal borefield under operation in the upper Midwest by modeling the borefield's temperature response to varying average monthly heating and cooling loads. The presented approach considered the borefield's interaction with the surrounding ground formation, which occurs through transient thermal conduction coupled with advective heat transfer from groundwater flow. A significant positive impact—up to 50% less temperature rise in the ground—was found by accounting for groundwater flow. Also, the presented study evaluated the system's performance by modeling a single borehole and estimating the coefficient of performance (COP) of the heat pump based on the temperature of fluid entering the heat pump (EFT). The results show that, absent appropriate mitigation strategies, overheating problems in the ground occur even in the first few years of GCHP operation. To balance the energy inputs/outputs to the ground, an operating scheme utilizing cold-water circulation during the off-season was evaluated. Under the simulated conditions, the energy imbalance was

fully recovered; thus, the proposed mitigation strategy may be a viable measure to sustain the operating efficiency of district-scale borefields over the long-term.

3.4.1 Introduction

Worldwide, space heating and cooling accounts for 48% of all energy use and, in the US that figure jumps to 66% when water heating is included (EIA 2009). Although the de facto approach is to burn fossil fuels such as natural gas and propane for space heating, these fossil-based options contribute directly to global warming. Ground-coupled heat pump (GCHP) systems use the thermal energy stored in the Earth and can be applied nearly anywhere to create an environmentally friendly, operationally low-cost and sustainable source for heating and cooling. If the US employed and incentivized well-designed and operated geothermal systems to a greater degree, the demand for imported energy would decrease and regional economic development would be stimulated because these systems are designed, drilled, manufactured, and installed using domestic resources and talent. Using a GCHP system reduces GHG emissions by 44% in comparison to a conventional air-source heat pump, up to 72% in comparison to electric resistance heating, and almost 40% in CO_2 emissions compared to a conventional gas boiler (Jenkins et al. 2009, EPA 2013). For every 100,000 homes with GSHP systems, an equivalent reduction in oil consumption of 2.15 million barrels per year would be achieved (EPA 1993). Large scale GCHPs (>50 kWh), have an enormous opportunity for energy and carbon savings; however, the balanced dissipation of energy from a borefield remains a primary challenge. Thus, if large borefields were to prove successful and economical, then GCHPs could well become the preferred method for heating and cooling large-scale facilities.

Ground Coupled Heat Pump Systems (GCHPs)

Vertical GCHPs are low-enthalpy systems that take advantage of a relatively constant subsurface temperature, which is higher than the ambient air temperature in the winter and lower in the summer, thus improving the mechanical efficiency of heat pumps used for space heating and cooling. This relatively constant temperature range within the near subsurface results from homeostatic heat flux, the rise and fall

of the heat radiating from above (the sun) and the heat emanating below (radioactive decay within the earth's interior). In the shallow subsurface (<10 m deep), the temperature fluctuates due to atmospheric interaction. At a greater depth (>50 m), the temperature approaches that of the natural geothermal gradient (Grant et al. 1982, Ozdogan-Dolcek et al. 2014). Thus, a GCHP can be applied anywhere, even in areas with low geothermal gradient (ASHRAE 2007).

GCHP systems typically include ground heat exchangers (GHXs) that have a sealed loop made of a high-density, polyethylene (HDPE) U-pipe that is buried in the ground and connected to a heat pump though which a carrier fluid is circulated. GCHPs, and the models used to design them, were originally intended for residential interiors rather than large buildings; consequently, special care must be taken when designing a system for a large commercial building (Kavanaugh, 1995). Because of the much larger number of boreholes required in commercial applications, the thermal interactions occurring between boreholes must be considered. In the US, it is suggested that space between the GHX and borehole be grouted to provide better thermal contact between the pipe and the surrounding soil/rock and also to prevent groundwater cross-contamination of the aquifer. Typical borehole depth is between 40 m and 150 m and has a diameter of 0.075 m to 0.15 m (Diao et al. 2004). The carrier fluid is circulated in a closed-loop system to deliver relatively warm (or cool) fluid to heat pumps and, in this way, regulates the interior temperature of the building.

Overview of GCHP Modeling Approaches

Although a significant number of analytical, numerical and hybrid models exist, only those most relevant to the design and performance evaluation of large-scale geothermal systems are reviewed here. Methods, in general, are created for two main purposes: (i) to determine the total length of ground loop needed and (ii) to evaluate long-term system performance. Some of the more noteworthy models are based on a combination of analytical and numerical solutions. Eskilson (1987) developed a g-function (non-dimensional parameter) model using a normalized step-response function that defines the relationship between the average borehole temperature and a step in the heat extraction/or rejection for pre-defined

borehole geometry. To determine a single GHX's temperature response to a unit step heat pulse, a two-dimensional finite-difference model was used. Subsequently, the temperature response of pre-defined configuration of multiple GHXs to the unit step heat pulse was estimated by using the superposition technique. These temperature responses could then be normalized to the g-function. This approach is widely accepted and used to determine response over periods of time ranging from one month to several years.

In addition to refining the assumptions in the Eskilso's first model (1987), the subsequent study looked at the condition of the fluid circulating through the GHX system. That is, the long-term thermal performance of various borehole configurations was analyzed by considering the thermal processes in the ground and in the borehole, including hydraulic coupling, pumping rate, and loading conditions (Claesson and Eskilson 1987). By assuming an average borehole temperature and mean fluid temperature, these researchers were able to demonstrate that the efficiency of the GHX system is a function of the amount of heat extracted from/injected to the ground. Claesson and Eskilson (1987) showed that minimum and maximum temperatures may take several years to manifest, especially in a borefield that consists of multiple boreholes in close proximity to each other. The worst design-case condition, for example, might occur more than 10 years after installation. Therefore, a comprehensive investigation of an extended time period should be considered to effectively evaluate the system's performance (Kavanaugh 1995).

An international standard by ASHRE (2007) noted that an accurate evaluation of the performance of a GHX requires a long-term analysis. In such analyses, long-term ground temperature changes are considered using the concept of "temperature penalty," (T_p) a term that refers to the effective increase or decrease of the undisturbed ground temperature due to a GCHPs operation. Kavanaugh (1995) first described the evaluation of T_p based on the application of Kelvin's line-source approximation, which predicts radial temperatures for a line source of heat output or input in an infinite media without axial effects. For sizing the GHX of a 10x10 borefield under two different ground conditions, this method has been refined by Kavanaugh and Rafferty (1997) and subsequently accepted as one of ASHRAE's standard

methods (ASHRAE 2003). As mentioned above, Eskilson (1987) calculated the dimensionless response (g-function) of a borefield, but not T_p directly. Bernier et al. (2008) presented the updated T_p values by rearranging Eskilson's g-function method to account for ground temperature imbalance over a long-term period.

Importance of Subsurface Geology for the GCHP Design

The geology of a GHX field plays an important role in the effective design and management of the field. The loop design must account for how heat is transferred in the geology (Busby et al. 2009, ASHRAE 2011, Spitler 2005). A field with closely spaced loops will ultimately lose efficiency when the heat from neighboring loops reduces the heat flow from a loop. An undersized field, one potentially resulting from an overestimation of the thermal conductivity of the geology, will cause long-term inefficiencies. Alternatively, an oversized field, one resulting from an underestimation of the thermal conductivity of the geology, might operate efficiently but would incur unnecessarily large upfront costs (ASHRAE 2011) and thus limit an otherwise successful operation. Heat flow in a GHX field is also controlled by the hydrogeology of the field (Dehkordi and Schincariol 2013, Diao et al. 2004, Hecht-Mendez et al. 2013). Saturated rock conducts heat better than unsaturated rock (Clauser and Huenges 1995, Horai and Simmons 1969, Meyer 2013, Zimmerman 1989). In addition, significant heat can be transported by groundwater flow.

Dehkordi and Schincariol (2013) evaluated a long-term performance of vertical GCHP systems and the effect that thermo-hydrogeological parameters on the system under consideration. By monitoring returning fluid temperature during a constant heat extraction (no seasonal thermal load), they simulated 25 years of operation. The results of this experiment indicated that the thermo-hydogeological parameters do impact the sustainability of the system. The undisturbed near-field and far-field ground temperature will either decrease or increase depending on the respective imbalance of the annual heating/cooling loads, and over a period of many years, this fluctuation will cause thermal imbalances; e.g., ground overheating due to a high amount of heat injection when the system is being used to cool the building. Such an imbalance

is especially likely to develop when the system relies on a large number of boreholes and predominantly when the system is used to cool commercial buildings like those operated by Epic Systems Corporation in Verona, WI, which is to date one of the largest GCHP installations in North America. A few studies focus on the operation of thermally imbalanced systems and potential ways to solve the problem. Zhou et al. (2014) presents a new operation mode that assesses the thermal imbalance problem in the ground by intermittently operating GHXs in summer at night with a cooling tower as the supplemental heat rejecter of the system. They demonstrated that coupling the operation of cooling tower with the GHXs during transition seasons could effectively resolve the temperature imbalance in the ground.

While GCHP systems have been widely studied and accepted as an alternative and sustainable energy source, possible performance deficiency such as overheating within the ground over the course of operation and impact that such overheating may have on the overall system is important to evaluate in terms of GCHPs' long-term sustainability. In this study, the efficiency of a GCHP, including its borehole components, is evaluated from the perspective of sustainability (of both the GCHP system and the ground in which the boreholes have been drilled), and the possible overheating problem is resolved through a different operation mode.

Study Area

Epic Systems Corporation operates a district-scale, cooling-dominated, low-enthalpy geothermal exchange (GHX) system to heat and cool the buildings on their 8,000-person campus in Verona, WI. The system has 25 km of underground piping; 12 ML of closed-loop, circulating water; 3,570 in-service geothermal wells (100–160 m in depth); and a capacity of 25.3 MW (7,200 tons)—enough energy to heat 2,500 homes. With an additional 2,500 wells coming into service, the goal is for the campus to be energy neutral between contributions from their solar fields, wind turbines, and GHX fields. The Epic geothermal system has grown from its original 564 boreholes in 2006 to more than 3,500 in 2013 (see Fig. 3.18) and is operated at a significant energy saving (Brandherm 2013).

The aforementioned field site in this study is well suited to investigating the role of geology and hydrogeology in controlling heat flow in a large GHX field. Located in the upper midwest, the exchange field has significant variations in geology and hydrogeology with depth (Krohelski et al. 2000). Fig. 3.19 shows the different lithologies at the site, some images of the rock in one of the boreholes, and the ranges of the thermal properties (Kavanaugh 1997, Meyer 2013, Walker et al. 2014) of the different formations. The lithologies vary significantly, even between different sandstone layers. The geology at the site consists of fill and glacial sediment over alternating layers of dolomite and sandstone underlain by shale. The bottom of the GHX loops sometimes encounter shale, depending on the surface elevation. According to several studies, the different lithologies should have different thermal properties (Clauser and Huenges 2009, Horai and Simmons 1969, Meyer 2013). Fig. 3.19 shows also a geophysical log from a boring on the site. The log illustrates the variability of the rock formations at this site. The upper rock (Prairie du Chien dolomite) is highly fractured, as shown by the variability of the caliper log. As shown in the gamma log, the Tunnel City sandstone has a mineralogy that differs significantly from that of the Wonewoc sandstone. The increased gamma signature of the Tunnel City formation is due to more clay and feldspathic cements than those found in the Wonewoc sandstone. The clay and feldspathic cements can be expected to lower the thermal conductivity of the rock when compared to the clean quartzite sandstone of the Wonewoc formation. The temperature in the boring shows a minimum at 50 m and a slightly increasing thermal gradient below that depth. The hydrogeology of the site is expected to play a role in heat transport by advection. Based on a regional groundwater flow model (Bradbury et al. 2013), there are two separate aquifers. In the shallow aquifer, groundwater flows westerly towards the Sugar River (listed as an exceptional waterway of Wisconsin) in the rock above the Tunnel City sandstone. In the deep aquifer groundwater flows east towards a municipal well in the rock below the Tunnel City sandstone. The hydraulic properties of the different formations can affect heat advection. Rocks with high hydraulic gradients and conductivities will transport more heat than those with lower gradients and conductivities. Therefore, for example, within the Wonewoc

sandstone one can expect the heat flux due to groundwater flow to be higher than that of the Eau Claire shale (Bradbury et al. 2013)

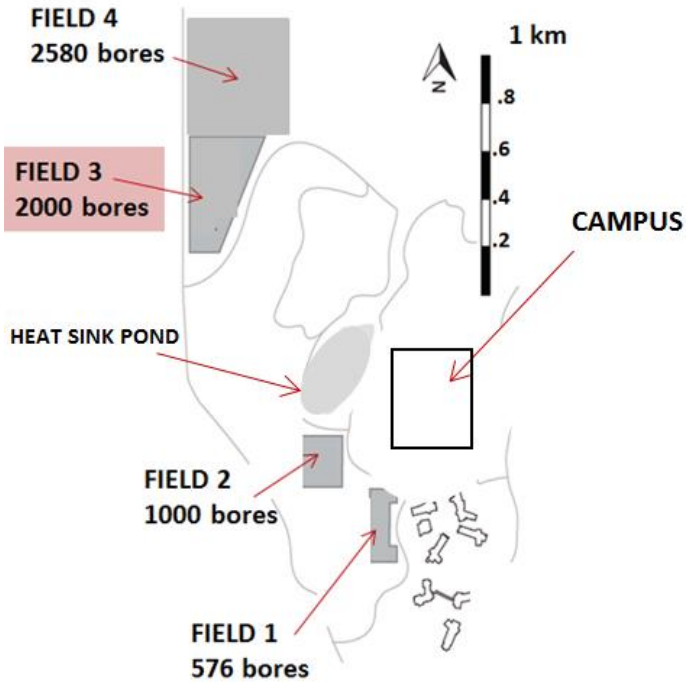

Figure 3. 18 District-scale geothermal heat exchange fields relative to Campus site

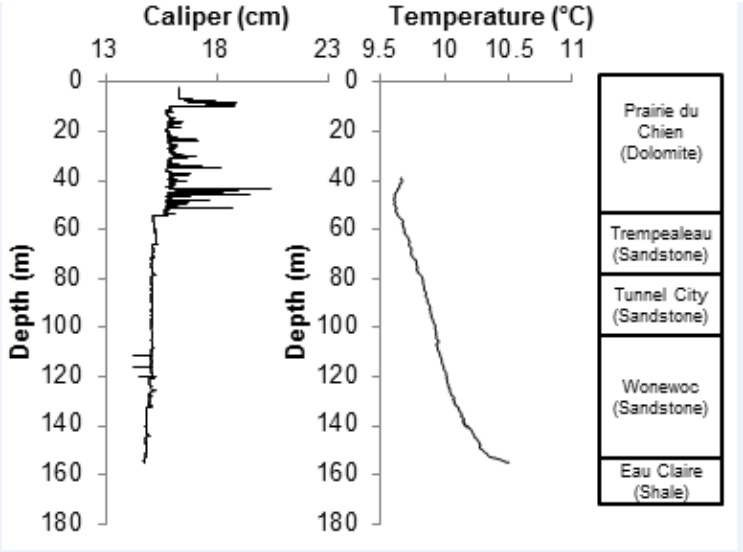

Figure 3.19. Caliper and Temperature logs with interpreted geology at the geothermal field. Caliper shows marked change in the rock quality across the formational divide between the Prairie du Chien group and the Trempelau group.

3.4.2 Model Development and Setup

Modeling was performed using computational fluid dynamics (CFD) implemented with the finite-volume method, which is well-known to be a useful technique for solving heat and mass transport through porous media (Choi and Kulacki 1992 & 1993, ANSYS 2014). CFD codes are structured around numerical algorithms that can tackle fluid-flow problems, which are governed by the momentum equation. Also, the momentum equation is supplemented by the continuity equation and the energy equation so that the model will be able to solve the conjugate heat and mass transport problem; this refers to the ability to compute conduction of heat through solids, coupled with convective heat transfer in composite porous media and solid layers. The solver uses a finite-volume method for discretizing the partial differential governing equations into solvable algebraic equations. As the most representative condition, the ground's thermal response to the heat loads applied by a GHX system can be expressed using a three dimensional time-dependent energy equation, including conduction and advection due to groundwater flow in porous medium as follows

$$n\rho_f c_f \frac{\partial T}{\partial t} + (1-n)\rho_s c_s \frac{\partial T_s}{\partial t} + \nabla.\left(v\left(\rho_f c_f\right)\right) = \nabla.\left(\lambda_{eff}\nabla T\right) + S \qquad \text{Eq. 3.11}$$

where T is the temperature, n is the porosity of the medium, ρ is the density of the medium, c is the specific heat capacity, λ_{eff} is the effective thermal conductivity of the medium, ν is velocity vectors in the x-, y-, z-direction, S is the fluid enthalpy source term. The two terms of Eq. 3.11 on the left-hand side represent the transient term (in the soil and in the fluid) and the convective energy transfer due to groundwater flow, respectively. On the right-hand side of Eq. 3.11 are the heat flux due to conduction and volumetric heat source term within the solid, respectively. The effective thermal conductivity in the porous medium is calculated as the volume average of the fluid conductivity and the solid conductivity as

$$\lambda_{eff} = n\lambda_f + (1-n)\lambda_s \qquad \text{Eq. 3.12}$$

Assuming that the temperatures of the fluid and solid medium are the same (i.e., no net heat transport one phase to another); in other words, assuming that there is thermal equilibrium (Nield 2013), the first term on the left side of the heat transport equation can be expressed as

$$n\rho_f c_f \frac{\partial T}{\partial t} + (1-n)\rho_s c_s \frac{\partial T_s}{\partial t} = \rho_m c_m \frac{\partial T}{\partial t} \qquad \text{Eq. 3.13}$$

in which $\rho_m c_m$ refers the volumetric heat capacity of the porous medium.

The model domain is assumed as an isotropic and homogenous medium, and Darcy's flow conditions are assumed by considering the viscous resistance due to the permeability of the solid medium ($1/m^2$) but not the internal resistance (losses) due to high flow velocity. The thermal and hydrogeological parameters of the model domain are presented in Table 3.5. Note that the thermal properties of the model domain are defined based on the design specifications, and the hydrogeological properties are taken from the most current Dane county regional groundwater flow model (MEP Associates 2014, Parsen et al. 2014). For the purpose of verification, the groundwater coupled heat transfer CFD model is compared with the outcomes by MT3DMS, which is a widely used program for simulating solute transport in porous media (e.g. aquifer) and which has also been adapted for heat transport experiments in recent studies (Martin et al. 2001, Cathomen 2002, Hecht-Mendez et al. 2010,). More information concerning the comparison of CFD and MT3DMS results can be found in a study done by Ozdogan-Dolcek (2015).

Modeling a 2D District-Scale Borefield (Base Case)

Borefield 3, as shown in Fig. 3.18(b) consists of 2000 boreholes and was simulated using a distributed, volumetric heat source/sink method and the design heating and cooling loads to determine the ground's temperature response to a monthly step change in the heat load. That is, the proposed computational simulation is hypothesized to accurately estimate a long-term trend of a large-scale borefield without consideration of a detailed geometry of all the borehole components (e.g., GHX loop, fluid, and grout). In a closed system, an imbalanced load can result in constant, year-upon-year changes in ground

temperature and an unsustainable system. The district-scale model was created as a way to determine how much of the thermal imbalance could be mitigated through thermal conduction and convection for sustainable long-term operation. Therefore, the entire borefield was simplified into a rectangular geometry with the evenly distributed volumetric heat generation rate, which was equivalent to the size of the actual borefield with the borehole spaced at 6.4 m (40 bores x50 bores) intervals. The model geometry (including dimensions) is shown in Fig. 3.20. Monthly-averaged heat injection and rejection rates were used as the source conditions (as shown in Fig. 3.21). The heat source and sink term can be changed by means of a user defined function (UDF), which is an externally written code in C programing language, loaded into the CFD package.

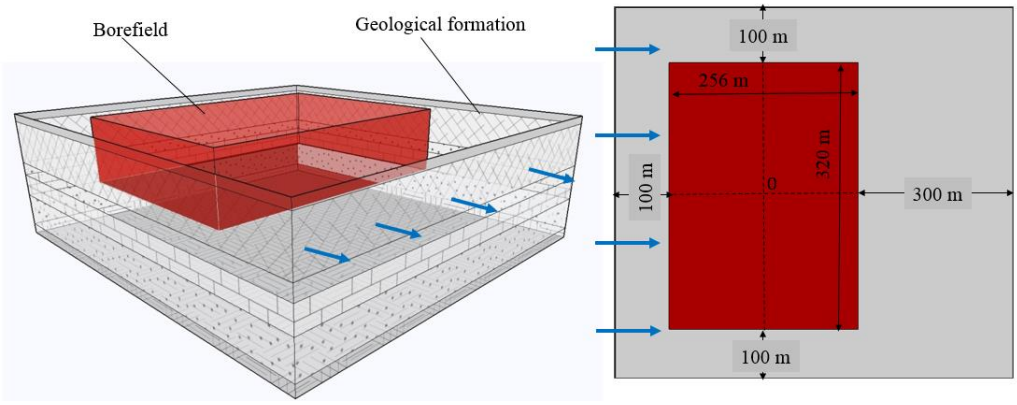

Figure 3. 20 Schematic view of model domain

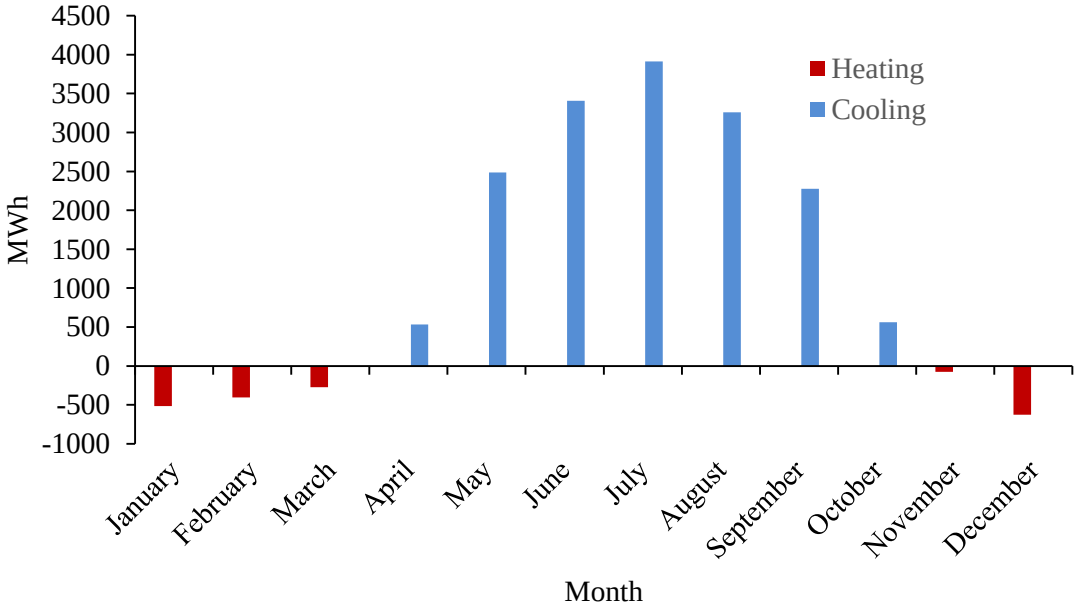

Figure 3.21 Annual net heating-cooling design loads used to size the Borefield 3 at Epic site (MEP Assoc. 2013) (Note: Negative values represent heat extraction).

Table 3.5 Model parameters used in Base Case simulation

Geologic Unit		**Description**	**Value**
n	[dimensionless]	Total porosity	0.3
n_{eff}	[dimensionless]	Effective porosity	varied
ρ	[$kg \cdot m^{-3}$]	Bulk density of the geologic medium	2650
c	[$J \cdot kg^{-1} \cdot K^{-1}$]	Bulk specific heat capacity of the geologic medium	900
λ	[$W \cdot m^{-1} \cdot K^{-1}$]	Bulk thermal conductivity of the geologic medium	3.82
Fluid			
ρ_f	[$kg \cdot m^{-3}$]	Density of fluid	998.2
c_f	[$J \cdot kg^{-1} \cdot K^{-1}$]	Specific heat capacity of the fluid	4182
λ_f	[$W \cdot m^{-1} \cdot K^{-1}$]	Thermal conductivity of the fluid	0.6
μ	[$kg \cdot m^{-1} \cdot s^{-1}$]	Dynamic viscosity	0.001003
Boundary Conditions			
q_v	[$m \cdot d^{-1}$]	Inlet groundwater velocity (Darcy's)	varied
q_h	[$W \cdot m^{-3}$]	Volumetric heat injection/extraction	UDF
T_i	[^oC]	Initial ground temperature	10.35
T_{inlet}	[^oC]	Inlet groundwater temperature	10.35
Adiabatic boundary at the top and bottom edge of the ground			

Modeling an Improved-2D single borehole

Because the mechanical efficiency of heat pumps is heavily dependent on the temperature of the fluid when it enters the heat pump (Entering Fluid Temperature or EFT), not only must the long-term temperature changes of the geothermal field be modeled, but also those of the recirculating exchanger fluid. The prediction of fluid temperature allows for the continuous prediction of a system's COP using performance data from the heat pump manufacturer. The model used in this study is similar to that developed by Zanchini and Terlizzese (2008) and used to evaluate the long-term performance of an

infinitely large borefield (Lazzari et al. 2010). These previous studies compared the model outputs to thermal response tests and the analytical solution for a cylindrical heat source. The present study achieves a validation of the model by comparing four months of experimental data taken from a residential GCHP application in Grand Marsh, WI. In addition, this study demonstrates how this model could be used to predict how the heat pump COP will change over time as the temperature of the borefield and entering fluid temperature change. Finally, this study uses this model to investigate the circulation of cold water through the borefield during winter months as a potential strategy for effectively maintaining thermal equilibrium in a large, thermally imbalanced borefield over the long-term.

Model setup

To model the fluid temperature for Borefield 3, design heating and cooling loads (see Fig. 3.21) were applied as internal heat generation within the exchanger fluid. An artificially high conductivity value was used to simulate turbulent mixing with the water (the inner cylinder region 'f' in Fig. 3.22), and a boundary layer (e in Fig. 3.22) was assigned a thermal conductivity using the Gnielinski correlation (Incropera et al. 2005). A flow rate of 0.25 kg/s was used based on field measurements.

$$Nu = \frac{\left(\frac{f\Phi}{8}\right)(Re_D - 1000)Pr}{1+12.7\left(\frac{\Phi}{8}\right)^{\frac{1}{2}}\left(Pr^{\frac{2}{3}}-1\right)} \quad \text{Eq. 3.14}$$

where, Nu, Re_D, and Pr represent the Nusselt, Reynolds, and Prandtl numbers, respectively, and $\mathbf{\Phi}$ is the friction factor from Colebrook-White equation

$$\frac{1}{\sqrt{\Phi}} = -2log_{10}\left(\frac{\varepsilon}{3.7D_h} + \frac{2.51}{Re_D\sqrt{\Phi}}\right) \quad \text{Eq. 3.15}$$

where ε is the roughness height (assumed to be 10^{-5} m) and D_h is the pipe's inner diameter.

where Nu, Re, and Pr represent the Nusselt, Reynolds, and Prandtl numbers, respectively.

Borehole elements representing the pipe, grout, and ground were included to model the site-specific properties surrounding the boreholes for each of the modeled scenarios. The thermal properties of the grout

were chosen based on standard grout properties (ρ = 1500 [kg/m^3], C_p=920 [J/kg·K], λ = 1.73 [W/m·K]). The thermal properties of the ground were the same as those used for the district-scale model (Table 3.5) and the pipe thermal properties were taken from actual measurement (Table 3.6).

The mean fluid temperature was monitored in the ANSYS-Fluent model (ANSYS 2104) by calculating the area-weighted average temperature of the water and boundary layer model entities ('f' and 'e' in Fig. 3.22). The effectiveness of the circulating cold water was evaluated by fixing the temperature of the water to 3 °C and monitoring the heat flux into it. This quantity of energy can be subtracted from the borefield imbalance, and the time needed to circulate this cold water in such a way that the borefield is thermally balanced can be determined.

From the mean fluid temperature output, the temperature of the fluid entering the heat pump (TEFT) during cooling, assuming a constant heat transfer along the entire length of the loop, can be determined as

$$T_{EFT,cooling} = T_m + \frac{\Delta T}{2} \quad \text{Eq. 3.16}$$

where T_m is the mean water temperature of two legs of U-pipe and ΔT represents the difference in temperature between the inlets and outlets of the U-loop GHXs, which from the first law of thermodynamics is

$$\Delta T = \frac{Q}{\dot{m} c_p} \quad \text{Eq. 3.17}$$

where Q is the thermal load being applied to the ground by a single borehole (negative if energy is rejected from the GHX and positive if energy is extracted), $\dot{m}$ is the mass flow rate, and c_p is the specific heat capacity of the water.

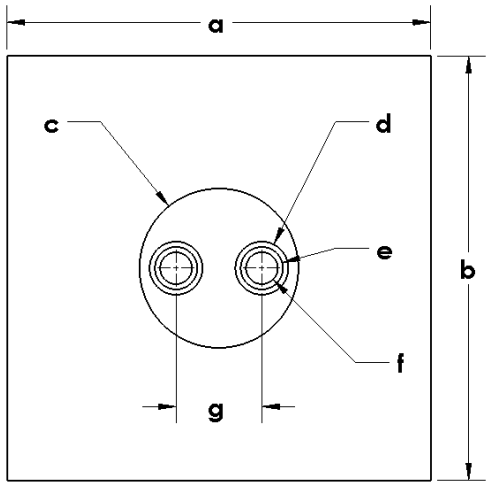

	Description	Borefield 3 model dimensions [m]	Residential single borehole model dimensions [m]
a	Spacing, x	6.40	20.00
b	Spacing, y	6.40	20.00
c	Borehole	0.140	0.150
d	Pipe	0.042	0.061
e	Boundary layer	0.032	0.051
f	Fluid	0.025	0.040
g	Pipes distance	0.081	0.081
Edges of domain are adiabatic boundaries. Model assumes no groundwater flow			

Validation of 2D single borehole model

Figure 3.22 Schematic view of model domain for 2D single borehole model and dimensions

Results of the 2D single borehole model were observed to be very sensitive to mesh size, time step size, and round-off criteria. Thus, a number of sensitivity analyses were performed to obtain the acceptable accuracy of the computational model. The largest inaccuracy was resolved using the double precision format to eliminate significant round-off error. To gain further confidence in the accuracy of the results, they were also compared to the experimental data from the ongoing residential GCHP system. A 4-month simulation of a GCHP system was run to provide a long-term comparison between the simulation results and the experimental data, as shown in Fig. 3.23. At the residential GCHP installation, temperature, flow, and electricity consumption, were recorded every 5 min to provide energy balance and COP data. The daily average rate of heat injected into the ground (a figured derived from the Grand Marsh field data) was applied to the model as internal heat generation within the fluid. The thermal properties of the ground were applied as weighted averages drawn from the existing literature and the measured values of the lithology present at the residential field site (as presented in Table 3.6).

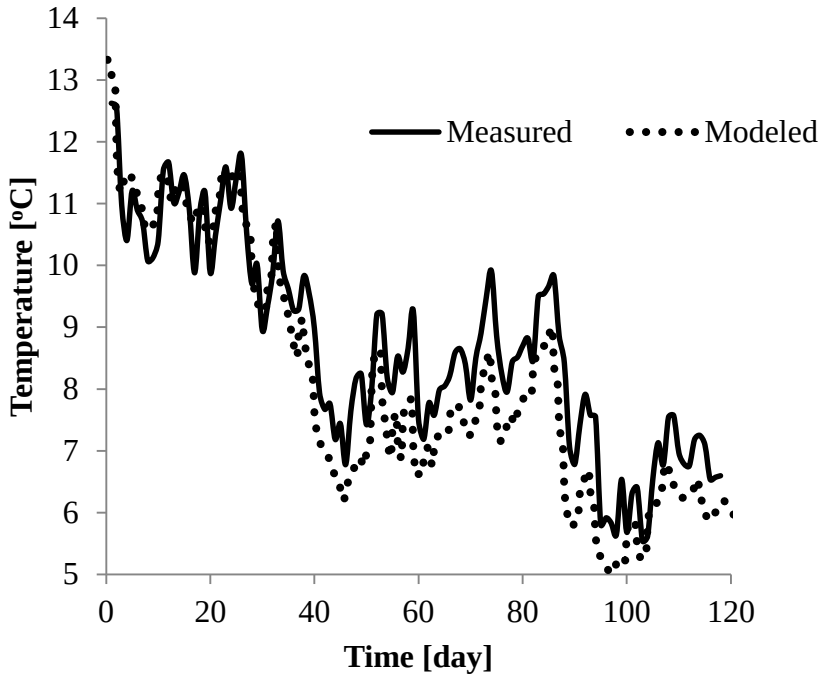

Figure 3.23 Comparison of CFD simulated and measured mean fluid temperatures from a GCHP system in Grand Marsh, WI

Table 3.6 Properties used in 2D single borehole model, Grand Marsh, WI

Property	ρ [kgm^{-3}]	c_p [$Jkg^{-1}K^{-1}$]	λ [$Wm^{-1}K^{-1}$]
Weighted-Average Geology	2323	1261	2.75
Grout	1500	820	1.50
HDPE U-Loop (Wang 2013)	950	2300	0.44
Fluid	998.2	4182	0.60

3.4.3 Results and Discussion

Temperature Field in A District-Scale Bore Field (Base Case)

Impact of groundwater flow

Simulated temperature was monitored at the borefield center (x=0 m) under different advective velocity conditions (from v_{adv}= 0 m/d to 1 m/d). Advective velocity is the ratio of Darcy's velocity to effective porosity where the groundwater actively flows through connected pores. Darcy's velocity is the hydrogeological parameter affecting the advective heat flux in the porous medium while advective velocity controls how fast the solute (heat) is moving. Since the time required for the temperature to dissipate is important in terms of GCHP system performance for the next heating-cooling cycle, we use the term advective velocity (v_{adv}) herein as the representative parameter of groundwater conditions. As we were focused on bulk water and heat movement rather than specific plume shape, we treated the surrounding formation as a homogeneous medium with no mechanical dispersion (mixing due to local velocity variation).

As seen in Fig. 3.24, the temperature changes for different advective velocities have the same pattern, which shows a cyclical temperature rise and fall over time that is due to the annual heating and cooling load cycle applied through GHXs to the ground. As expected, borefield ground temperature increased significantly over the 20-year period due to the load imbalance that existed between the heating and cooling cycles (cooling-dominated). The temperature at the center of the borefield rises linearly up to ~50 ^{o}C when there is no groundwater flow (v_{adv} = 0 m/d); i.e., when heat is transferred by conduction only. A low velocity case (v_{adv} = 0.01 m/d) showed no appreciable difference between low-flow and the no-flow conditions. The temperature profile under a velocity of 0.2 m/d, which is the most representative value obtained at the campus-scale borefield site, rises linearly for the first 10 years before tapering to an 8% less temperature rise as compared to the no-flow condition. This indicates that groundwater flow at the borefield site is contributing to heat transport by carrying the heat away. A simulation conducted with the highest

conceivable velocity, 1 m/d, showed less temperature rise over the first couple of years and the temperature reached an asymptotic average of 18°C. This velocity, by providing a relatively low-constant ground temperature, can be favorable for the geothermal borefield in terms of ground temperature sustainability as well as GCHP performance; however, the presence of this velocity is unlikely based on the information from literature for this site.

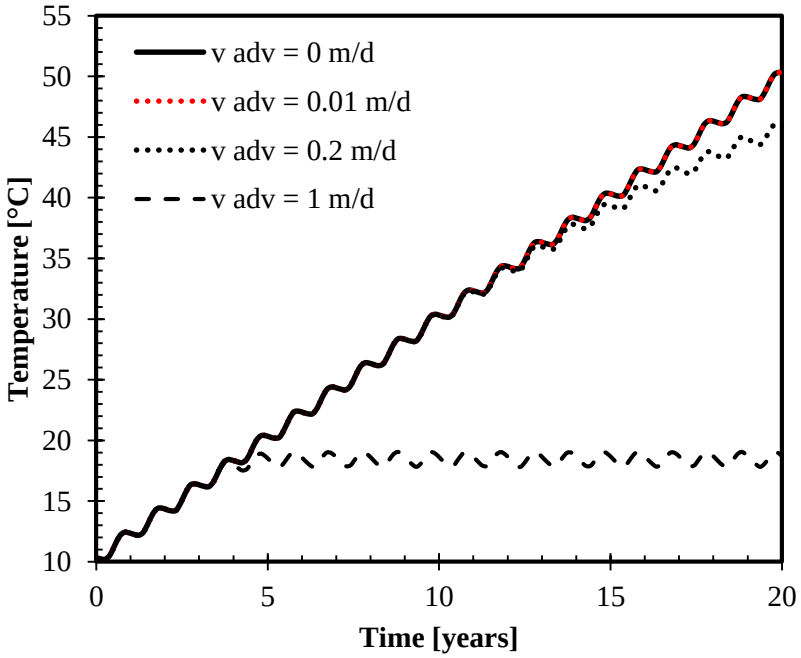

Figure 3.24 Temperatures at the center of borefield over time under conditions with no groundwater flow and with groundwater flow at various advective velocities (Prairie du Chien Group Dolomite with n_{eff} = 0.05)

The impact of groundwater flow can also be seen in Fig. 3.25 (a), which shows temperature distribution along a horizontal distance (from east to west) after a 10-year simulation. Ground temperature increased near the borefield, reaching a maximum temperature within the borefield area. The impact of groundwater flow with a velocity of 0.01 m/d is again negligible while the impact of a field-specific groundwater flow condition with a velocity of 0.2 m/d is clearly seen, shifting the temperature distribution curve 40 m yet the maximum borefield temperature remains the same (~30°C). Further increasing the velocity to 1 m/d shifts the temperature curve dramatically away and makes the maximum borefield temperature significantly cooler (26°C). Fig. 3.26 shows the temperature contours around the borefield and the surrounding ground under no groundwater flow (ν_{adv} = 0 m/d) and with a groundwater flow (ν_{adv} = 0.2 m/d). Clearly, the borefield temperature is much lower when a groundwater flow exists and the heat is not only diffused but also shifted in the direction of the flow, whereas heat is only diffused locally by conduction when there is no groundwater flow. Much of the upper Midwest is geothermally favorable for cooling-dominant sites due to cool ground temperatures (12°C) and low thermal gradients (8 °C/km) (Meyer 2013). The results from this study show that transmissive aquifers (e.g., ν_{adv} = 0.2 m/d), make an especially suitable location for systems primarily used for space cooling. However, large-scale borefields that annually reject a large amount of heat to the ground during summer will unlikely be offset by the additional heat flux from groundwater flow and will still likely cause overheating in the ground year after year. Thus, for large-scale borefields, a heat mitigation strategy is needed to balance annual loads and maintain a neutral ground temperature.

Significance of bedrock porosity

The measured porosity of rock in this study field can vary from 0.02 to 0.3 (WGNHS 2014). As discussed in the previous section, the ground formation (Prairie du Chien Dolomite) modeled in this study is highly fractured with karst features that can cause high variation in porosity. The effect of porosity on the heat transport of a particular geology can be predicted for the overall porosity range by using a possible minimum effective porosity (n_{eff}) of 0.05 and a possible maximum n_{eff} of 0.3. Fig. 3.25(a) and Fig. 3.25(b) show that the temperature distribution curve for a formation with n_{eff} of 0.05 is nearly the same as compared to a formation with n_{eff} of 0.3 at a velocity ranging from 0 m/d to 0.01 m/d and 20% and 50% higher at a velocity of 0.2 m/d and 1 m/d, respectively. The difference is because Darcy's flux is the inverse ratio of effective porosity; therefore, a n_{eff} of 0.3 provides a higher groundwater flux, and this higher flux results in more advective heat transfer. Such implies that the heat transport due to advection is strongly dependent on the rock's effective porosity (n_{eff}), and therefore, this parameter should be taken into consideration. Also, fluid density variation due to the high temperature in the borefield may cause natural convection that may lead to additional heat dissipation in the porous media. However, a series of sensitivity analyses showed the groundwater velocity driven by buoyancy to be less than 1.12e-22 m/s based on the conditions in the study site, deeming it negligible for subsequent calculations.

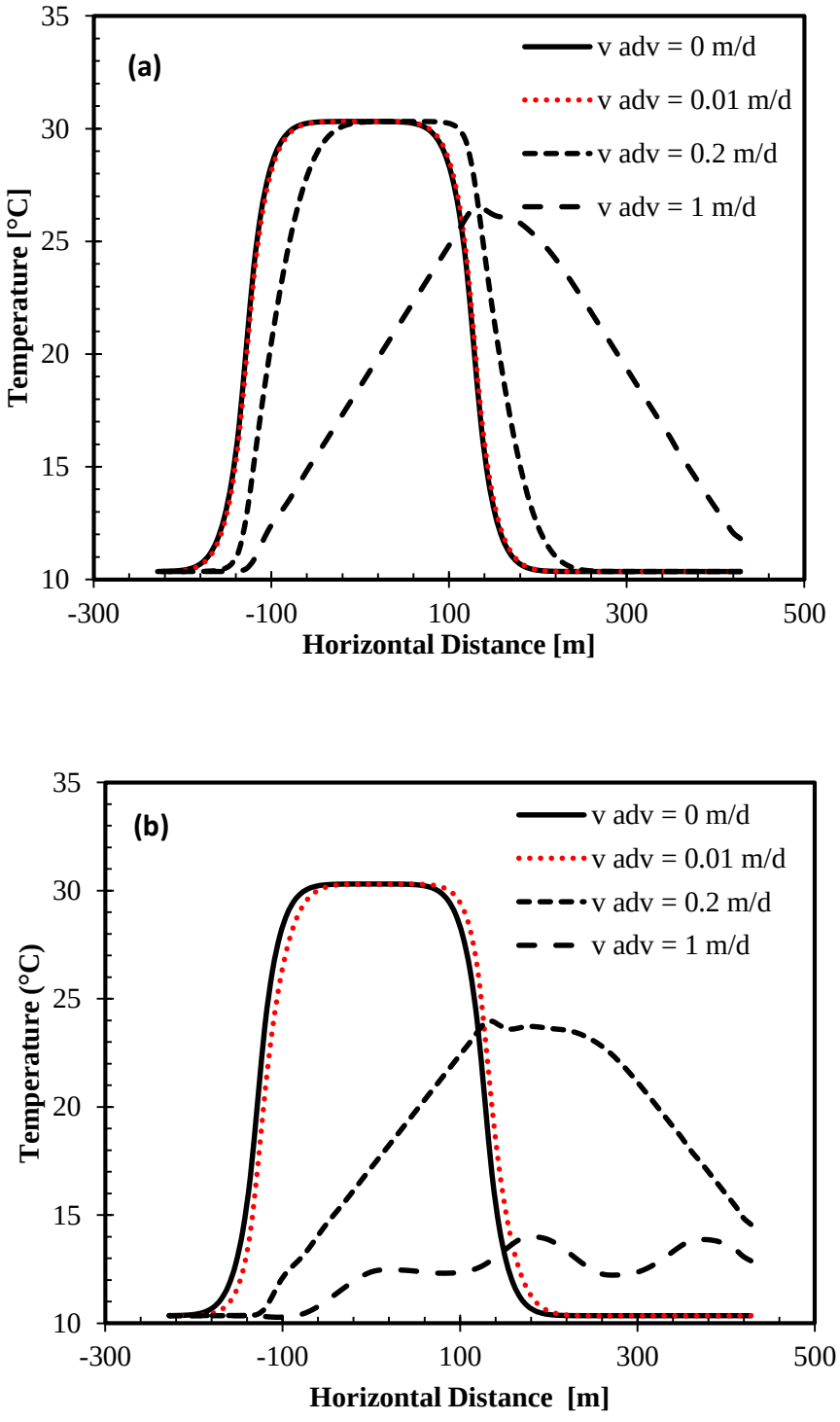

Figure 3.25 Temperature along horizontal axis of borefield for various advective velocities for 10 year simulation (Prairie du Chien Group Dolomite with (a) n_{eff} = 0.05, (b) n_{eff} = 0.30)

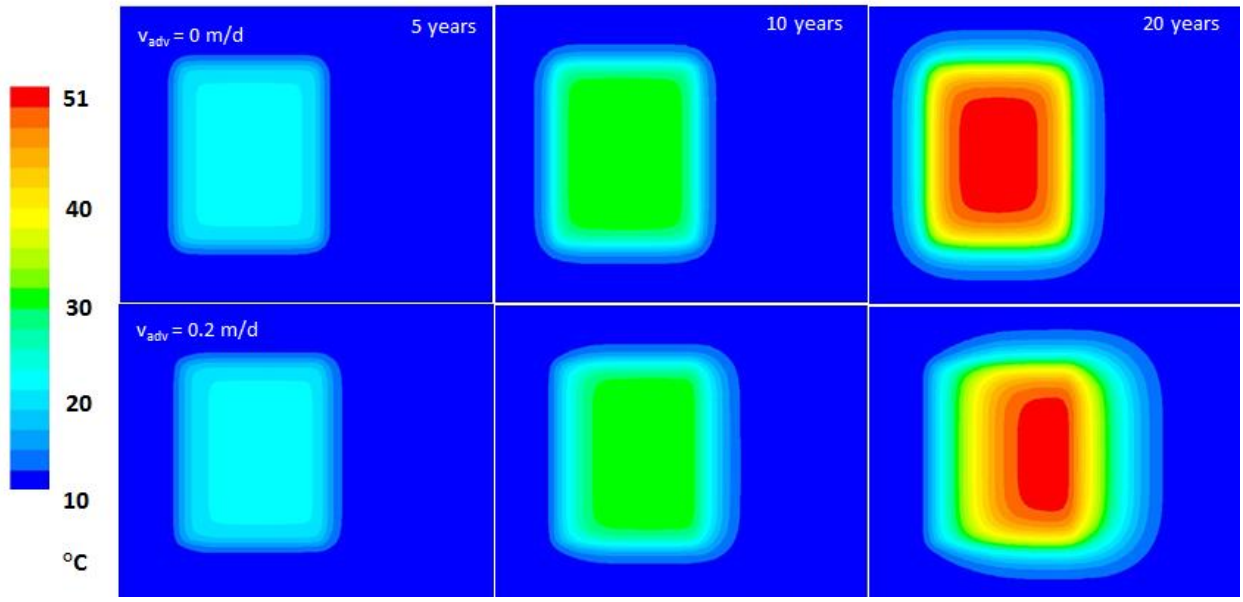

Figure 3.26 Temperature contours under no groundwater flux (v = 0 m/d) and groundwater flux (v = 0.2 m/d) for 5, 10 and 20 years

Performance Evaluation of GCHP System

As discussed, previous results obtained by the district-scale borefield model indicated that energy imbalance is a potential issue under the given design conditions. Groundwater flow lowers the borefield ground temperature although this effect does not manifest at the center of the borefield until 10 years after operation begins. Even after the first year of operation of GCHP, the borefield temperature has already risen, and this will most likely decrease the efficiency of the system. To determine the impact that overheating has on the GCHPs performance during 20 years of operation, the temperature of the fluid as it returns from the GHX and enters the heat pump is the most important parameter for evaluating the heat pump performance (as estimated by the 2D, single-borehole model). Using Eq. 3.16 and the modeled results, the temperature of the fluid entering the heat pump was estimated. The information associated with the cooling COP versus the entering fluid temperature relationship found in the heat pump's manual could be used for this purpose. The mean water temperature obtained by the single borehole model versus borefield ground temperature from the base case model (no groundwater flow) over 20-year operation is

presented in Fig. 3.27 (a). The amplitude of the mean water temperature increases in much greater spikes than the ground temperature due to the borehole's resistance (e.g., fluid, pipe, and grout). As expected, the slope of the two temperature profiles are the same, thus showing good conformity between the two models in terms of reasonability of their assumptions and the computational process used. As shown in Fig. 3.27 (b), ground with higher temperature will have higher EFT, thus resulting in a lower COP for a cooling dominant operation based on the representative performance data from the Multistack™ water-cooled heat pump datasheet.

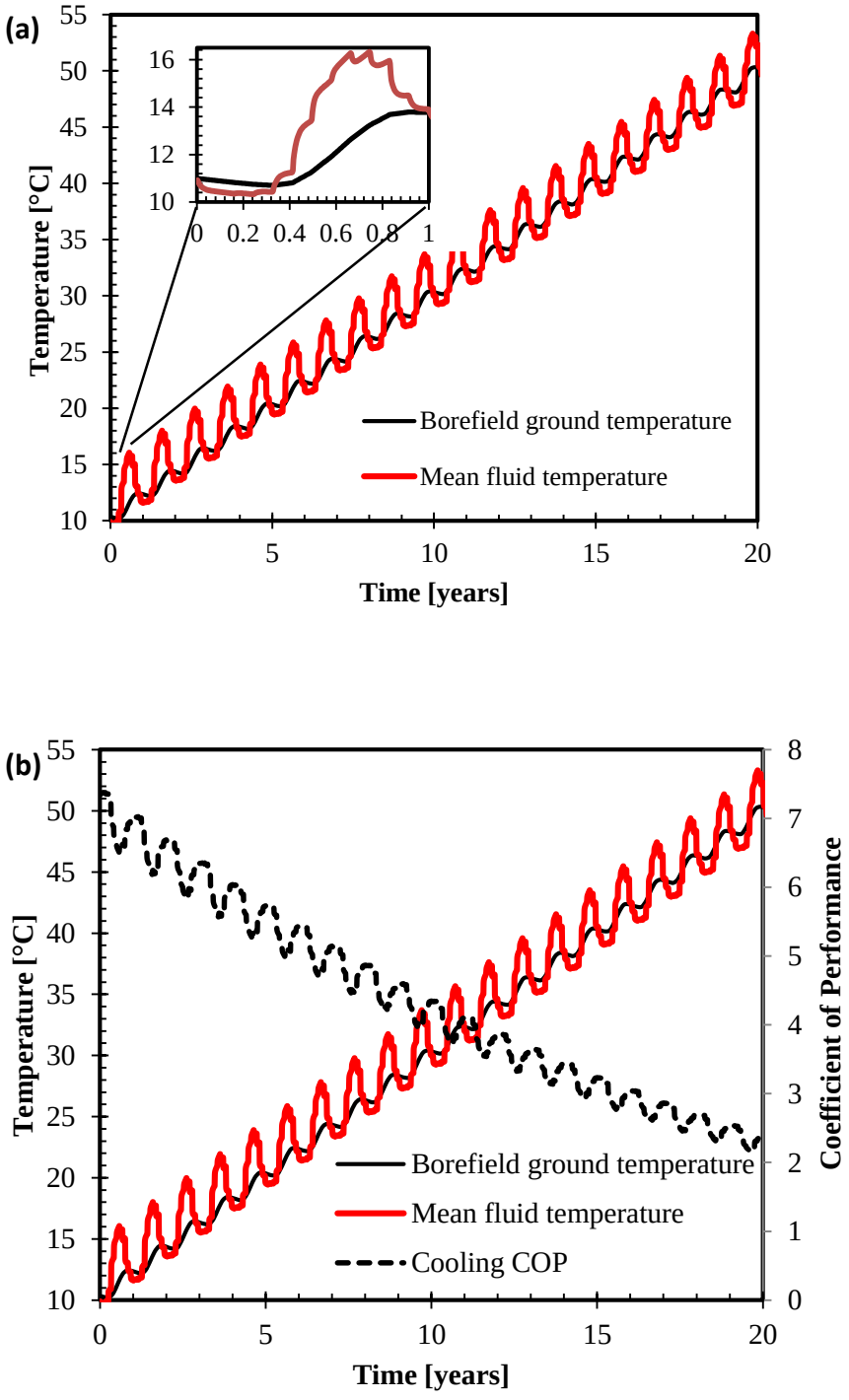

Figure 3.27 (a) Mean fluid temperature change from single borehole model versus borefield ground temperature from base case model over time (b) Cooling COP change with increasing EFT from the borefield during cooling mode for a Multistack MS010X_W with leaving temperature of 6 °C

3.4.4 Mitigation Strategy

Current Operational Strategies

Facilities management on site is well aware of potential overheating due to past issues with Borefield 1 reaching temperatures of over 30°C after it was installed in 2006; in response, they have pursued a strategy of aggressive expansion to reduce the total load on any one field, adding over 5,000 boreholes in the following 9 years. However, as the system load remains highly unbalanced, additional operational strategies have been implemented to eliminate or reuse waste heat where possible. Current ones include heating parking structures, preheating domestic hot water, and deicing of patios and sidewalks.

Ground Temperature Response under Intermittent Operation

As shown in previous model results, a GCHP system with a large thermal load imbalance can dramatically increase the borefield temperature, resulting in significant reductions in heat pump COP. To improve the borefield heat balance, a one-year, intermittent operation period was introduced after every five years of operation. With this proposed operation period included, the borefield temperature decreased by about the same temperature value of 6 ^{o}C under the no groundwater flow condition and with a groundwater flow at v_{adv} = 0.2 m/d (see Fig. 3.28). A one-year, intermittent period once every five years over 20 years of operation under the groundwater flow condition will aid in ground temperature recovery. However, using this mitigation strategy alone will not achieve a fully balanced borefield temperature.

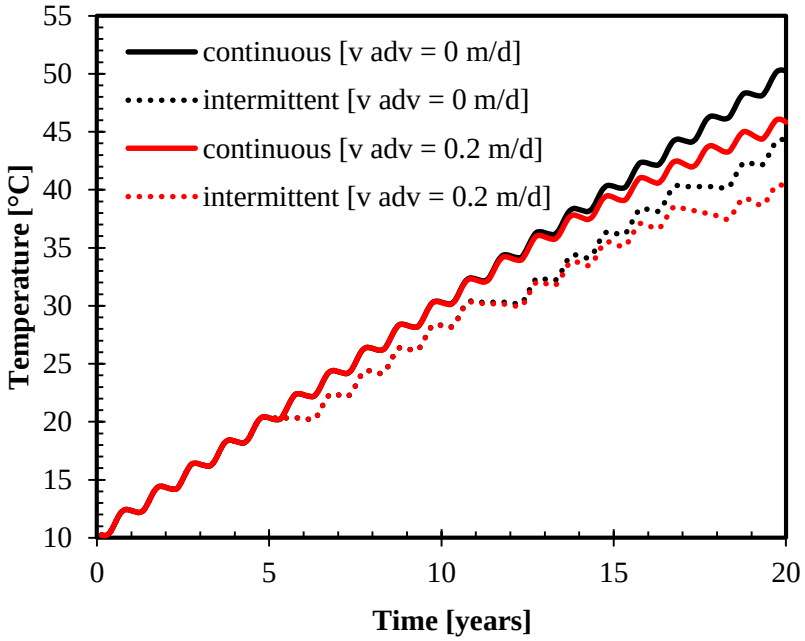

Figure 3.28 Temperature response under the continues versus intermittent operation of heating-cooling cycles (Prairie du Chien Group Dolomite, n_{eff} =0.05)

Ground Temperature Recovery under Cold-Water Circulation

Given the results obtained when applying the previously proposed strategy (see Fig. 3.28), a more active mitigation strategy is proposed. This strategy would involve the circulation of cold water (3 ^{o}C assumed) through the GHXs during times when there are low loading requirements and cold ambient air temperature (i.e. winter). Such would allow the cold-water circulation schedule to be staggered among several borefields. The cold water circulation was simulated using the 2D single borehole model by setting the water entity ('f" in Fig. 3.22) to a fixed value of 3 ^{o}C. The campus-scale field site has a pond that is used for stormwater retention, and during the winter and early spring, heat could be constantly sunk into the ice-capped pond with the addition of snow from the surrounding area. Several schedules for how the borefields might be staggered were tested.

The first scenario tested involved the circulation of cold water at the end of the heating season (March). This method distributes the entire March load over the first one and two weeks of the month in

the scenarios representing 3 and 2 weeks of cold-water circulation, and adding the March load to the February load in the scenario in which cold-water is circulated for the entire month of March. The times when the heat load is intensified represent times when cold water would be circulated through the other borefields, which could not be used simultaneously for heating or cooling. The results for cold-water circulation of a month or less are shown in Fig. 3.29. None of these cold-water circulation scenarios fully recovered the annual thermal imbalance. Therefore, a second strategy involved balancing the thermal load every other year. This method entailed doubling the heat extraction load during December, January, February and March of the first year and circulating cold water during those 4 months during the second year. As seen in Fig. 3.30, this strategy succeeded at leveling the thermal imbalance created over the previous two years.

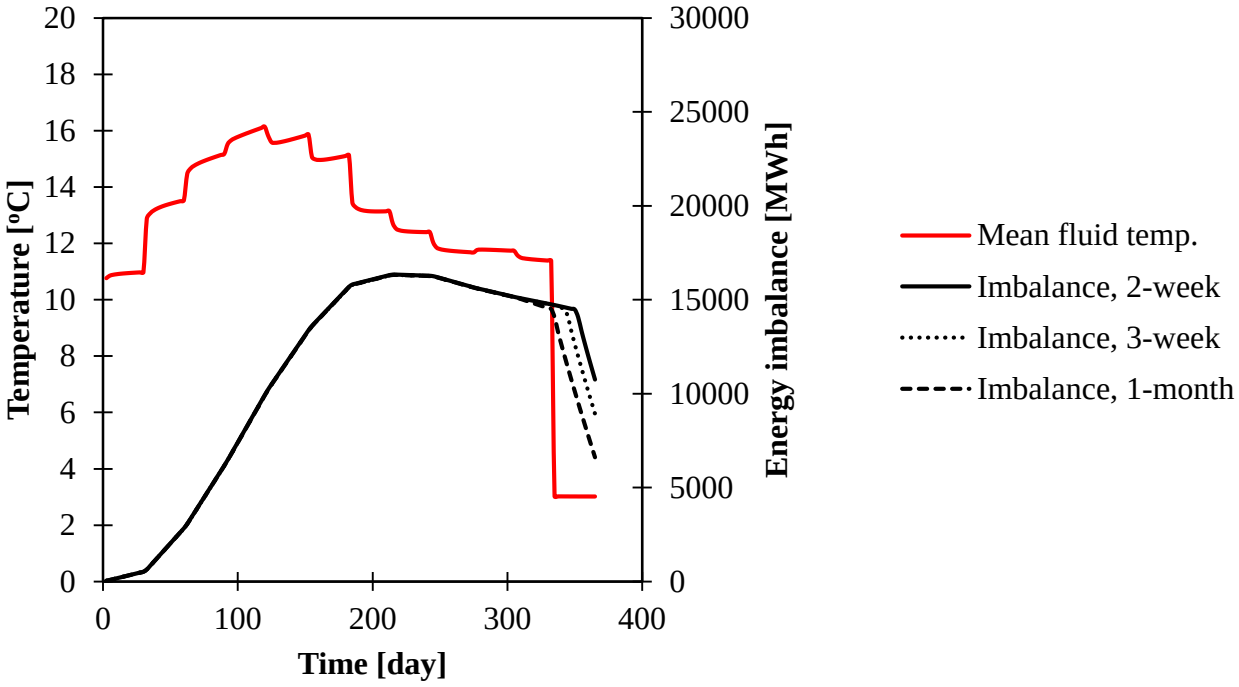

Figure 3.29 Energy imbalance over time under the cold-water circulation during end of March

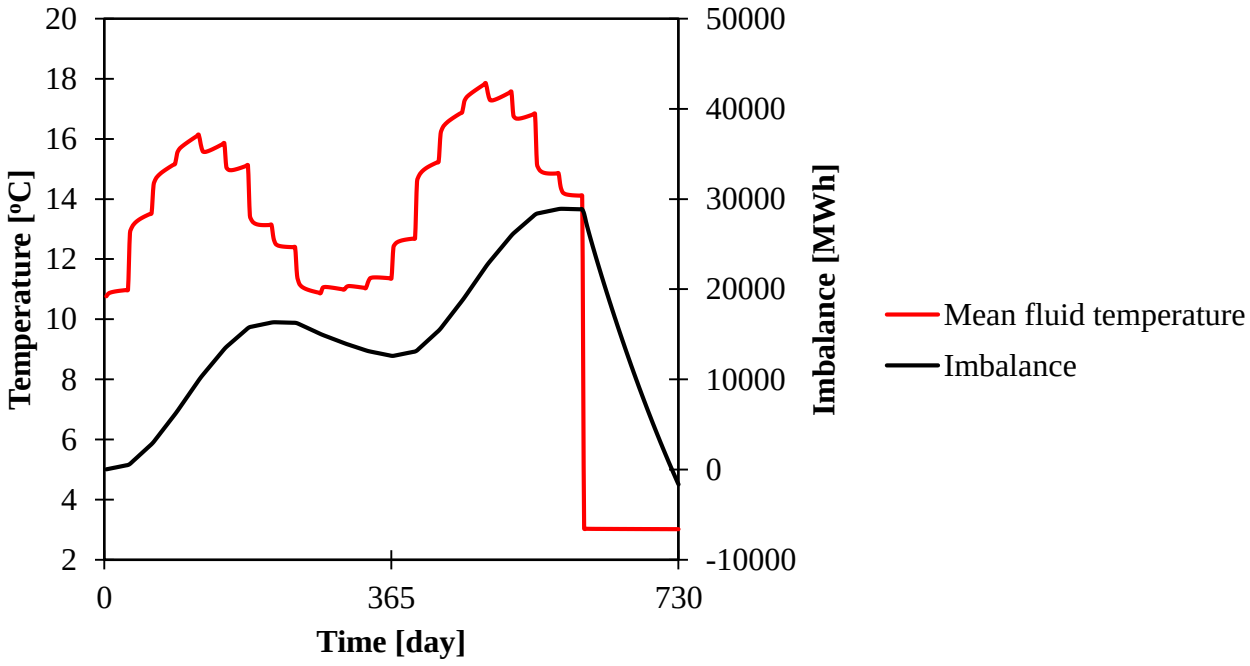

Figure 3.30 Temperature and energy imbalance over time under cold-water circulation during heating season

3.4.5 Conclusions

This study examined the ground temperature changes obtained from a real-world campus-scale geothermal borefield by modeling predesigned annual heating and cooling loads. Ground temperature changes under these design conditions were simulated using a 2D transient, groundwater flow-coupled model by means of CFD. The impact of ground hydrogeological conditions (such as groundwater flow at various advective velocities—0 m/d-1 m/d) was measured. From the results we obtained, we were able to conclude that the borefield ground temperature significantly increases over a 20-year GCHP operation and correlates positively with groundwater flow conditions. If the system operates continuously under the design conditions, the temperature regulation efficiency of the ground and the GCHPs will be reduced over time due to increased ground temperature. To evaluate the heat pump performance (COP) over a 20-year period, 2D, single-borehole models, which considered borehole resistances (fluid, pipe and grout), were simulated and validated for an operating GCHP system. Results showed that an increase in borefield ground temperature reduced the COP of the heat pump dramatically to the point where heat pump will no longer perform efficiently for the next operation cycles. To overcome the ground-overheating problem, some mitigation strategies are proposed. The first strategy involves introducing a one-year intermittent idling cycle after every five years of operation. Modeling results showed that the ground temperature did not sufficiently recover after the intermittent idling cycle. The second strategy entailed circulating cold water (3 ^{o}C) through the GHXs under two different scenarios. In the first scenario, cold water was circulated at the end of the heating season (March) for various time durations (1 week to 1 month). None of these cold-water circulation runs fully recovered the annual thermal imbalance. The second scenario involved doubling the heat extraction load during December, January, February and March of the first year (when cold water is being circulated through another borefield) and circulating cold water during those 4 months in the second year. This procedure succeeded at recovering the thermal imbalance created over the previous two years. In summary, we have identified a potential solution for the reduced efficacy of GCHPs, which results from changes in the ground temperature over long periods of time. Our models revealed that the alternating

operation of multiple borefields on opposite two-year cycles (i.e. doubling heat extraction during the cold months of one year and circulating cold water the second year) can efficiently maintain ground temperatures and thus prolong the effective use of GCHPs as an environmentally and economically useful tool for space heating large, campus-scale facilities.

3.4.5 References

American Society of Heating, Refrigerating and Air-Conditioning Engineers (ASHRAE). 2003. "Geothermal Energy." ASHRAE Handbook. HVAC Applications.

American Society of Heating, Refrigerating and Air-Conditioning Engineers (ASHRAE). 2007. "Geothermal Energy." ASHRAE Handbook. HVAC Applications.

American Society of Heating, Refrigerating and Air-Conditioning Engineers (ASHRAE). 2011. "Geothermal Energy." In 2011 ASHRAE Handbook - HVAC Applications.

ANSYS. 2014. "ANSYS FLUENT Theory Guide." http://www.ansys.com. Canonsburg, PA: SAS IP.

Bradbury, K.R., Borchardt, M.A., Gotkowitz, M., Spencer, S.K., Zhu, J., and Hunt, R.J. 2013. "Source and transport of human enteric viruses in deep municipal water supply wells." *Environmental Science and Technology*, 47(9), 4096–4103.

Brandherm, R. 2013. Personal comminication.

Busby, J., Lewis, M., Reeves, H., and Lawley, R. 2009. "Initial geological considerations before installing ground source heat pump systems. *Quarterly Journal of Engineering Geology and Hydrogeology*, 42(3), 295–306.

Clauser, C., and Huenges, E. 1995. "Thermal conductivity of rocks and minerals. In T. Ahrens, rock physics and phase relations-a handbook of physical constants." Washington: AGU reference shelf, 3(1080-305X), 105–126.

Choi, C.Y., and Kulacki, F.A. (1992) Mixed convection through vertical porous annuli locally heated from the inner cylinder, *ASME Journal of Heat Transfer*, 114:1, 143-151.

Choi, C.Y., and Kulacki, F.A. (1993) Non-Darcian effects on mixed convection in a vertical packed-sphere annulus, Technical Note, *ASME Journal of Heat Transfer*, 115:2, 506-510.

Cathomen, N., F. Stauffer, W. Kinzelbach, and F. Osterkorn. 2002. Thermische Grundwassernutzung. Auswirkung von W¨armepumpenanlagen auf die Grundwassertemperatur. Gas Wasser Abwasser 82(12), 901–906.

Dehkordi, S.E. and Schincariol, R.A. 2013. "Effect of thermal-hydrogeological and borehole heatexchanger properties on performance and impact of vertical closed-loop geothermal heat pump systems." *Hydrogeology Journal*, 22(1), 189–203.

Diao, N., Li, Q., and Fang, Z. 2004. "Heat transfer in ground heat exchangers with groundwater advection." *International Journal of Thermal Sciences*, 43(12), 1203–1211.

Energy Information Administration (EIA). 2009. "Residential Energy Consumption Survey (RECS)."

Environmental Protection Agency (EPA). 2013. "Inventory of U.S. greenhouse gas emissions and sinks: 1990–2011." Washington D.C.

Eskilson, P. 1987. "Thermal analysis of heat extraction boreholes." Ph.D. Thesis. University of Lund, Lund, Sweden.

Fossa, M. and Minchio, F. 2013. " The effect of borefield geometry and ground thermal load profile on hourly thermal response of greothermal heat pump systems." *Energy*, 51, 323–329.

Grant, M.A., Donaldson, I.G., and Bixley, P.F. 1982. "Geothermal reservoir engineering." *Academic Press*, San Diego, California. 369 p.

Hecht-Méndez, J., Molina-Giraldo, N., Blum, P., Bayer, P. 2010. " Evaluating MT3DMS for heat trasnport simulation of closed geotermal systems." *Ground Water*. 48 (5), 741–756.

Hecht-Méndez, J., Paly, M., Beck, M., and Bayer, P. 2013. "Optimization of energy extraction for vertical closed-loop geothermal systems considering groundwater flow." *Energy Conversion and Management*, 66(10.1016), 1–10.

Horai, K. and Simmons, G. 1969. "Thermal conductivity of rock-forming minerals." *Earth and Planetary Science Letters*, 6(5), 359–368.

Kavanaugh, S. 1995. "A design method for commercial ground-coupled heat pumps." American Society of Heating, Refrigerating and Air-Conditioning Engineers (ASHRAE) Transactions, 101(part 2), 1088–1094.

Kavanaugh, S., Rafferty, K., and Geshwiler, M. 1997. "Ground-source heat pumps: Design of geothermal systems for commercial and institutional buildings." Chap. 3. Atlanta: American Society of Heating, Refrigerating and Air-Conditioning Engineers (ASHRAE).

Krohelski, J.T., Bradbury, K.R., Hunt, R.J., and Swanson, S.K. 2000. "Numerical simulation of groundwater flow in Dane county Wisconsin." *Wisconsin Geological and Natural History Survey*, Bulletin 98.

Lazzari, S., Priarone, A., Zanchini, E. 2010. " Long-term performance evaluation of borehole heat exchnager fields with groundwater movement." Proceeding of the COMSOL Conference, Paris.

Martin, R.J., S.F. Bender, S.W. Gaulke, and J. Wallace. 2001. "Simulation of groundwater flow and heat transport on Grand Cayman Island." In MODFLOW 2001 and Other Modeling Odysseys, Conference Proceedings, eds. S. Seo, E.P. Poeter, C. Zheng, O. Poeter, 776–782. International GroundWater Modeling Center, Colorado School of Mines,Golden, Colorado.

MEP Associates, LLC. 2014. Personal Comminication. Eau Claire, Wisconsin.

Meyer, L. 2013. "Thermophysical properties of Wisconsin rocks for application in geothermal energy." Master Thesis. University of Wisconsin-Madison.

Nield, D.A., and Bejan, A. 2013. Convection in Porous Media. ISNB: 978-1-4614-5540-0. Springer. 778p.

Ozdogan-Dolcek, A., Tinjum, J.M., and Hart, D.J. 2014. "Numerical modeling of ground temperature response in a ground source heat pump system (GCHP)." *American Society of Civil Engineers (ASCE) Geo-Congress 2014*, Atlanta.

Ozdogan-Dolcek, A. 2015. "Numerical modeling of heat transport for the ground coupled heat pump (GCHP) systems and associated life cycle assessments." Ph.D. Dissertation. Univeristy of Wisonsin-Madison.

Parsen, M.J., Bradbury, K.R., Hunt, R.J., Feinstein, D.T. 2014. "A new groundwater flow model for Dane County, Wisconsin." Report preapred for the Capital Area Planning Commission, Dane County, WI. Wisconsin Geological and Natural History Survey, University of Wisconsin-Extension.

Spitler, J. 2005. "Ground-source heat pump system research-past, present, and future." *Heating, Ventilation, Air Conditioning, and Refrigration Research*, 11(2), 165–168.

Walker, M.D., Meyer, L.L., Tinjum, J.M., and Hart, D.J. 2014. "Thermal property measurement of stratigraphic units with modeled implications for expected performance of vertical ground source heat pumps." J*ournal of Geological and Geotechnical Engineering.* In Review.

Wisconsin Geological and Natrual History Survey *(*WGNHS). 2014. "Understanding porosity and Density [data]." Retrieved fromhttp://wgnhs.uwex.edu/maps-data/data/rock-properties/understanding-porosity-density/

Zanchini, E., and Terlizzese, T. 2008. "Finite-element evaluation of thermal response tests performed on U-tube borehole heat exchangers." *Proceedings of the COMSOL Conference.* Hannover.

Zhou, P., Chen, C., Wu, J., Hu, G., Guo, Y., & Li, K. (2014). "Study on heat transport of soil thermal recovery of ground source heat pump system. *In Proceeding of the 8th International Sympoisum on Heating, Ventilation and Air Conditioning*. 2, 449–460.

Zimmerman, R. 1989. " Thermal conductivity of fluid-saturated rocks." Journal of Petroleum Science and Engineering." 3, 219–227.

CHAPTER 4 -LIFE-CYCLE ASSESSMENT AND COMPARISON OF VARIOUS GROUND COUPLED HEAT PUMP SYSTEMS BASED ON A WISCONSIN CASE STUDY

A full life-cycle assessment (LCA) of a residential GCHP system has been implemented based on monitored and ongoing operation of a fully instrumented GCHP system in Grand-Marsh, WI. This study is in preparation for submission in *Renewable and Sustainable Energy Review*.

Abstract: Within the heating, ventilation, and air conditioning (HVAC) sectors, ground coupled heat pumps (GCHPs) offer a potentially economical, low-carbon energy approach to lowering of the global energy budget. This study investigates the performance of a conventional vertical GCHP configuration with three boreholes (VERT), a conventional horizontal GCHP (HORZ), an unconventionally deep (300 m) single borehole GCHP (SING) system, and a conventional split natural gas air conditioning unit (NGAC). This study also compares potential for reduced greenhouse gas (GHG) emissions via the GCHP systems in Wisconsin, USA, using a comprehensive "cradle-to-grave" life-cycle analysis (LCA), which is implemented using SimaPro. Assuming the current Wisconsin electrical grid of 5.5% renewables, heating and cooling loads of a 186 m^2 residence, a coefficient of performance (COP) of 4 and a 25-year lifetime, an average of 272 metric ton CO_2 equivalent emissions is calculated for SING. Top contributors are heat-exchanger operation (93.3%), borehole drilling (2.4%), and circulation pump operation (1.5%). This amounts to GHG emissions savings of 10% and 19% over VERT and HORZ GCHPs, respectively, and 27% over NGAC. Sensitivity analyses determine that a grid with renewables penetration of 50% could save 68% GHG emissions over natural gas. As the use of fossil fuel decreases and the grid becomes cleaner, GCHP systems become even more beneficial from the perspective of lifetime GHG emissions. A COP of 5 could further reduce GHG emissions by 38%, indicating that the COP is a significant factor of GCHP environmental impacts.

4.1 INTRODUCTION

4.1.1 Energy and HVAC

Discovery of new fossil-based resources is increasingly more difficult, while energy demand is increasing due to expanding population and developing nations. From 2000 to 2010, world energy consumption increased by 23% and is projected to grow by 56% between 2010 and 2040 (EIA 2013). Meanwhile, there is a growing concern surrounding warming of the earth due to greenhouse gas (GHG) emissions from fossil fuel energy sources. Though carbon dioxide (CO_2) is naturally emitted through the carbon cycle, fossil fuel burning has been directly tied to the exponential atmospheric increase in CO_2 levels since the Industrial Revolution (USDOS 2007). Fossil fuels such as coal, petroleum, and natural gas currently account for 80% of world energy use and 77.5% in the US. CO_2 concentrations are at a record high of 397.23 parts per million [Tans et al. 2014], and at the current growth rate, the consumption of fossil fuels alone is projected to increase emissions by 46% by 2040 (EPA 2013). Extensive climate research has demonstrated the connection between increased GHG concentrations and global temperature rise, shifting snow and rainfall patterns, and extreme climate events, among other effects (EPA 2013). The superposition of these issues and concerns has created urgent global pressure to develop and integrate innovative and renewable energy solutions into all sectors of society.

The heating and cooling of buildings comprises a substantial portion of world energy use, and thus is an important focus area. In 2009, residential energy use accounted for 22% of total annual energy consumption in the US (EIA 2013). Heating, ventilation, and air conditioning (HVAC) comprise 48% of residential energy consumption in the US and 57% of the total in Wisconsin, as shown in Fig 4.1. Including water heating, these figures increase to 66% nationally and 72% in Wisconsin. In the US, 55.4% of HVAC is sourced from natural gas (EIA 2009). This is due to the widespread use of natural gas furnaces for space heating. Though typically the least expensive option in the US (EIA 2013), natural gas is a fossil fuel and thus contributes to global warming. In light of increased societal concern about energy sources and their environmental impacts, heating and cooling solutions with lower GHG emissions are essential. This study

focuses on the emissions and practicality of ground source heat pump (GCHP) systems as an alternative form of HVAC.

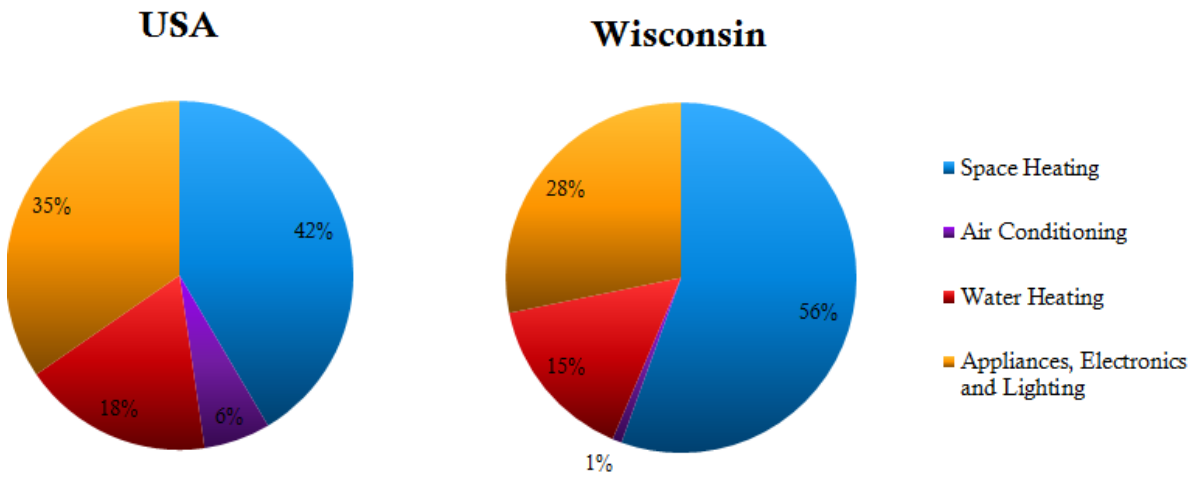

Figure 4.1 Residential energy consumption by end-use in the United States and in Wisconsin in 2009, adapted from US Energy Information Administration, Annual Energy Review 2013

4.1.2 Introduction to Ground Source Heat Pumps (GCHP)

GCHPs, also known as geothermal heat pumps, geoexchange, thermal exchange, or energy exchange (Dickie et al. 2010), provide a potential energy-saving alternative for heating and cooling buildings. Though comprising only 0.2% of the total installed HVAC systems, GCHP use is predicted to increase exponentially in upcoming decades (Saner et al. 2000). Rather than directly consume fuel or electricity, GCHPs use the earth as a heat source and heat sink and thus can be applied even in areas with low geothermal gradient. Depending on the weather and geological conditions at the site, the temperature below a depth of six meters into the earth's crust remains relatively constant at 10–15 ºC. The first GCHPs were open-loop systems in which groundwater intermixed with the loop fluid, but closed-loop GCHPs are now preferred to prevent groundwater contamination (Raffery 200). Horizontal systems circulate fluid through horizontal pipes in trenches at least 1.5 m below the ground. Horizontal systems work well for small heating and cooling loads and large plots of land, which are more common in residential use. Since drilling is not required, horizontal systems often have a low upfront cost. Vertical GCHPs consist of a sealed

loop of High Density Polyethylene (HDPE) U-pipe, buried in the ground and connected to a heat pump through which water or antifreeze is circulated, typically 80 m to 110 m deep (Natural Research Canada 2009). Drilling and completing the borehole increases the initial cost, but allows for greater heat transfer when space is limited, as occurs with large systems or in urban areas. In a closed-loop system, a fluid (typically water mixed with antifreeze) circulates through pipes in a borehole or trench in the ground to take advantage of the temperature consistency in the ground. Heat is transferred from the ground to the fluid for heating during the winter, and it is released through the ground by means of the fluid during the summer. Heat is then transferred through a ground loop heat exchanger from the carrier fluid to a refrigerant, which is compressed and evaporated in a heat pump to extract heat for the building in the form of hot water or warm air. Electrical input is needed to power the heat exchangers and circulation pumps that exchange the heat from/to the ground to/from the residence.

GCHPs operate according to the basic thermodynamic principles of heat transfer. Complex models and equations exist to determine the length of a borehole that is necessary for a functional GCHP to provide a specified quantity of heat transfer [10]. The following simplified linear model developed from Fourier's Law is used to determine the heat transfer load q in a borehole (Ingersol et al. 1954):

$$\mathrm{q} = \mathrm{L} \times \left(\mathrm{T_g} - \mathrm{T_w}\right) \times \lambda \qquad \text{Eq. 4.1}$$

where q is the rate of heat transfer from the ground to the circulating fluid or vice versa [W], L is the borehole length [m], $\mathrm{T_g}$ is the ground temperature [K], $\mathrm{T_w}$ is the temperature of the water (or carrier fluid) entering the ground [K], and λ is the thermal conductivity of the ground (soil or rock) surrounding the borehole [W/m·K]. The average ground temperature is used in this approximation. Higher thermal conductivity, longer length, and elevated ground temperatures thus yield increased transfer of energy from the ground.

In GCHPs and any typical refrigeration system, energy efficiency is measured by the coefficient of performance (COP) and the energy efficiency ratio (EER). The COP is the ratio of useful energy, which is a system's output energy to its input energy use to run the system. Conventional GCHPs have a COP of 3 to 4 (i.e., an efficiency of 300% to 400%), far greater than the theoretical 100% limit for other sources of HVAC. The COP is calculated using power or energy with the following formula [6]:

$$\mathrm{COP} = \frac{\text{total heating capacity [BTU/hr]}}{\text{power input[W]} \times 3.412[\ \mathrm{BTU/hrW}]} = \frac{\mathrm{e} + \mathrm{q}}{\mathrm{e}} \qquad \text{Eq. 4.2}$$

where e is the input electrical energy and q is the heat transferred from the ground. During the life cycle of a GCHP, electricity input is needed to run the compressor within the heat exchanger and the circulation pumps. While the COP is used to define efficiency during heating, EER is a term specifically applied to cooling (Dickie et al. 2010) and is defined as

$$\mathrm{EER}\ \left[\frac{\mathrm{BTU}}{\mathrm{hrW}}\right] = \frac{\text{total cooling load}\ \left[\frac{\mathrm{BTU's}}{\mathrm{hr}}\right]}{\text{power input [W]}} \qquad \text{Eq. 4.3}$$

High-enthalpy systems, such as Enhanced Geothermal Systems (EGS), are typically drilled very deep and used to generate electricity. GCHPs, on the other hand, are low-enthalpy systems used only for HVAC, ranging from 23 m to 150 m deep (Natural Resources Canada 2009). For residential use, boreholes are rarely deeper than 100 m, since borehole depth is limited by the increased difficulty and cost of drilling into bedrock layers. The deep single borehole (SING) system, proposed by a drilling contractor in Wisconsin, is an unconventionally deep (~300 m) vertical GCHP that provides an elevated entering water temperature (EWT) to a closed-loop heat exchange system (Tinjum 2013). This higher temperature eliminates the need for antifreeze and allows the use of pure water as the loop fluid. The SING system is hypothesized to have a high COP due to elevated thermal conductivity in the bedrock layers and an increased temperature due to prolonged exposure to the natural geothermal gradient. Thus, it offers potential

advantages over conventional vertical loops, horizontal loops, and natural gas heating systems for HVAC applications. Though cost is an important factor, this study aims to explore and quantify potential environmental advantages in terms of GHG emissions over a GCHP system's lifespan. Drilling and electricity use are expected to be the key emitters, but the exact emission balance between drilling and electricity use is what motivates this study.

4.1.3 Introduction to Life Cycle Analysis (LCA)

Accurately assessing environmental impact requires a structured and widely accepted methodology. Life cycle analysis (LCA), also known as life cycle assessment was developed in the early 1990s and has become an increasingly popular methodology to evaluate environmental impacts of a product across its entire life from material extraction to end of life; i.e., from "cradle-to-grave" (SimaPro7 2010). In an age of "greenwashing" where the word "sustainability" is used carelessly, LCA uses real scientific analysis as methodology to judge a product's environmental impact rather than assumptions based on marketing or historical evidence. By explicitly defining inputs, outputs, boundaries, and assumptions, LCA develops a clear criterion from which to compare products with similar functions.

LCA implementations consist of four key stages defined by the International Organization for Standardization (ISO 14040 and 14044) (Rebitzer et al. 2004). First, the "Goal and Scope" defines parameters and boundary conditions of each study. This section assigns a "functional unit" (FU) to the product as a comparison basis to other products with a similar function. Data is collected during the "Life Cycle Inventory" (LCI) stage, in which raw materials and energy processes are defined and linked to emissions and material depletions that will occur. Next, in the "Life Cycle Impact Assessment" (LCIA) stage, the LCI results are aggregated and adjusted into midpoint and endpoint characterization categories in order to understand their environmental relevance. The final LCA stage—"Interpretation"—assesses the significance of the LCA results in the context of the goal and scope and conducts an uncertainty analysis and sensitivity analyses on the data (SimaPro7 2010).

Though a wide range of products use LCA, one of its most pivotal implementations is determining the environmental impact of energy sources, or life cycle energy assessment (LCEA). Considering increasing energy demand and the concern of global warming, global warming potential (GWP) is an important characterization category of LCA (Raadal et al. 2011). GWP is considered a midpoint category, typically quantified by GHG emissions using units of CO_2 equivalent (CO_{2eq}). Although the predominant atmospheric GHG is CO_2 (84%), methane, nitrous oxide, carbon monoxide, and fluorinated gases contribute significantly (EPA 2013). The CO_2 equivalence value of each GHG differs by analysis method.

4.1.4 Related Work

Since the 1980s, hundreds of studies have been conducted analyzing GHG emissions of energy sources and yield a wide range of results. The International Panel on Climate Change (IPCC) aggregated these papers and conducted a harmonization of the CO_2 emissions for coal, natural gas, petroleum, nuclear, wind, solar, hydroelectric, and biogas electricity production (2011). It must be noted that, while fossil fuel sources emit GHGs onsite and renewable sources do not, the emissions considered in LCEAs are both localized and delocalized and are associated with plant construction, operation, uranium mining and milling, and plant decommissioning (Sovacool et al. 2008). Since GCHPs do not directly produce electricity, they were neglected in the IPCC study.

GCHPs have been cited in industry and literature as “renewable energy,” a “green solution,” and even “carbon neutral” (Baxi 2013). Though there have been studies on GHG emissions, no extensive LCA background exists to firmly support these claims. A Europe-specific cradle-to-grave LCA on GCHPs found average GHG emissions of 63 metric tons (mt) CO_{2eq} for a lifetime of 20 years (Saner et al. 2000). This study used the Continental European electricity mix with 0.599 kg CO_{2eq}/kWh but performed case studies on specific locations. Comparing GCHPs to alternate HVAC sources showed savings ranging from -31% to 88% depending on electrical grid, location, climate, and passive-cooling capabilities. This study, as well

as a large majority of GCHP LCAs, is specific to Europe and thus results cannot be simply extrapolated to the US.

A study from the US Air Force analyzed CO_2 emissions and costs due to the electricity input of GCHPs over a life cycle in all 50 US states and compared these emissions and costs to conventional natural gas AC split systems (Fredin 2009). Average GHG emissions in Wisconsin were 329.5 mt CO_{2eq} and calculated to emit 21% more than the natural gas system. Though the Air Force study contained Wisconsin-specific data, it considers only CO_2 emissions rather than total GHG emissions and focuses only on the emissions during the operation of the GCHP rather than cradle-to-grave emissions. A third study conducted by the Energy Center of Wisconsin contrasted costs and emissions of GCHPs for five building scenarios in three regions of Wisconsin (Hackel 2009). In a residential scenario, GCHPs demonstrated CO_2 savings of 163 kg, 1,054 kg, and 15,830 kg CO_{2eq} over natural gas, propane and electricity only configurations respectively. Similar to the study by Fredin (2009), only electrical input during operation was considered. Other emissions are considered but they are calculated individually, rather than in terms of GWP. The most well established method, TEWI (Total Equivalent Warming Impact), was developed at Oak Ridge National Laboratory in the early nineties to quantify direct and indirect GHG emissions over the whole lifetime into a single number expressed in terms of CO_2 mass equivalents. One particular example from Forsen (2005) showed indirect emissions related to the generation of electricity (97.8%) are by far the largest contributor to GHG emissions. All these studies agree that GHG emissions vary primarily due to grid composition. However, to date, there has been no cradle-to-grave analysis comparing total GHG emissions of unconventionally deep GCHPs to other GCHPs configurations in Wisconsin.

4.2. MATERIALS AND METHODS

4.2.1 Goal and Scope

The main goals of this study are the following:

1. Determining GHG emissions from the Deep Single Borehole (SING) GCHP system in Wisconsin (note: emissions are not localized, but rather attributed to energy processes during the life cycle)
2. Comparing GHG emissions over the lifecycle of
    a. a conventional vertical GCHP configuration with three boreholes (VERT)
    b. a conventional horizontal GCHP (HORZ)
    c. an unconventionally deep single borehole (SING)
    d. a conventional split system natural gas air conditioning unit (NGAC)
3. Determining the top contributors to these emissions

These goals are accomplished by performing a "cradle-to-grave" LCA to trace the energy flows and resources for all stages of the life. Historically, LCAs were conducted using simple equivalence equations (i.e., TEWI). With the addition of many materials and iterative looped processes, it becomes increasingly more complex to trace each step. In this study, the LCA is carried out using SimaPro 7.3.3 software, a market-leading LCA software developed by the Dutch company PRé Consultants. Material and energy flows are organized according to the four LCA stages: goal and scope, LCI, LCIA and interpretation. SimaPro has direct links to LCI databases and LCIA methods.

Functional Unit and Site Description

The life cycle of a GCHP consists of flows into and out of nature and the technosphere defined by the functional unit (FU). The functional unit is the fundamental flow in which all other resource flows relate to, and it measures the function of product (SimaPro7 2010). In this study, the FU is the heat flow required to provide space heating and cooling to a single-family residence in central Wisconsin over a 25-year

period, in kWh. The house size is assumed to be 186 m^2, the median size of a single-family residence in the Midwest (US Census 2010). Although the ground loop components are predicted to have a lifetime of at least 50 years and up to 256 years according to some studies (Tarnowski and Bandauf 2007), the heat exchanger and duct system are cited to demand repairs after 25 years. With replacements of above ground parts, GCHPs have the potential for a longer lifetime, but the LCA is standard to assume a worst-case scenario life of 25 years. The site is essentially idealized but modeled around a residence near Grand Marsh, Wisconsin, where UW-Madison has recently installed a VERT system.

There are complex ways to model heating load and heat transfer from GCHP systems on a monthly, daily, and hourly basis. Adapting heating load data from a similar study using Trane Trace 2000 software, this study assumes a heating load of 14.3 kW and a cooling load of 12.7 kW (Fredin 2009). Degree days measure the number of hours per year the GCHP needs to work at full power, both in heating and cooling mode. Wisconsin's climate is heating dominated, with an average of 2,548 heating degree days (HDD) and 513 cooling degree days (CDD) based on the analysis done by Fredin (2009) Annual energy consumption is assumed to remain constant over the entire lifetime. Thus, over a 25-year lifetime, a total of 1,075,265 kWh of energy is required to heat and cool the building.

The geology at the site is comprised of overburden soils, Cambrian sandstone, and Precambrian granite bedrock with depths defined in Table 4.1 (Meyer 2013). Though not constant across the state, this is a typical stratigraphy of Wisconsin and matches the conditions at the base site in Grand Marsh.

Table 4.1 Geological strata of the site based on Grand Marsh, WI, and associated thermal conductivity of each rock formation (Kavanaugh et al. 1997, Meyer 2013)

Geological formations	Depth start (m)	λ* (W/m·K)	Average λ (W/m·K)
Overburden Soils	0 - 45	1.5 - 2.4	1.95
Cambrian Sandstone	45 - 115	2.1 - 3.5	2.80
Precambrian Granite	115+	1.9 - 5.2	3.55
* adapted from Meyer (2013) and Kavanaugh et al. (1997)			

System Description

The life cycle of GCHP system consists of five stages: production of all materials in the ground loop and heat exchanger, transportation of materials to the site, earthwork and construction onsite, operation, and disposal. These stages and main inputs are shown in Fig. 4.2.

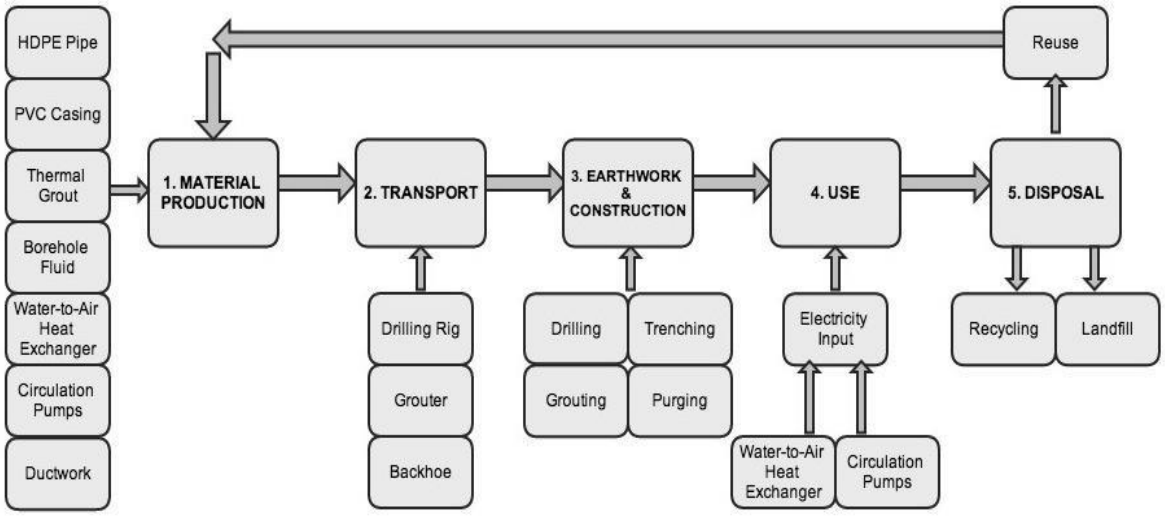

Figure 4. 2 Life-cycle stages of the deep single borehole system from material inputs to disposal and main flows of each unit process

To achieve the functional unit, the SING system is defined in this analysis as a single 361.2-m-deep well with a single HDPE U-tube, and water as the heat carrier fluid. The well is cased in PVC to 60.1 m to prevent unstable upper soil formation from caving-in and grouted to provide more contact between U-tube and surrounding soil. In heating dominated climates such as Wisconsin, trenches must be drilled below the deepest annual frost line (1.07 m in Wisconsin). In this study, a 1.5-m trench depth is used. The SING proposal couples a water-to-water heat exchanger with a water-to-air heat exchanger and a buffer tank to provide heating and cooling to air, domestic hot water use, and radiant floor heating. For simplicity, this study considers only the space heating component of SING (i.e., water-to-air heat exchanger, fan coils, and duct system) and disregards the water heating load (water-to-water heat exchanger, buffer tank, and floor coils).

To conduct a comparison, alternative scenarios are selected that fulfill the same functional unit as SING. First, a triple-well VERT model is drawn directly from the system at Grand Marsh with borehole depths of 103 m, 111 m and 148 m. Second, a typical HORZ is considered. The pipe length in the horizontal system is assumed to be equal to that in VERT. Reviewed literature cites average COPs of 3.0 for horizontal GCHPs (Wu et al. 2010, Wu et al. 2014) and 3.5 for vertical GCHPs (Hackel 2009). Additionally, the preliminary results from ongoing study of a residential VERT system in Grand Marsh, Wisconsin, confirms that four month's of heating COP of 3.2 is in acceptable range. Hence these literature values are accepted for this study. Heat exchangers and pumps are the same for all GCHPs. Since natural gas accounts for over half of HVAC energy, a natural gas furnace is used as another alternate scenario. Natural gas only provides heating, so furnaces are coupled with a typical air-to-air conditioner to comprise a NGAC split system unit.

The COP of the SING geothermal system was predicted to be as large as 5 (Tinjum 2013). A linear model is implemented based on Eq. 4.1 and Eq.4.2. Thermal conductivity λ of each system is taken to be the average of each stratigraphic layer normalized over the total length of the borehole. This method gives approximate thermal conductivities shown in Table 4.2. Assuming the input electricity is less than the heat

transfer from the ground, the COP is approximately proportional to thermal conductivity of the ground. Assuming COPs of 3.0 and 3.5 for the HORZ and VERT systems based on the literature (Wu et al. 2014, Hackel 2009) and our current real VERT GCHP operation in Grand Marsh, Wisconsin, the linear trend for SING is solved to find a COP of 4, considering a constant EWT [T_w] and maximum ground temperature $T_g$for the SING system. However, the COP is not only dependent on the linear relationship, but also on the design of SING. Deeper systems provide high EWT due to elevated thermal conductivity in the bedrock layers and an increased ground temperature due to natural geothermal gradient, which result in a higher COP. The EER of each system is assigned a value of 14.4 based on Wisconsin-specific calculations through the Air-Conditioning, Heating and Refrigeration Institute (AHRI) (Fredin 2009). Results are summarized in Table 4.2.

Table 4.2 Well depths, thermal conductivity and COP assumptions for the three GCHP systems targeted in this study

System	Well Depth (m)	Avg. Thermal Conductivity (W/m·K)	COP	EER
HORZ	1.5	2	3.0	14.4
VERT	103/111/148	2.7	3.5	14.4
SING	361	3.3	4.0	14.4

4.2.2 Life Cycle Inventory (LCI)

Life Cycle Inventory (LCI) is the data collection stage of LCA. The inventory is composed of inputs to and outputs from nature, the technosphere, and the econosphere and defines emissions to air, water, and soil (Pre Consultant 2010). In this study, input parameters and emission information were gathered from the Ecoinvent 2.2 unit process database, the world's largest and most widely accepted LCI database (Frischkrecht and Jungbluth 2007). Unit processes track the materials and sub-processes that compose a

process. Data unavailable on Ecoinvent was adapted from two other databases, Industry Data 2.0 and U.S. LCI, as well as published literature and equipment specifications.

In all LCA calculations and every database, unit processes inherently come with uncertainty. This uncertainty is due to reliability, completeness, temporal correlation, geographical correlation, further technical correlation, and sample size of data in question (SimaPro 2008), and can be modeled on SimaPro. This study assumes log-normal standard deviations of 1.50 for all material production data and an uncertainty of 2.00 for all earthwork, transportation, use and decommission data. This choice, though arbitrary itself, reflects a greater number of estimates in a process to increase its statistical uncertainty. According to SimaPro, uncertainty from technosphere flows is rarely above 2.00 (SimaPro 2008), and since inputs in this study come from the technosphere, the uncertainty choice is justified.

Material Production

Materials can be categorized by the three loops of the GCHP system: ground-loop, refrigeration-loop, and distribution-loop. Production of machines used in the earthwork and construction processes are considered negligible. Material inputs are quantified by mass and are summarized in Table 4.3. All inputs are from the Ecoinvent 2.2 database, except PVC, which is taken from the US LCI database.

HDPE pipe is typically used as the borehole U-tube and for the supply and return headers because of its durability and low cost (Dickie et al. 2010). This study uses SDR 11 5.1 cm HDPE pipes. Since 5 m to 6 m spacing is recommended between boreholes (Kavanaugh and Rafferty 1997), header lengths are assumed as 6.71 m for SING and longer for VERT; pipe mass is calculated accordingly. In all cases, tap water is used as the heat carrier fluid and required mass is computed from pipe length. The Grand Marsh wells are cased in PVC to increase system strength and reduce the heat loss in the upper, less-thermally conductive regions of the well. PVC is typically chosen because it is lightweight, resistant to corrosion, inexpensive, and relatively easy to install. Other common casing materials are carbon steel, stainless steel, concrete or no casing at all, but PVC casing is used as a worst-case scenario. 61 m of Schedule 40 20.32

cm PVC casing are inserted into each well during drilling. Below 61 m, the borehole has no casing and is drilled with a diameter of 0.15 m.

In Wisconsin, boreholes are required to be backfilled with thermal grout (Dickie et al. 2010). Grouting serves two primary functions: to fill the hole with a seal to limit groundwater contamination and to enhance thermal conductivity and heat transfer between the heat carrier fluid and the surrounding soil. Historically, grouts have been pure bentonite clay or cement, but grouts are evolving to include a mixture of silica sand, bentonite, amendments such as graphite, and water; with ratios dependent on the target thermal conductivity. This study uses a 1:4:2.9 ratio of Thermal Grout Lite bentonite to silica sand to water to achieve a target thermal conductivity of 1.52 W/m·K (WaterFurnace 2012). Grout is calculated to fill all empty space between the borehole and the HDPE pipe.

The refrigeration loop consists of circulation pumps and a water-to-air heat pump. Two stainless steel Grundfos 15-55SF/LC circulation pumps are used and mass are assumed to be 100% stainless steel. This study uses a WaterFurnace Envision Geothermal/Water Source Heat Pump, model NDV038, with an R-410A scroll compressor, air coils, and a blower (WaterFurnace 2012). Heat pumps are composed primarily of sheet steel, galvanized steel, copper, a refrigerant, and water. Considering heat pump and fan coil inputs from a LCA study by Shah et al. (2008), the mass of the WaterFurnace heat pump is multiplied by a correction factor to estimate the material inputs as shown in Table 4.3. The NGAC system has no ground-loop components and uses a natural gas furnace and standard AC unit rather than a heat pump. Input values are taken from the study done by Shah et al. (2008) justified due to similar site conditions: a 181.2 m^2 residence occupied by a single family. WaterFurnace and the AC use R-410a, a zeotropic refrigerant blend of 50% R-32 and 50% R-125. R-134a is available in the EcoInvent 2.0 database and is similar to R-410a in many regards. Both refrigerants are replacements for R-22a and have no contribution to ozone depletion. According to ANSI/ASHRAE (2010), R-134a has a GWP of 1300 (i.e. 1300 kg CO_{2eq}) and R-410a has a GWP of 1730 (Sand et al. 1991, McQuay 2002), so R-134a is used with a correction factor of

1730/1300. Although some sources claim that refrigerants must be changed annually due to leakage (Forsen 2005) change is assumed unnecessary.

Lastly, heated or cooled air is distributed for both GCHP and NGAC scenarios from the fan coil unit to the residence through a duct network along the ceiling and floors. The duct system in this study is also adapted directly from the study by Shah et al. (2008), with 0.76 mm galvanized steel sheets and 50 mm fiberglass insulation.

Transport

LCI's must account for the transportation of all materials and construction equipment to the site, which is taken to be Grand Marsh, Wisconsin. In this study, the origin of some materials are known and others are not. Bentonite comes from Mills, Wyoming, silica sand from Portage, Wisconsin, and the WaterFurnace heat exchanger was manufactured in Fort Wayne, Indiana. When origin is unknown, this study assumes a transport distance of 100 km. Transport is assumed by truck for all inputs except for the heat exchanger, which travels 675 km by rail and then the rest of the way by truck. Transport values are input to SimaPro using tonne-km (tkm) units, which is equal to the mass of the object in metric tonnes (mt) multiplied by total transport distance in kilometers.

Earthwork and Construction

The primary energy processes in GCHP installation are trenching the site, drilling the borehole(s), grouting the borehole(s), and purging air out of the system. Densities, energy densities and specific energies of fuels were taken from the Wolfram Alpha online database. For electricity processes this study does not take into account the grid at each material production site but rather assumes the grid incorporated into SimaPro. Equipment specifics and fuel use are taken from the actual construction process at the base site in Grand Marsh.

During the trenching process, a backhoe is used to dig a trench to install the boreholes. For best results, the fluid should leave the borehole at a lower depth than it enters the mechanical room. HDPE pipes must be covered by deep soil in order to minimize effect of climate on fluid temperature. Ease of trench digging is a variable of soil compaction and soil type. The Grand Marsh scenario is considered, where a New Holland LB90B backhoe (75 kW diesel engine) spent 5.5 hours trenching an area of approximately 1.858 m^2. The following equation is used to estimate E_t, the energy required for trenching, in all scenarios:

$$E_{t-GCHP}\,[MJ] = 5.5\ hr \times HP_{eng} \times \frac{2.682\ MJ}{HPhr} \times \frac{A_t\,[m^2]}{1.858\ m^2} \qquad \text{Eq. 4.4}$$

where HP_{eng} is the horsepower of the engine [HP] and A_t the area of the trench $[m^2]$. The trench required for SING is approximately one third the size of that required for VERT, and A_t = 185.8 m^2 for HORZ. In the horizontal case, groundwork consists of only trenching and no required drilling.

There are many methods to drill boreholes depending on the geology and depth required. Drilling through bedrock granite is far more energy-intensive than drilling through sandstone (DOE 2006). Using a Simco 7000 rotary drilling rig with a diesel engine, assuming Table 4.1 stratigraphy, and using fuel consumption estimates from industry, a simple linear model is developed to estimate drilling energy consumption E_d:

$$E_d\,[MJ] = \rho_{dies} Se_{dies} [0.0967\ d_{ss} + 0.680\ (d_w - d_{ss})] \qquad \text{Eq. 4.5}$$

where ρ_{dies} is the density of diesel [kg/gal], Se_{dies} the specific energy of diesel [MJ/kg], d_{ss} is the depth of the sandstone and soil composite layer [ft] and d_w the total length of the well [ft]. The difference $d_w - d_{ss}$ represents the penetration into the granite layer. The limited model assumes well depths of 23.23 m (250 ft) minimum, but is applicable here as an order of magnitude estimate. For more specific inputs, complex modelling, such as Cost of Renewable Energy Spreadsheet Tool (CREST) developed by the NREL, is suggested to balance installation and operation costs.

A grouter, in this case an 18 kW gasoline-powered GeoLoop 50-500, mixes grout and pumps it into the well through a tremie pipe. With the total volume of grout as defined in material production and a flow rate of 0.001893 m^3/s as listed in the equipment specifications (Geo-Loop Inc. 2013), the following equation determines the total gasoline F_g used:

$$F_g[\text{gal}] = \frac{HP_{eng}\,[\text{HP}] \times V_g\,[\text{gal}] \times 0.0447 \left[\frac{\text{MJ}}{\text{HPmin}}\right]}{v_g \left[\frac{\text{gal}}{\text{min}}\right] \times Se_{gas}\left[\frac{\text{MJ}}{\text{kg}}\right] \times \rho_{gas}\left[\frac{\text{gal}}{\text{kg}}\right]} \qquad \text{Eq. 4.6}$$

where $HP_{eng}$is the horsepower of the engine, V_g the volume of grout used, v_g the flow rate of grout through the tremie pipe, Se_{gas} the specific energy of gasoline and ρ_{gas} the density of gasoline. No grout is used in HORZ.

Lastly, air must be purged out of the HDPE pipes to ensure steady flow. Using a 1.5 kW Purge Pro from Geothermal Supply Co. (2013) that operates off 120-V electricity, purging energy E_p is estimated using:

$$E_p\,[\text{kWh}] = 0.7457 \times HP_{eng} \times t_p \qquad \text{Eq. 4.7}$$

where HP_{eng} is the horsepower of the engine and t_p the time spent purging. Approximately one hour is spent purging for VERT, and the same is assumed for SING and HORZ as the pipe length is the same. Pipe fusion was found to contribute only 0.001 kWh, hence smaller energy processes such as fusion are not considered. There is no significant energy processes affiliated with the NGAC system, since it only requires placement of parts by hand.

Operation

Energy inputs during the use phase consist of electricity used by the heat exchangers and circulation pumps. The site at Grand Marsh is in the process of tracking this data. For the purposes of this study, GCHP energy use is estimated with a theoretical model based on climate and building load. This model, adapted

from the study by Fredin (2009), divides the building load into heating and cooling consumption. According the model, there are four annual electricity inputs determined by the following equations:

$$\text{GCHP Cooling [kWh]} = \frac{\text{Cooling Load } \left[\frac{\text{BTU}}{\text{hr}}\right] \times \text{ CDD [hr]}}{\text{EER } \left[\frac{\text{BTU}}{\text{hrW}}\right] \times \text{ 1000 } \left[\frac{\text{W}}{\text{kW}}\right]} \quad \text{Eq. 4.8}$$

$$\text{GCHP Circ. Pump Cooling [kWh]} = \frac{\text{Pump Power [W]} \times \text{ CDD [hr]}}{\text{Motor Efficiency [\%]} \times \text{ 1000 } \left[\frac{\text{W}}{\text{kW}}\right]} \quad \text{Eq. 4.9}$$

$$\text{GCHP Heating [kWh]} = \frac{\text{Heating Load } \left[\frac{\text{BTU}}{\text{hr}}\right] \times \text{ HDD [hr]}}{\text{COP } \times \text{ 3145 } \left[\frac{\text{BTU}}{\text{kWh}}\right]} \quad \text{Eq. 4.10}$$

$$\text{GCHP Circ. Pump Heating [kWh]} = \frac{\text{Pump Power [W]} \times \text{ HDD [hr]}}{\text{Motor Efficiency [\%]} \times \text{ 1000 } \left[\frac{\text{W}}{\text{kW}}\right]} \quad \text{Eq. 4.11}$$

Energy loads and degree days are used from previous study done by Fredin (2009) and COP's are used from Table 4.2. Motor efficiency is taken as 88% (WaterFurnace 2012) and combined circulating pump power 50 W (GroundAlpha 2013). Solving and adding up Eq. 4.8 – 4.11, total annual electricity input is determined and then extrapolated to the entire 25-year lifetime to define LCI inputs for the use phase shown in Table 4.3.

The natural gas air conditioning split system (NGAC) uses natural gas for heating and electricity for both air conditioning and to run the fan in the furnace. Assuming equal lifetime and equal heating and cooling loads for a natural gas system, the following equations calculate electricity and natural gas use [18]:

$$\text{NGAC Cooling [kWh elec.]} = \frac{\text{Cooling Load } \left[\frac{\text{BTU}}{\text{hr}}\right] \times \text{ CDD [hr]}}{\text{EER } \left[\frac{\text{BTU}}{\text{hrW}}\right] \times \text{ 1000 } \left[\frac{\text{W}}{\text{kW}}\right]} \quad \text{Eq. 4.12}$$

$$\text{NGAC Heating [kWh elec.]} = \frac{\text{Fan Power [W]x HDD [hr]}}{\text{Motor Efficiency [\%]} \times \text{ 1000 } \left[\frac{\text{W}}{\text{kW}}\right]} \quad \text{Eq. 4.13}$$

$$\text{NGAC Heating [kWh NG]} = \frac{\text{Heating Load } \left[\frac{\text{BTU}}{\text{hr}}\right] \times \text{ HDD [hr]}}{\text{AFUE } \times \text{ 3145 } \left[\frac{\text{BTU}}{\text{kWh}}\right]} \qquad Eq.4.14$$

where EER is taken to be 14.4, the annual fuel utilization efficiency (AFUE) of natural gas is given a mid-efficiency value of 80% motor efficiency 85% and fan power 249 W.

Electricity inputs are modeled from the current electrical grid in Wisconsin. Though it is recommended to use marginal electricity for the purpose of GCHP (Hackel 2009), for simplification, this study uses average Wisconsin electricity values from 2011 as reported by the EIA (2013) with 62.5% coal and only 5.5% renewables. These values are programmed into the SimaPro product stage database for analysis.

Disposal

After a GCHP's 25-year lifetime, several disposal scenarios are possible. Refrigeration and distribution loop components can be replaced and reconnected with the ground loop for at least one more life cycle, but worst-case scenarios of complete decommission is taken. In this scenario, water is removed from the U-tube and pipes are cut at ground level, but the rest of the system lays intact underground to allow the possibility of reuse in the future. The refrigeration and distribution loops for GCHP and NGAC are treated as explained in the study by Shah et al. (2008), with 90% of the materials by mass recycled and the remaining 10% disposed in a landfill. To input this scenario into SimaPro, a new waste scenario is modeled from "Waste Scenario US/U" from the Ecoinvent 2.2 database (Hischier et al. 2010).

Table 4.3 Life cycle inventory input materials and processes for SING, VERT, HORZ and NGAC systems

Ground Coupled Heat Pumps (GCHPs)						Natural Gas Air Conditioning (NGAC)			
Component	**Material/Process**	**Unit**	**SING**	**VERT**	**HORZ**	**Component**	**Material/Process**	**Unit**	**NGAC**
Material Production						**Material Production**			
Thermal Grout	Bentonite Grout	kg	1,100	1,450	0	NG Furnace	Steel	kg	46
	Silica Sand	kg	4,400	5,800	0		Galvanized Steel	kg	18
	Tap Water	kg	3,209	4,229	0		Aluminum	kg	9
Pipe	HDPE Pipe	kg	670	776	670		Copper	kg	3
Casing	PVC Pipe	kg	489	1,467	0	AC Unit	Steel	kg	78
Borehole Fluid	Tap Water	kg	1,562	1,562	1,562		Galvanized Steel	kg	35
Water-to-Air Heat Exchanger	Steel	kg	113	113	113		Copper	kg	17
	Galvanized Steel	kg	44	44	44		Aluminum	kg	17
	Copper	kg	14	14	14		Refrigerant	kg	6
	Refrigerant R-140A	kg	2	2	2	Ductwork	Galvanized Steel	kg	265
	Tap Water	kg	5	5	5		Fiberglass	kg	140
Circulation Pumps	Stainless Steel	kg	6	6	6	**Transport**			
Ductwork	Galvanized Steel	kg	265	265	265	All	Truck	tkm	63
	Fiberglass	kg	140	140	140	**Operation**			
Transport						NG Furnace	Natural Gas Combustion	kWh	1,189,387
All (except Heat Exchanger)	Truck	tkm	3,851	4,606	872	AC Unit	120V Electricity	kWh	57,907
Heat Exchanger	Freight	tkm	107	107	107	**Decommission**			
Earthwork & Construction						Materials	Recycle	%	90
Drilling	Diesel	MJ	70,028	26,924	0		Landfill	%	10
Trenching	Diesel	MJ	492	1,476	7,380.00				
Grouting	Gasoline	gal	0.18	0.54	0				
Purging	120V Electricity	kWh	1.5	1.5	1.5				
Operation									
Heat Exchanger	120V Electricity	kWh	276,352	310,335	355,645				
Circulation Pumps	120V Electricity	kWh	4,504	4,504	4,504				
Decommission									
Materials	Recycle	%	90	90	90				
	Landfill	%	10	10	10				

4.2.3 Life Cycle Impact Assessment (LCIA)

Life Cycle Impact Assessment (LCIA) connects each of the inventory inputs to their corresponding environmental impact. Resource and emission flows from the inventory are connected to a series of midpoint and endpoint indicators. Required LCIA structure, determined by ISO 14044, consists of: *selection* of relevant impact categories and models, *classification* of each inventory entry to impact categories, and *characterization* of these impacts using equivalence factors determined by selected assessment method (SimaPro 2010). Additionally, normalization and weighting may be applied to determine the relative impact of each category.

SimaPro incorporates dozens of impact assessment methods. This study uses the Tool for the Reduction and Assessment of Chemical and other environmental Impacts (TRACI 2), an impact assessment method developed specifically for the US by the Environmental Protection Agency (EPA) (Hischier et al. 2010). Though TRACI 2 contains a variety of midpoint impact categories, this LCA focuses only on GWP, defined as "potential global warming based on chemical's radiative forcing and lifetime" (Bare 2002). US specific characterization factors are used for CO_2 and carbon monoxide biogenic and fossil flows from the Ecoinvent database, as shown in Table 4.4.

Table 4.4 Biogenic and fossil characterization factors for CO and CO_2 used in TRACI 2, adapted from Hischier et al. 2010.

Ecoinvent name	**GWP characterization factor (kg CO_2-eq)**
Carbon dioxide, biogenic	0
Carbon dioxide, fossil	1
Carbon monooxide, biogenic	0
Carbon monooxide, fossil	1.57
Methane, biogenic	23
Methane, fossil	23

4.3 RESULTS AND ANALYSIS

4.3.1 Deep Single Borehole System

The compiled inventory of each stage of the deep single borehole (SING) system's life is assessed using global warming characterization from TRACI 2. Over its entire 25-year life cycle, the SING GCHP was calculated to emit 271,618 kg CO_2 eq. The operation phase of the heat pump is associated with the most emissions. Specifically, electricity to run the compressor in the water-to-air heat exchanger is shown significantly to be the largest contributor to global warming, responsible for over 93% of total emissions as demonstrated in Fig. 4.3. All emissions associated with electricity use are directly connected to the percentage of fossil fuels on the electrical grid.

The second largest GHG emissions contributor is the drilling of the 361.2 m borehole (2.4%). Rotary drilling rigs function by combusting diesel fuel, shown to emit 10.1 kg CO_2 per gallon (EPA 2013) and 13.9 kg CO_2 eq per gallon. As expected, drilling a deep well results in significant GHG emissions, but they are over an order of magnitude less significant than heat pump operation. The third largest contributor is the electricity to run the circulating pump during SING operation (1.5%). These emissions also correlate

to the associated emissions with the Wisconsin electrical grid. However, associated emissions are two orders of magnitude less than emissions from running the heat exchanger.

The production of system's ductwork, HDPE pipe, and PVC casing contribute 0.7%, 0.7% and 0.6% to total GHG emissions, respectively. Although these are primary contributors during the assembly of the GCHP, they are shown to be practically negligible when considered over the entire lifetime. All other factors -- production of other materials, all transportation of materials and earthwork excluding drilling contribute less than 0.3% to total emissions, and can be considered inconsequential for this study.

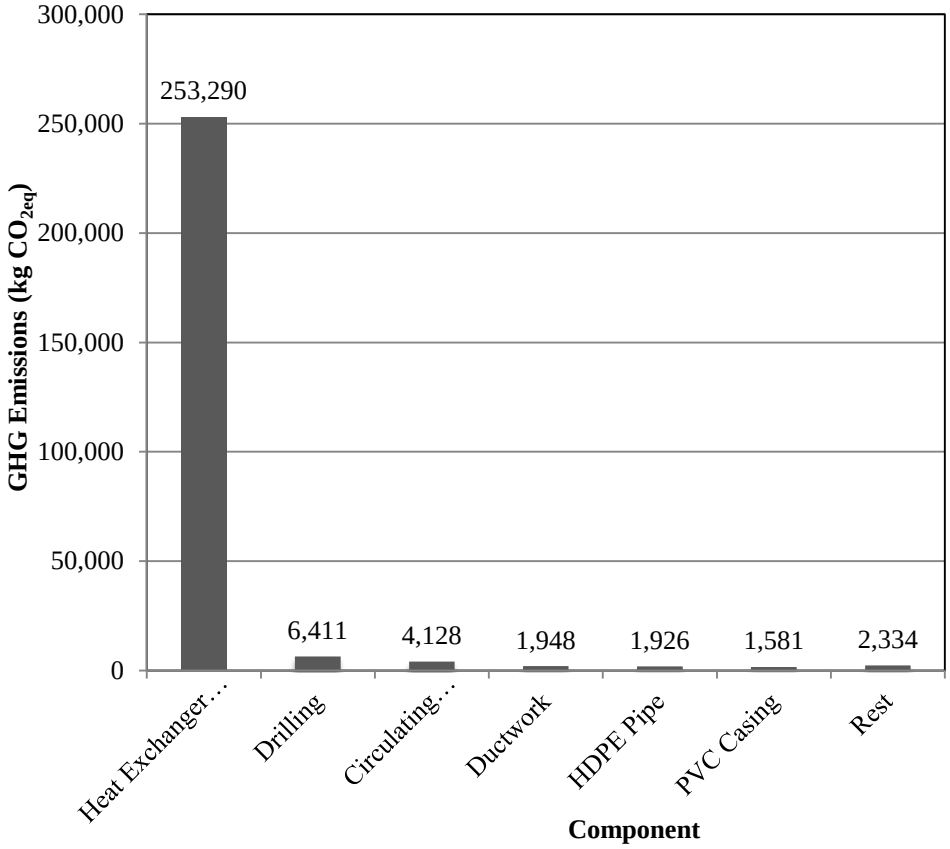

Figure 4.2 Largest contributors to total GHG emissions (271,618 kg CO_{2eq}) of the SING GCHP during the entire 25-year lifetime in order of contribution

4.3.2 Comparison to Conventional Systems

GHG emissions associated with the SING system must be compared to alternative scenarios to assess their relevance and implications. All stages of the life cycle of the two other GCHPs, VERT and HORZ, and the conventional NGAC are analyzed using TRACI 2 GWP impact assessment method and are compared to SING in Fig. 4.4

VERT has the highest emissions during material production, followed by SING, NGAC, and lastly HORZ. This is primarily due to the use of PVC to case all three boreholes, which accounts for 47% of all emissions during its material production. SING only has one borehole and HORZ has none. During earthwork and construction, as expected the SING system emits the most CO_2 eq: 40% more than VERT and 14% more than HORZ. Although VERT requires drilling and around three times more trenching, and HORZ requires around fifteen times more trenching energy, the emissions due to drilling the 361.2 m borehole in SING far exceed those due to trenching. Emissions during transportation contribute less than 5% of total emissions during assembly, so they can be considered negligible. SING emissions during material production and VERT emissions during earthwork and construction compensate, thus during assembly SING and VERT are essentially tied as the largest emitters, with SING leading by only 3%. Disposal contributes less than transportation, so it is also negligible.

The operation phase of the life cycle shows an entirely different trend. GHG emissions increase almost linearly, with SING emitting 11% less than VERT, 22% less than HORZ, and 29% less than NGAC. The emissions from the GCHPs are due directly to electricity consumption. From these calculations, the Wisconsin grid emits 0.92 kg CO_{2eq}/kWh. Since SING consumes 11% less electricity than VERT and 22% less that HORZ, and since all scenarios use the same electrical grid, these results are trivial. For the NGAC scenario, emissions during operation are due to the superposition of natural gas combustion and electricity use. Although natural gas is shown to emit 0.27 kg CO_{2eq}/kWh (71% less than the electrical grid), the NGAC

system consumes 71% more total energy than HORZ. Since some of this energy is electricity to run the air conditioner, NGAC operation cumulatively emits more.

For each scenario, emissions during operation are more than an order of magnitude greater than those in all other life stages combined. Furthermore, the emission difference between successive scenarios during operation is greater than total emissions in all other stages. Thus, over an entire lifetime, the GHG emission trend from the operation phase significantly dominates. Collectively, SING saves on average 10% emissions over VERT, 19% over HORZ, and 28% over NGAC.

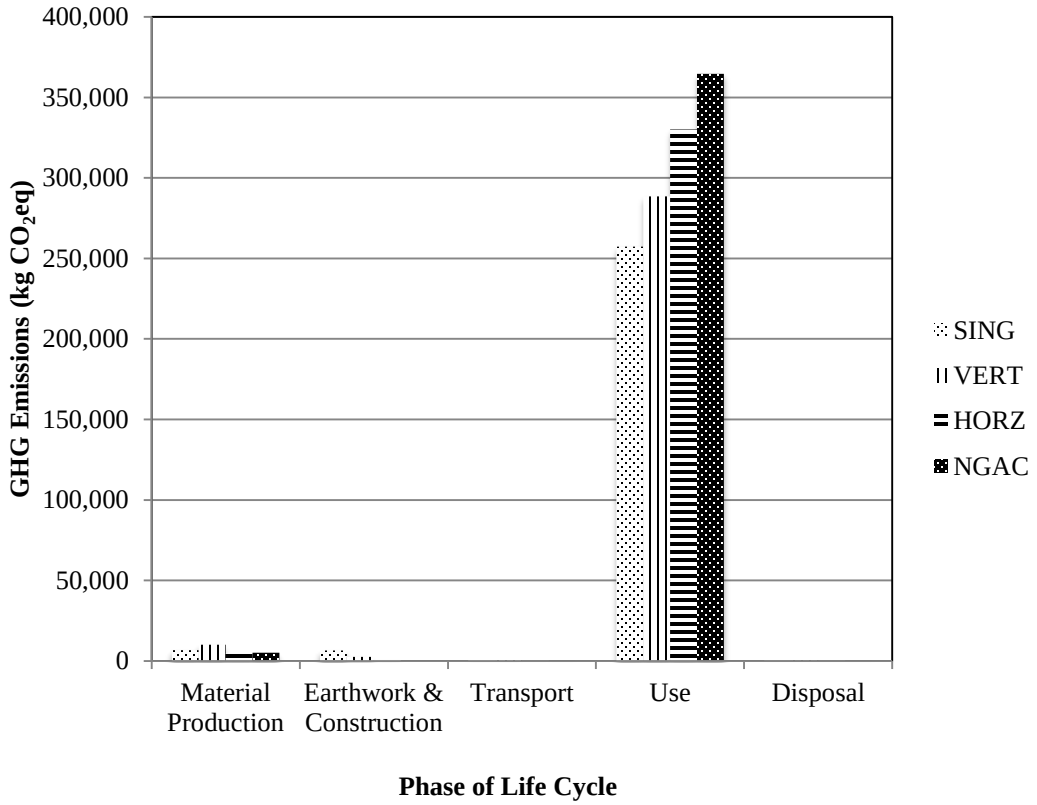

Figure 4.3 Comparison of GHG emissions during each phase of a 25-year life cycle for SING, VERT, HORZ and NGAC scenarios.

4.3.3 Uncertainty Analysis

Before drawing any conclusions based on the calculated life cycle emissions, it must be noted that LCA delivers average emission values for each system. As explained in the inventory analysis, each data entry in SimaPro is subject to some degree of imprecision. Uncertainty analysis, required in the interpretation stage of LCA, documents the effect of imprecise data on the results of the impact assessment. This allows for the comparison of the precision of different data sets. Using TRACI 2, Monte Carlo regressions are conducted on the GHG emission results from all four systems using 1,000 iterations at a confidence level of 68.3% (one standard deviation) and results are plotted in Fig. 4.5.

Accounting for data uncertainty, the maximum emissions for SING are approximately equal to the average emissions for the NGAC system and the minimum emissions for NGAC are approximately equal to the average emissions for SING. Although the average values show a near linear trend in which SING emits less than other alternatives, it can essentially be concluded that each scenario emits the same order of magnitude of GHGs. The maximum values of uncertainty were chosen for a worst-case scenario analysis, so it is possible that in reality the standard deviation is smaller and the average trend is more precise.

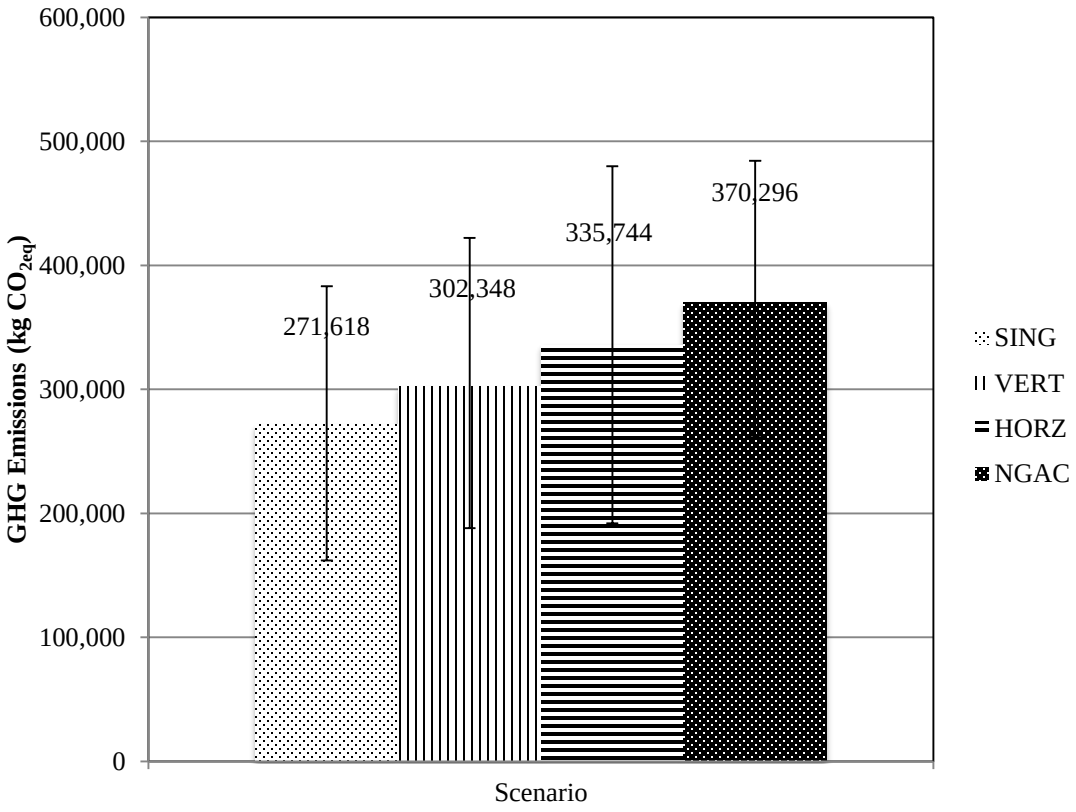

Figure 4.4 Comparison of total life cycle GHG emissions over 25-year life cycles using Monte Carlo uncertainty analysis to one sigma (68.3% uncertainty)

4.3.4 Sensitivity Analysis

In addition to uncertainty analysis, LCA interpretation requires implementation of a systematic change of input parameters to identify the most critical parameters and motivate further data collection. The following sensitivity analyses compare the SING system and the NGAC system.

The COP of a GCHP dictates the amount of electrical energy consumed by the heat exchanger. For SING, this study estimates a COP of 4. Since the operation phase is significantly the largest contributor to emissions, it is important to understand how life cycle GHG emissions change with COP. Equations 2.2 to 2.6 are manipulated for various COP values between 2.5 and 5, and an impact assessment is conducted for SING at these various COPs. Fig. 4.6 plots the associated emissions against the GHG emissions for NGAC.

The plotted values for SING resemble a power series trend, and fitting the data to a curve gives the following equation for GWP in kg CO_2 eq:

$$\mathrm{GWP} = 820{,}152(\mathrm{COP})^{-0.796} \qquad \text{Eq. 4.16}$$

NGAC is associated with emission of 370,296 kg CO_2 eq. Solving Eq. 4.16 for this value gives a COP of 2.72. Thus, SING systems with a COP greater than 2.72 should have less GHG emissions than the NGAC system. If SING was found to have a COP of 5, the value predicted in the SING as proposed, it would save 37% GHG emissions over a conventional NGAC system.

SING and NGAC emit approximately the same order of magnitude with the current Wisconsin grid. However, as per EIA, amount of renewables are projected to increase and the amount of coal is projected to decrease nationally in the following decades (EPA 2013). Political and economic pressures have pushed 27 US states, including Wisconsin, to adopt various. Renewable Portfolio Standards (RPS). Wisconsin's neighbors, Minnesota, Illinois and Ohio, all require 25% renewables by 2025 (C2ES 2013). Currently Wisconsin has 5.5% renewables, and its RPS requires 10% by 2015 (Tuerch et al. 2013). Though lawmakers have no subsequent percentage benchmarks in mind at this time, it is likely that this number will increase in the future. To conduct a sensitivity analysis to estimate the interplay between a cleaner electrical grid and GHG emissions from SING, five hypothetical grid projections are calculated up to 50% renewables in increasing increments of 10%. To simply model these projections, contributions from coal are directly replaced by contributions from wind energy and the electrical grid is taken to be constant over the entire 25-year lifetime.

Projections for the SING and NGAC systems are plotted in Fig. 4.7. With Wisconsin's RPS, SING GHG savings over NGAC should increase from 27% to 30% by 2015. Assuming a linear model, the slope for SING increases over five times faster than that of NGAC. If Wisconsin reaches a 30% renewable grid, which is in the range of RPS goal for other US states, SING could save 48% emissions. With a 50%

renewable grid, up to 68% emissions could be saved. At this point, SING and NGAC emissions are no longer on the same order of magnitude.

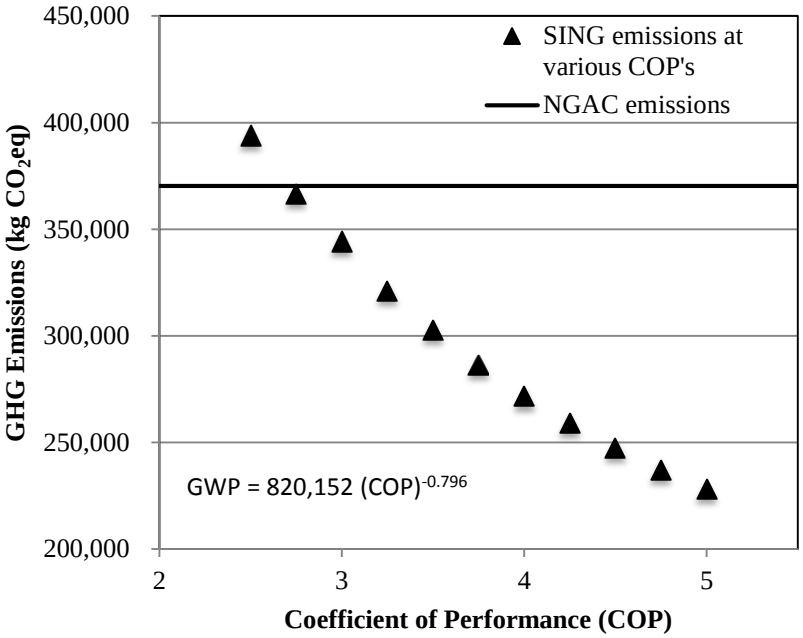

Figure 4.5 Sensitivity analysis of GHG emissions from the SING system for various COP values between 2.5 and 5 plotted against the emissions due to a NGAC system.

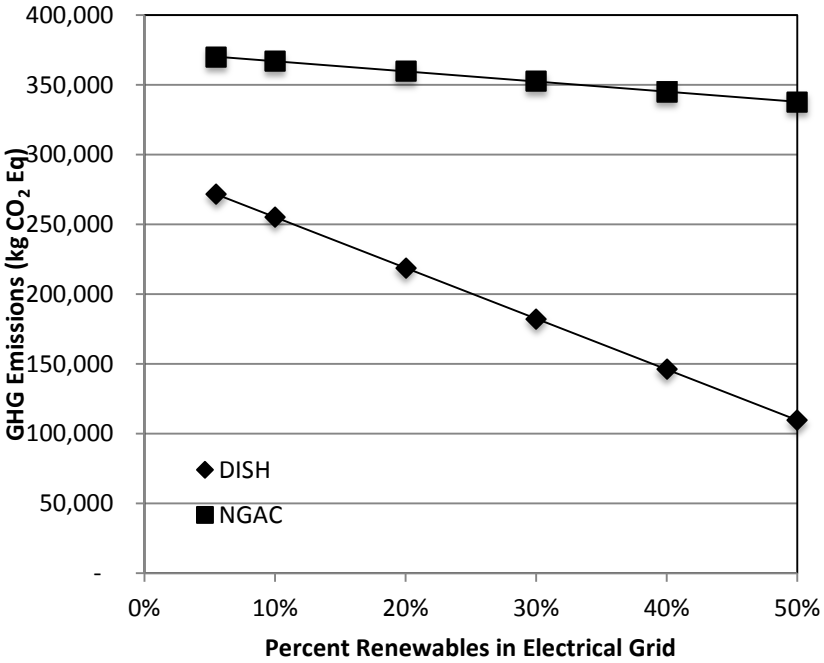

Figure 4.6 Sensitivity analysis of GHG emissions from the SING system for hypothetical grids in which energy generated from coal is replaced with energy generated from wind

4.4 Conclusion and Recommendations

GCHPs are considered environmentally friendly due to their low emission of GHGs. For conventional GCHPs, one study from Europe showed GHG emissions around 63 mt CO_{2eq} for 20-year lifetime (Saner et. Al 2000) and a Wisconsin specific study found average emissions of 329.5 mt CO_{2eq}. This study uses a comprehensive LCA to quantify the GHG emissions of SING, an unconventional GCHP with a single 361.2 m deep borehole, in a Wisconsin residence. Assuming a COP of 4.0, the SING system on average emits 272 mt CO_{2eq} over its entire 25-year lifetime, including material production, transportation of materials, earthwork and construction, operation, and disposal. The top three contributors to these emissions are electricity to operate the heat exchanger (93.3%), diesel combusted to drill the borehole (2.4%), and electricity to run the circulating pump (1.5%). In terms of emissions, the burden of drilling deep into bedrock was shown practically insignificant in comparison to electricity use during system operation.

To evaluate the significance of these emissions, SING was compared to other HVAC options. SING was shown to save 10% GHG emissions over VERT, 19% over HORZ, and 27% over a NGAC. Data indicates that GHG savings increase with deeper well configurations. However, accounting for the statistical uncertainty of inventory data, all that can be concluded is that these four systems lie within the same order of magnitude. To one standard deviation, SING emissions lie between 188 mt and 422 mt, and no GCHP system is substantially more carbon neutral than a NGAC alternative. This relationship can change with an increase in renewable energy in the grid. Assuming a COP of 5.0, SING could save 37% GHG emissions over a NGAC system. With a 50% renewable grid, SING saves 68% emissions. Other HVAC sources such as oil fired boilers emit even more GHG over their lifetime than NGAC (Saner et al. 2000) Hence, as the grid becomes cleaner all GCHPs will become the less carbon intensive option.

For a single unit, the SING saves less than 100 mt CO_{2eq} over a lifetime, which alone is negligible. A thought experiment was conducted to scale emissions savings up to the entire state. It is supposed that

all NGAC systems in Wisconsin are immediately replaced with GCHP systems. Wisconsin consumes 140 Trillion kJ (132 Trillion BTU) annually for HVAC purposes alone (EIA 2009). According to Fig. 4.1, 55.4% of this energy use is attributed to natural gas. This would account for around 450,000 NGAC systems in the state. Replacing each of these with a GCHP would save 1.8 million mt of GHG emissions from entering the atmosphere annually and reduce Wisconsin's GHG emissions by 1.5%. Furthermore, assuming the entire US had Wisconsin's climate, ground conditions and grid, emissions are scaled up to the entire US population to find GHG savings of 97.5 million mt CO_{2eq}. Making this change could also reduce national emissions by 1.5% and thus global emissions on the order of 0.3%.

This study is a fundamental framework and order of magnitude estimate to determine whether or not GCHP are a feasible heating and cooling solution specifically in Wisconsin. Certain potential problem within research methodology and assumptions must be accounted for to explain error and suggest further research. There is inherent uncertainty in SimaPro databases caused by model choices and incompleteness of data sets that cannot be accounted for statistically. The EcoInvent database is specific to Switzerland and many other inputs are based on European data. The real lifetime of a NGAC system is estimated as 20 years, so the 25-year lifetime assumed this study is a best-case scenario for NGAC (Shah et al. 2008). This study estimates 25 years into the future, yet assumes static conditions. In reality, there is a complex interplay of variables; the COP may vary over the lifetime due to heat depletion and climate fluctuations as the grid becomes cleaner and technological innovations improve. Determining how these variables interact could be a motivation for a future study.

Ultimately, the results of this study will be used to create an interactive spreadsheet for Wisconsin contractors and homeowners to determine GHG emissions of GCHP systems, allowing analysis to compare varying input parameters such as system type, borehole length, ground conditions, building load and climate. For a follow-up study, the most important revision main point should be determining energy consumption and SING's COP to greater precision. Since electricity use is the most significant contributor

to emissions, this data needs to be the most precise. The only way to measure electricity use with complete accuracy is to physically run the GCHP and explicitly measure the power intake of each piece of equipment and the heat transferred from the ground. It is also suggested to use building energy simulation tools such as Trane Trace or TRNSYS to determine building load, COP, and electricity input. Next, comprehensive programming should be implemented to connect the spreadsheet directly to SimaPro or incorporate the relevant GHG emission metrics directly into a database. When designing low-carbon energy solutions, GHG emissions are just one of many factors to consider. Coupling of a life cycle cost analysis (LCCA), perhaps including potential carbon taxes on emission savings, would strengthen this study and further analyze the feasibility of implementing the SING system or GCHPs in Wisconsin.

4.5 References

ASHRAE. 2010. Designation and Safety Classification of Refrigerants. American Society of Heating, Refrigerating and Air-Conditioning Engineers, Inc.

ASHRAE 2007. Geothermal Energy. ASHRAE Handbook. American Society of Heating, Refrigerating and Air-Conditioning Engineers, Inc. Atlanta, GA.

Baxi. 2013. Benefits of ground source heat pumps.

Bare J.C. 2002. The Tool for the Reduction and Assessment of Chemical and Other Environmental Impacts (Traci). Journal of Industrial Ecology, 6:49-78.

C2ES. 2013. Renewable and Alternative Energy Portfolio Standards.

Canada Mortgage and Housing Corporation. 2008. A Guide to Residential Home Heating. ISBN 978-0- 660-19848-4.

Clayton, L. 1987 Pleistocene Geology of Adams County, Wisconsin. Wisconsin Geological and Natural History Survey. Information Circular 59.

Daikin, McQuay. 2002. Refrigerants. Application Guide AG 31-007.

Dickie, E.J. 2010. Energy Exchange - Geothermal Exchange and Beyond. 3rd ed. British Columia, Canada.

EIA (Energy Information Administration). 2009. Residential Energy Consumption Survey (RECS).

EIA (Energy Information Administration). 2012. Annual Energy Outlook 2012 Early Release.

EIA (Energy Information Administration). 2011. Annual Energy Review. Washington: Department of Energy.

EIA (Energy Information Administration). 2013. International Energy Outlook 2013. Report Number: DOE/EIA-0484

Finkbeiner, M. et al. 2006. The New International Standards for Life Cycle Assessment: ISO 14040 and ISO 14044. Int J LCA 11 (2) 80 – 85.

Forse, M. 2005. Heat pumps technology and environmental impact. European Heat Pump Association & SweSING Heat Pump Association.

Fredin, P. 2009. Ground Source Heat Pumps vs. Conventional HVAC: A Comparison of Economic and Environmental Costs. Department of the Air Force Air University, Wright-Patterson Air Force Base, Ohio. Thesis.

Frischknecht, R. and Jungbluth, N. 2007. Implementation of Life Cycle Impact Assessment Methods. Ecoinvent report No. 3, v2.0. Swiss Center for Life Cycle Inventories. Dübendorf, Switzerland.

GHG Protocol. 2012. Quantifying the Greenhouse Gas Emissions of Products: PAS 2050 & The GHG Protocol Product Standard.

Geopro, Inc. 2013. Thermal Grout Lite Specifications.

Hackel, S. 2010. 10 Year Update: Emissions and Economic Analysis of Geothermal Heat Pumps in Wisconsin.

Hart, D. 2013. Personal Communication.

Hischier, R. and Weidema, Bo. 2010. Implementation of Life Cycle Impact Assessment Methods. Final report Ecoinvent v2.2 No. 3. Swiss Centre for Life Cycle Inventories, Dübendorf, CH. Retrieved from http://www.ecoinvent.org/fileadmin/documents/en/03_LCIA-Implementation-v2.2.pdf.

Ingersoll, L. R., Zobel, O. J., and Ingersoll, A. C. 1954. Heat Conduction with Engineering, Geological and Other Applications. New York: McGraw-Hill.

IPCC (International Panel for Climate Change). 2011. Annex II: Methodology. In IPCC: Special Report on Renewable Energy Sources and Climate Change Mitigation.

Kavanaugh, S., Rafferty, K., and Geshwiler, M. 1997. Ground-source heat pumps: Design of geothermal systems for commercial and institutional buildings. Atlanta: *American Society of Heating, Refrigerating and Air-Conditioning Engineers*.

MIT (Massachusetts Institute of Technology) and US DOE (Department of Energy). 2006. The Future of Geothermal Energy: Impact of Enhanced Geothermal Systems (EGS) on the United States in the 21st Century. Massachusetts Institute of Technology, Cambridge, MA.

Natural Resources Canada. 2009. Heating and Cooling with a Heat Pump. Office of Energy Efficiency.
PRé Consultants. 2010. Introduction to LCA with SimaPro 7.

PRé Consultants. 2008. SimaPro Database Manual.

Raadal HL, Gagnon L, Modahl IS, Hanssen O. 2011. Life cycle greenhouse gas (GHG) emissions from the generation of wind and hydro power. *Renewable and Sustainable Energy Reviews*, 15: 3417–3422.

Rafferty, K. 2000. Design Issues in the Commercial Application of GSHP Systems in the U.S. Geo-Heat Center Bulletin.

Sand, J.R., S.K. Fischer, and V.D. Baxter. 1997: Energy and Global Warming Impacts of HFC Refrigerants and Emerging Technologies. Arlington, VA, USA.: U.S. Department of Energy and AFEAS.

Saner, D., Juraske, R., Kubert, M., Blum, P., Hellweg, S., Bayer, P. 2010. Is it only CO_2 that matters? A life cycle perspective on shallow geothermal systems. *Renewable and Sustainable Energy Reviews* 14:1798–1813.

Shah, V.P., D. Col Debella and R.J. Ries. 2008. Life cycle assessment of residential heating and cooling systems in four regions in the United States. *Energy and Buildings*, 40 (4), 503-513.

Sovacool, B.K. 2008. Valuing the greenhouse gas emissions from nuclear power: A critical survey. *Energy Policy*, 36, 2940-2953.

Tarnowski, C. and S. Baldauf. 2006. Ageing resistance of HDPE-geomembranes – Evaluation of long-term behavior under consideration of project experiences. Retrieved from http://www.gseworld.com/content/documents/articles/Ageing%20resistance%20of%20HDPE-geomembranes.pdf.

Teurck, D.G., P. Bachman and M. Headman. 2013. WPRI Report: The Economic Impact of Wisconsin's Renewable Portfolio Standard. The Wisconsin Policy Research Institute Report vol. 26 no. 4: March Retrieved from http://www.wpri.org/Reports/Volume26/Vol26No4/Vol26No4.pdf.

Tinjum, J. 2013. Personal Communication.

US Census. 2010. Median and Average Square Feet of Floor Area in New Single-Family Houses Completed by Location.

US DoS (Department of State). 2007. Fourth Climate Action Report to the UN Framework Convention on Climate Change: Projected Greenhouse Gas Emissions. Washington, DC, USA.

US EPA (Environmental Protection Agency). 1993. Space Conditioning: The Next Frontier. Office of Air and Radiation, 430-R-93-004. Washington, DC.

US EPA (Environmental Protection Agency). 2013. Inventory of U.S. Greenhouse Gas Emissions and Sinks:1990–2011. Washington, DC. Retrieved from http://www.epa.gov/climatechange/Downloads/ghgemissions/US-GHG-Inventory-2013-Main-Text.pdf.

Walker, B. 2013. Personal Communication.

Water Furnace International, Inc. 2012. Envision Series NDV038 Specification Catalog. Fort Wayne, IN: *Water Furnace International*, Inc.

Wisconsin State Climatology Office. 2013. Wisconsin Winter Climate.

Wu, Y., G. Gan Guo-hui and A. Verhoef. 2010. Experimental measurement and numerical simulation of horizontal-coupled slinky ground source heat exchangers. *Applied Thermal Engineering*, 30 (16): 2574–2583.

Wu, R., Tinjum, J., and Likos, W. 2014. Coupled thermal conductivity dry-out curve and soil-water characteristic curve in modeling of shallow horizontal geothermal ground loops. *Journal of Geotechnical and Geological Engineering*, 33 (2), 10706-014.

CHAPTER 5- CONCLUSIONS AND RECOMMENDATIONS

This study is organized that detailed conclusions are given for each aspect of the work in Chapter 3 and 4. Further, a detailed literature study (Chapter 2) was conducted on the design and simulation tools for modeling the vertical-ground heat exchangers (GHXs) used in ground-coupled heat pump (GCHP) systems, which compared of different numerical methods (e.g. Finite-difference method, Finite-element method, and Finite-volume method) that have been used for modeling the heat transfer process in the GHX and in the surrounding geological formations (Chapter 3). Here, we will briefly summarize the work and the most important conclusions and recommendations associated with the numerical model developed herein, and the environmental life cycle assessment (LCA) of GCHPs.

Model Development

As a preliminary computational model, one-year of cumulative thermal response of the ground around a vertical ground heat exchanger (GHX) operating in both heating and cooling modes was simulated using a finite-element method in conjunction with ABAQUS, as described in Section 3. The purpose of this study was to observe changes that would occur in the soil temperature when a 300-m-deep borehole embedded through varying lithologies was exposed to a constant heat load. The monthly averaged surface temperature change and the natural geothermal gradients were considered and applied as boundary conditions. The modeling results reveal that deep GHXs may be more efficient in heating- dominate applications because it takes advantage of the geothermal gradient and is less sensitive to seasonal temperature change that shallow GHXs are more exposed to. The ground temperature profiles along the borehole vary significantly due to lithology changes; therefore, the lithology change along the length of GHX s should be taken into consideration for designing the GHXs. The line-source (LS) method by Ingersoll (1954) has been deemed the most valid analytical approach for the heat transfer process of GHXs and thus was used to validate our computational model. However, the actual borehole heat load depends on the thermal resistance between the fluid, which circulates through the GHXs, and the grout in the borehole,

in addition with changes with time and depth. Thus, to account for the variations in borehole heat load, more complex numerical analyses including axial convective heat transport due to fluid flow in the GHX pipe as well as conduction processes in the borehole components and surrounding ground became the next level of complexity in our models.

An advanced three-dimensional (3D) transient computational fluid dynamic model (CFD) was created to more accurately account for the fluid conditions. This model was validated with previous experimental and analytical studies done by Erol and François (2014). Although 3D modeling provides an explicit representation of the entire borehole and GHXs within 1 m^3 volume, the computational time was dramatically increased (i.e., 72 h for 50h simulation). Because the actual length of GHXs and surrounding ground is large, development of an improved 3D model that is computationally effective would be necessary for future modeling efforts.

A two-dimensional (2D) model was simulated using the same numerical method as that of 3D model as mentioned above. This 2D model is equivalent to the 3D model of one meter depth and with adiabatic upper and lower surfaces. The fluid flow was not explicitly modeled, rather the constant fluid temperature was applied at the pipe walls. The results from 3D model were compared with this 2D model. Our findings show strong agreement between temperature profiles along the radial distance (from borehole center to border of the surrounding ground). This justification significantly increased the computational efficiency and became a motivation to improve our 2D model.

We improved the 2D by accounting for the temperature gradient along the GHX length in addition to dynamic fluid conditions, which implies the fluid temperature change under the heating and cooling loads being applied to borehole by fluid. We validated our model experimentally using data collected from 4-months of operation at an active, instrumented residential GCHP application in Grand Marsh, WI.

We developed a 2D model that represents the actual operating district-scale borefield at Epic in Verona, WI. This model considered groundwater flow conditions. A long-term (20-yr) energy balance between the actual design heating/cooling loads and the surrounding ground were assessed from the

sustainability point of view for commercial GCHPs. Total heating and cooling loads were applied as volumetric heat generation sources to a 2D district-scale model.

From the 2D district-scale transient model, we found that the heat applied to the borefield model was unable to dissipate efficiently from the borefield to the surrounding ground. Although the boreholes were not explicitly represented in this model, but rather assumed as pure conduction, heat accumulated in and nearby the borefield, thus resulting in high ground temperatures. Interestingly, the effect of thermal properties of the surrounding ground was found insignificant for the district-scale borefield in contrast to a model for a single borehole within an infinite surrounding medium. This revealed that the thermal interaction occurring between boreholes creates a short-circuit, resulting in huge local resistance. Additionally, because the cooling load of the system is higher than the heating load, the ground temperature never reaches thermal equilibrium and continues to increase over the modeled time span of 20 years. Further, the associated COP analysis showed that the temperature rise in the ground increased the entering water temperature, dramatically reducing the efficiency of the heat pump. Therefore, we next worked toward developing solution strategies for the overheating problem in the existing borefield.

To meet this end, we coupled an improved 2D single borehole model from Section 3 with our 2D district-scale borefield model using the same heating and cooling building loads because the improved 2D model has the ability to simulate dynamic fluid conditions in the pipe. The associated COP was estimated. The results from this combined model were compared with the 2D district-scale model and a strong agreement between ground temperature and entering water temperature was found. Therefore, our improved 2D single borehole model was then used to develop various cooling strategies due to its computational efficiency. We found that cold water (3 ^{o}C) circulation from the end of March to mid-April was the most feasible solution for achieving ground temperature equilibrium; however, this alone was not sufficient to provide a complete energy balance in the ground. We found that we could achieve a fully balanced thermal condition when we doubled the heat extraction during December, January, February and March of the first year and then circulated cold water during the same 4 months of the second year.

Environmental Life Cycle Assesment of Ground Source Heat Pump System

To evaluate the environmental impacts of GCHP systems, a life-cycle assessment (LCA) was performed using market-leading software (Sima-Pro). CO_2 emissions from different types of GCHPs including vertical, horizontal, and vertical but unconventionally deep (~300 m) ground heat exchangers were simulated and compared with conventional heating and cooling system. With the current Wisconsin electrical grid containing 5.5% renewables, heating and cooling loads at 186 m^2 residence, a coefficient of performance (COP) of 4 and a 25-year lifetime, an average of 272 metric ton CO_2 equivalent emissions was calculated for the unconventionally deep GHX. Top contributors were heat-exchanger operation (93.3%), borehole drilling (2.4%), and circulation pump operation (1.5%). Sensitivity analyses determine that a grid with renewables penetration of 50% could save an additional 68% GHG emissions over natural gas. As the use of fossil fuel decreases and the grid becomes cleaner, GCHP systems become even more beneficial from the perspective of lifetime GHG emissions. A COP of 5 could further reduce GHG emissions by 38%, indicating that the COP is a significant factor in calculating the environmental impacts.

Recommendations

The 2D, transient finite-volume model of a ground heat exchanger is a significant improvement over current computationally intense 3D numerical models. In this model, thermal effects of GHX pipes (such as grout and dynamic fluid conditions) on heat transfer as well as the impact of the surrounding ground's thermo-physical and hydrogeological conditions (e.g., groundwater flow) are considered.

2D district-scale modeling of predesigned heating and cooling loads for over 20-years of GCHP operation may be less accurate. Use of additional research utilizing the data collected from an actual operating borefield may ensure enhanced accuracy for long-term sustainability assessment.

The improved 2D single borehole model is limited to conditions with no groundwater flow. The pre-existing 2D model can be improved by including groundwater flow through the system. This may be achieved by using periodic boundary conditions in CFD using an external code, user defined function. As presented in this study, a significant impact from groundwater flow (40 % less temperature rise compare to

one with no groundwater flow) on the heat transfer process in a district-scale borefield can be accounted for.

Generalized dimensionless solutions for a single borehole and for a multi-borehole fields can be beneficial for utilizing the developed 2D model herein to make it suitable for any type of design. System optimization is highly recommended in terms of design and geological conditions (such as number of boreholes, their configuration (e.g. interval, length), and direction of groundwater flow, present of discontinues in the formation (e.g. fractures)), with the goal of minimizing the thermal impact to the ground as a way to avoid extreme temperature anomalies and improve system performance over the lifetime of GCHP systems. These analyses will then allow for an estimation of the energy balance needed to quantify the effects that the GCHPs will have on the surrounding ground temperature while in operation.

Testing different scenarios while considering the sensitivity of the entering fluid temperature, the heat exchange rates as they relate to geological factors (ground thermal conductivity and ground thermal gradient), and design specifications (grout and pipe thermal conductivity) with this model provides promising research for future assessments. The interpretation of the results and the parametric studies performed will help the engineering community develop simplified solutions based on proper physical formulations.

In the future, it would be beneficial to couple a life-cycle with a cost assessment (LCCA) to gain a true understanding of the cost-to-benefit metrics for the GCHP systems, particularly for the engineering communities having commercial GCHP systems design. To analyze the life-cycle costs with regard to capital, the annual and periodic costs will strengthen the feasibility of implementing GHXs in Wisconsin. A COP directly depends on the temperature of the entering fluid temperature. A more accurate COP calculation would provide a more accurate estimation of the electricity used during the heating and cooling period. Using the current field conditions at the Epic site, a time-dependent (i.e., daily, monthly) COP should be calculated as a direct input in LCA and LCCA for accurate future assessments.

CHAPTER 6- REFERENCES

ABAQUS.(2012). Theory Manual 6.12 Heat Transfer 2.11. Retrieved from online web site: http://abqdoc.byv.kth.se:2080/v6.12/books/stm/default.htm.

ANSYS. (2012). ANSYS FLUENT Theory Guide.http://www.ansys.com. Canonsburg, PA: SAS IP.

Arash Mohammadi and Ali Jazayeri. (2012). Numerical Simulation of Combustion in Porous Media. Computer and Information Science.

ASHRAE. (1995b). Commercial/Institutional Ground-Source Heat Pumps Engineering Manual. Caneta Research Inc., *American Society of Heating, Refrigerating and Air-Conditioning Engineers.*

ASHRAE. (2007). Geothermal Energy.ASHRAE Handbook. HVAC Applications. *American Society of Heating, Refrigerating and Air-Conditioning Engineers.*

A. Demirci, K. Gorgulu, Y.S. Duruturk. (2004). Thermal conductivity of rocks and its variation with uniaxial and triaxial stress. *International Journal of Rock Mechanics & Mining Sciences*, 41,1133-1138.

A.M. Gustafsson, L.Westerlund, G.Hellstrom. (2010). CFD-Modeling of NAtural Convection in a Groundwater-filled Borehole Heat Exchanger. Applied Thermal Engineering, 30. 683-691.

ASTM C177. (1985). Standart test method for steady-stateheat flux measurements and thermal transmission properties by means of the guarded-hot-plate apparatus.

ASTM C518. (1991). Standart test method fro steady-state heat flux measurements and thermal transmission properties by means of the heat flow meter apparatus.

ASTM. (2009). E1225, Standard Test Method for Thermal Conductivity of Solids by Means of the Guarded-Comparative-Longitudinal Heat Flow Technique. ASTM International. *ASTM International.*

Attig, J. W., Bricknessl, M., Carson, E. C., Clayton, L., Johnson, M. D., Mickelson, D. M., & Syverson, K. M. (2011). Glaciation of Wisconsin: Educational Series 36, Fourth edition. Madison, WI: Wisconsin Geological and Natural History Survey.

Bernier MA, Pinel P, Labib R, Paillot R . (2004). A multiple load aggregation algorithm for annual hourly simulations of GCHP systems. *HVAC&R Res* , 10(4):471–87.

Birch, R. and H. Clark. (1940a). The thermal conductivity of rocks and its dependence upon temperature and composition. *American Journal of Science*, 529-558.

Blackwell, D. D., Negraru, P. T., and Richards, M. C. (2007). Assessment of the Enhanced Geothermal System Resource Base of the United States. *Natural Resources Research*, 283-308.

Bose, J. E. (1984). Closed Loop Ground Coupled Heat Pump Design Manual. Engineering Technology Extension Oklahoma State University.

Bakker, A. (2002). Applied Compututional Fluid Dynamics. http://www.bakker.org.

Cengel, Y. A. (2007). Heat and Mass Transfer 3rd ed. New York: The McGraw-Hill Companies, Inc.

Chiasson, A. D. (2012). Thermal Response Testing Of Geothermal Wells For Downhole Heat Exchanger Applications. Thirty-Seventh Workshop on Geothermal Reservoir Engineering, Stanford University, Stanford, California, January 30 - February 1, 2012.

Clauser, C. Huengens, E. (1995). Thermal conductivity of rocks and minerals. Washington, DC.: In A Handbook of Physical Constants, Rock Physics and Phase Relations; Ahrens, T. J., Ed.; AGU:.

Colburn, A. (1933). Trans. Am. Inst. Chem. Eng.

C.K. Lee and H.N. Lam. (2008). Computer simulation of borehole ground heat exchangers for geothermal heat pump systems. *Renewable Energy* , Vol. 33.1286–1296.

Carslaw, H. S., and J. C. Jaeger. (1947). Conduction of Heat in Solids. Oxford, UK: Claremore Press.

Cengel, Y. A. (2007). Heat and Mass Transfer 3rd ed. New York: The McGraw-Hill Companies, Inc.

Cermak, V. (1993). Lithosphere thermal requmes in Europe. Phys. Earth Planet, 79,179-193.

Claesson, J., Eskilson, P. (1987). Conductive Heat Extraction by a Deep Borehole. Sweden: Lund University.

Claesson, J., Eskilson, P. (1987). Simulation Model for Thermally Interacting Heat Extraction Boreholes. Sweden: Lund University.

Claude Jaupart and Jean-Claude Mareschal. (2011). Heat Generation and Transport in the Earth. New York: Cambridge University Press: ISBN 9780521894883.

Clauser, C. Huengens, E. (1995). Thermal conductivity of rocks and minerals. Washington, DC.: In A Handbook of Physical Constants, Rock Physics and Phase Relations; Ahrens, T. J., Ed.; AGU.

Dickson, M. H., and Fanelli, M. (2004). What is Geothermal Energy. Pisa, Italy: *International Geothermal Association.*

Dott, R. H., & Attig, J. W. (2004). Roadside Geology of Wisconsin. Missoula, Montana: Mountain Press Publishing Company.

D. W. Waples and J.S. Waples. (2004). A Review and Evaluation of Specific Heat Capacities of Rocks, Minerals, and Subsurface Fluids. Part 1: Minerals and Nonporous Rocks. *Natural Resources Research,* 97-122.

Department of Energy. (2013). Choosing and Installing Geothermal Heat Pumps. Retrieved from ENERGY.GOV: http://energy.gov/energysaver/articles/choosing-and-installing-geothermal-heat-pumps.

Dickie, E. (2010). Energy Exchange. Canada.

Energy Information Administration (EIA). (2013). International Energy Outlook . USEIA.

Energy Information Administration. (2011). Annual Energy Review 2011. Washington: Department of Energy.

Franklin W. Schwartz and Hubao Zhang. (2004). Fundamentals of Ground Water. New Delhi: John Wiley & Sons, Inc.

Franklin W. Schwartz and Hubao Zhang. (2004). Fundamentals of Ground Water. New Delhi: John Wiley & Sons, Inc.

Gnielinski, V. (1976). Int. Chem. Eng. 16, 359.

Gehlin S. (2002). Thermal Response Test- Method Development and Evaluation. Doktoral Thesis 2002:39. Lulea University of Technology. Sweden.

Gene L. LaBerge and Paul E. Myers. (1983). Precambrien Geology of Marathon County, Wisconsin. Madison, W: Wisconsin Geological nad Natural History Survey .

Gueguen, Y. and Palciauskas, V. (1994). Introduction to the physics of rocks. New Jersey: Princeton University Press.

H. Zeng, N. Diao, Z. Fang. (2002). A finite line-source model for boreholes in geothermal heat exchangers. *Heat Transfer Asian Res*. 31, 558-567.

H. Zeng, N. Diao, Z. Fang. (2003). Heat Transfer Analysis of boreholes in vertical ground heat exchanger. *International J. Heat Mass Transfer*, 4467-4481.

Hart, D. P. and Couvillion, R. (1986). Earth Coupled Heat Transfer. *Publication of the National Water Well Associatio*n.

H. F. Wang and M. P. Anderson. (1982). Introduction to groundwater modeling: Finite difference and finite element methods. Freeman and Co, 237 pp.

Hart, D. P. and Couvillion, R. (1986). Earth Coupled Heat Transfer. Publication of the National Water Well Association.

Hellstrom, G. (1991). Ground Heat Storage. Thermal Analysis of Duct Storage Systems. Lund, Sweden: Part I Theory. University of Lund, Department of Mathematical Physics.

Holman, J. (1992). Heat Transfer, 7th ed. New York: McGraw-Hill.

http://www.cfd-online.com/Wiki/Navier-Stokes_equations. (n.d.).

Hyunjun, O. (2014). Thermal resistivity of dry-out curves for thirteen sandy soils. Master Thesis. University of Wisconsin-Madison.

I. M. Abdulagatov, Subkhanverdi N. Emirov, Zumrud Z. Abdulagatova, and Sabir Ya. Askerov. (2006). Effect of Pressure and Temperature on the Thermal Conductivity of Rocks. *J.. Chem. Eng*. Data, 22-33.

IGCHPA. (1991). .(Bose, J.E., Editor) Design and Installations Standards. Stillwater,. Oklahoma: International Ground Source Heat Pump Association.

Incropera, F.P., DeWitt, D.P., Bergman, and Lavine. (2007). Fundamentals of Heat and Mass Transfer. 6th ed. John Wiley & Sons, Inc.

Ingersoll, L. R., O. J. Zobel, and A. C. Ingersoll. (1954). Heat Conduction with Engineering,Geological, and Other Applications. New York: McGraw-Hill.

J.H. Sass, A. L. (1971). Heat flow on the western United States. Geophysic.Res.

Jun Wand, Enshen Long, Wen Qin. (2013). Numerical Simulation of Ground Heat Exchnagers based on Dynamic Thermal Boundary Contidions in Solid Zone. *Applied Thermal Engineering*, 106-115.

J.H.Ferziger, M.Peric. (2002). Computational Methods for Fluid Dynamics. Germany: ISNB 3-540-42074-6, Springer.

J.Hughes, P. (December 2008). Geothermal Heat Pumps: Market Status, Barriers to Adoption, and Actions to Overcome Barriers. Oak Ridge National Laboratory: U.S. Departmetn of Energy.

K.Nagano, T. Katsura , S. Takeda. (2006). Development of a design and performance prediction tool for the ground source heat pump system. *Applied Thermal Engineering*, 26.1578–1592.

Kavanaugh, S. (1995). A Desing Method for Commercial Ground-Coupled Heat Pumps. A*SHRA Transactions*, 1088-1094.

Kavanaugh, S., Rafferty, K., and Geshwiler, M. (1997). Ground-source heat pumps: Design of geothermal systems for commercial and institutional buildings. Atlanta: *American Society of Heating, Refrigerating and Air-Conditioning Engineers*.

Kavanaugh, S.P. and K. Rafferty. (1997). Ground Source Heat Pumps- Design of Geothermal Systems for Commercial and Institutional Building. ASHRAE .

Keene, A. K. (2012). Mitigating Ballast Fouling Impact And Enhancing Rail Freight Capacity. Madison: Master Thesis:University of Wisconsin.

Khabakhpasheva, E. (n.d.). Turbulent Flow. Thermopedia, DOI: 10.1615/AtoZ.t.turbulent_flow.

Kelvin, S. W. (1882). Mathematical and Physical Papers, II. cited by Ingersoll, et a. (1954), 41.

Kusuda, T., Achenbach, P. R. (1965). Earth Temperature and Thermal Diffusivity at Selected Stations in the U.S. *ASHRAE Transactions*, Vol. 71.

Martin, L. (1965). The Physical Geography of Wisconsin. USA: The University of Wisconsin Press.

Matthew D. Walker, Lauren L.Meyer,James M.Tinjum, David J.Hart. (2014). Thermal Property Measurement of Stratigraphic Units with Modeled Implications for Expected Performance of Vertical Ground Source Heat Pumps. *Geological and Geotechnical Engineering Journal*.

Meyer, L. (2013). Thermophysical Properties of Wisconsin Rocks for Application in Geothermal Energy. Madison: Master Thesis:University of Wisconsin.

Mohammadi, A. Jazayeri, A. and Ziabasharhagh, M. (2008). Numerical Simulation of Convective Heat Transfer in Spark Ignition Engine. Proceeding of ASME international combustion engine, Illinois, USA, April 27-30 Chicago.

Mickelson, D. N. (1974). Glacial events in North-central Wisconsin. in Knox, J.C.

Muraya, N. K. (1995). Numerical Modeling of the transient thermal interference of ertical U-tube heat exchangers. TX: Ph.D. Thesis, Texas A&M University, College Station.

Muraya, N. K., D. L. O'Neal and W. M. Heffington . (1996). Thermal Interference of Adjacent Legs in a Vertical U-Tube Heat Exchanger for a Ground-Coupled Heat Pump. *ASHRAE Transactions*, 102(2):12-21.

N. Diao, Qinyun Li, Zhaohong Fang. (2004). Heat transfer in ground heat exchangers with groundwater advection. *International Journal of Thermal Sciences* 43, 1203-1211.

Ozbek, H. (1976). Thermal conductivity of multi-fluid saturated porous media. University of California Berkeley: Ph.D. Thesis.

P. Wang, P. Qin. (2011). CFD modeling of ground source heat pump exchanger and experimental verification. *IEEE*, 2050-2053.

Petukhov, B. S. and J.P. Hartnett, Eds. (1970). Advances in Heat Transfer. New York: Academic Press.

P.M. Congedo, G. Colangelo, G. Starace. (2012). CFD simulations of horizontal ground heat exchangers: A comparison among different configurations. *Applied Thermal Engineering*, 33-34.

R.Al-Khoury, T. Kolbel, R.Schramedei. (2010). Efficient Numerical Modeling of Brehole Heat Exchanger. *Computers and Geosciences*, 36.1301-1315.

R.W.Fox and A.T.McDonald. (1994). Introduction to Fluid Mechanics. 4th ed., Canada: *John Wiley & Sons, Inc*, pp27-33 & pp182-209.

Rottmayer SP, Beckman WA, Mitchell JW. (1997). Simulation of a vertical U-tube ground heat exchanger in an infinite medium. *ASHRAE Trans.*, 103(2):651–9.

S. Javed, F.Fahlen, J. Claesson. (1999). Verical Ground Heat Exchangers: A Review of heat Flow Models. Goteborg, Sweden: Chalmers University of Technology.

S. Sanaye and B. Niroomand. (2009). Thermal Economic MOdeling and Optimization of Vertical Ground-Coupled Heat Pump. *Energy Conversion and Management* , 50.1136-1147.

Todd W. Rayne, Kenneth R. Bradbury, and David M. Mickelson. (1996). Variability of hydraulic conductivity in uniform sandy till, Dane County, Wisconsin. Madison: WISCONSIN

Turcotte, Donald L. and Gerald Schubert. (1983). GEODYNAMICS Application of Continuum Physics to Geological Problems. USA: John Wiley and Sons, Inc.

Versteeg, H. K. and Malalasekera, W. (1995). An Introduction to Computational Fluid Dynamics the Finite Volume Method. ISNB 0-444-00985-X, England: Prentice Hall, Edinburg.

Vikas Bansal , Rohit Misra, Ghanshyam Das Agrawal, Jyotirmay Mathur. (2010). Performance analysis of earth–pipe–air heat exchanger for summer cooling. *Energy and Buildings* 42, 645–648.

V. Khalajzadeh, G. Heidarinejad, J. Srebric. (2011). Parameter Optimization of a Vertical Ground Heat Exchanger Based on Response Surface Methodology. *Energy and Buildings*, 43. 1288-1294.

Vosteen, H., & Schellschmidt, R. (2003). Influence of temperature on thermal conductivity, thermal capacity and thermal diffusivity for different types of rock. *Physics and Chemistry of the Earth*, 499-509.

Winterton, R. H. (1998). Int. J. Heat Mass Transfer. 41, 809.

Wisconsin Geological and Natrual History Survey. (2005). Bedrock Geology of Wisconsin [map]. Retrieved from Wisconsin Geological and Natrual History Survey:http://wisconsingeologicalsurvey.org/pdfs/pgszpdf/bedrock_geology.pdf.

Zheng, Z., Wang, W., and Ji, C. (2011). A Study on the Thermal Performance of Vertical U-Tube Ground Heat Exchangers. *Energy Procedia*, 12, 906-914.

Yavuzturk C, Spitler J D. (1999). Short Time Step Response Factor Model for Vertical Ground Loop Heat Exchangers. *ASHRAE Transactions*, 105(2):475-485.

Yavuzturk, C. (1999). Modeling of vertical ground loop heat exchangers for ground source heat pump systems. Oklahoma: Doctoral Thesis, Oklahoma State.

APPENDIX A

MODEL JUSTIFICATIONS

A.1 Temperature Response of Multiboreholes and Single Borehole

A.2 Development of Improved 2D Single Borehole Model

A.1 Temperature Response of Multi-Boreholes and a Single Borehole

Modeling of heat flow beneath the Earth's surface requires high performance computing tools to run, particularly in the case of large-scale borefields (>100 bores) within a reasonable time and performance level. The computational demand can be significantly reduced if symmetry within the borefield is considered. Symmetric thermal interactions between adjacent ground heat exchangers in an infinitely-large and equally-spaced borefield act as zero heat-flux boundaries (adiabatic). Therefore, a single borehole model with adiabatic boundary conditions on all four sides (see Fig. A.1a and A.1b) should sufficiently represent the heat transfer process around the ground heat exchanger in the large borefield. To test this assertion, we compared temperatures at the boundary between boreholes in a 4x4 borefield and on the adiabatic boundary of our single representative borehole. The results from the single borehole show strong agreement with the results obtained from an interior single borehole of 4x4 borefield, which greatly reduces the computational time and modeling effort (see Fig A. 2.). This model is sized based on the actual geothermal borefield performing at the Epic site in Wisconsin. Material parameters and boundary conditions used in this model are shown in Table B.1.

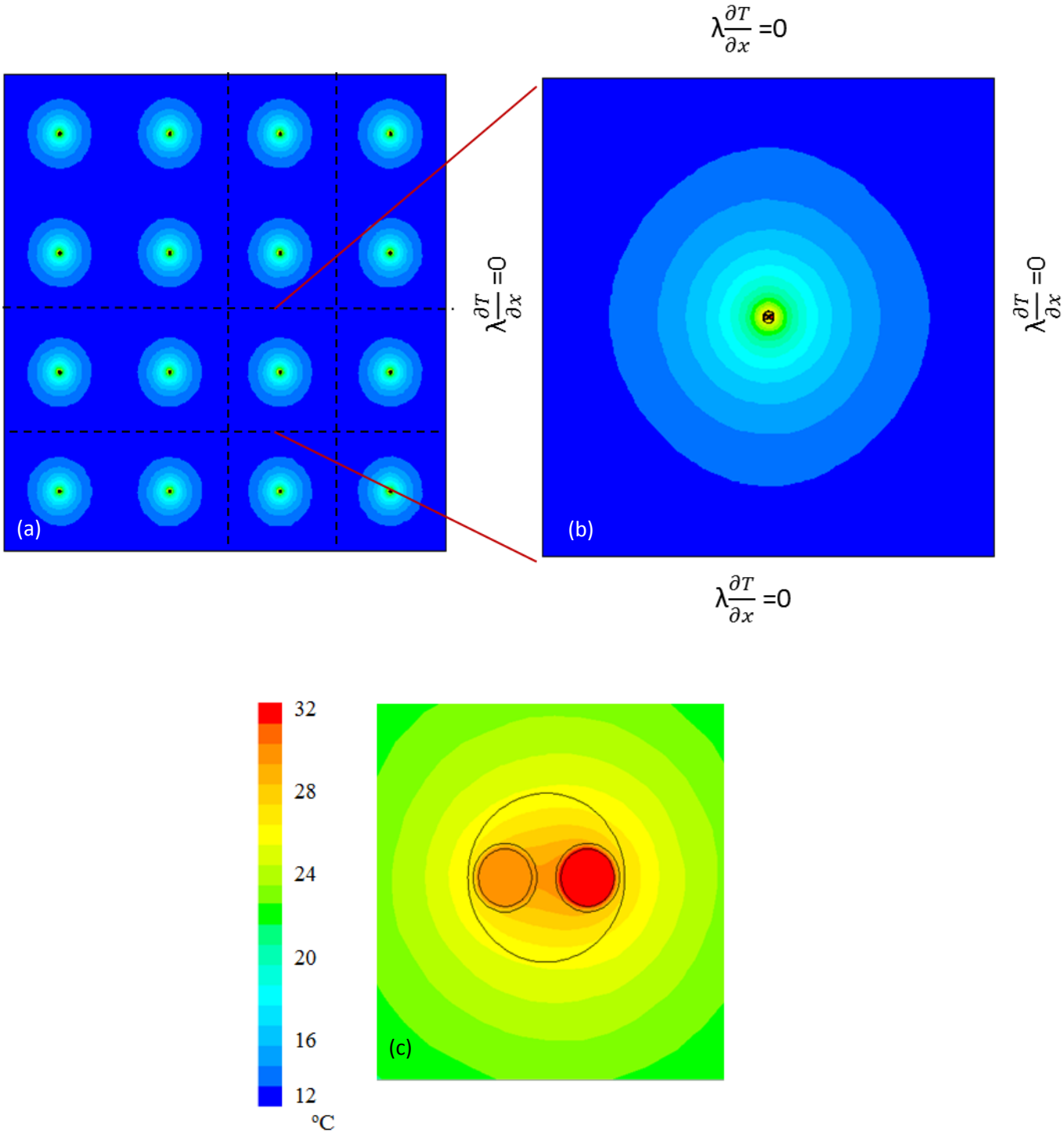

Figure A. 1 a) Temperature contours for 4x4 borefield (model size is 24.4 m x 24.4 m with 6.1 m borehole spacing), (b) for a single borehole model (equivalent to one from multi-borehole, model size is 6.4 m x 6.4 m), (c) a single borehole model (close view of b)

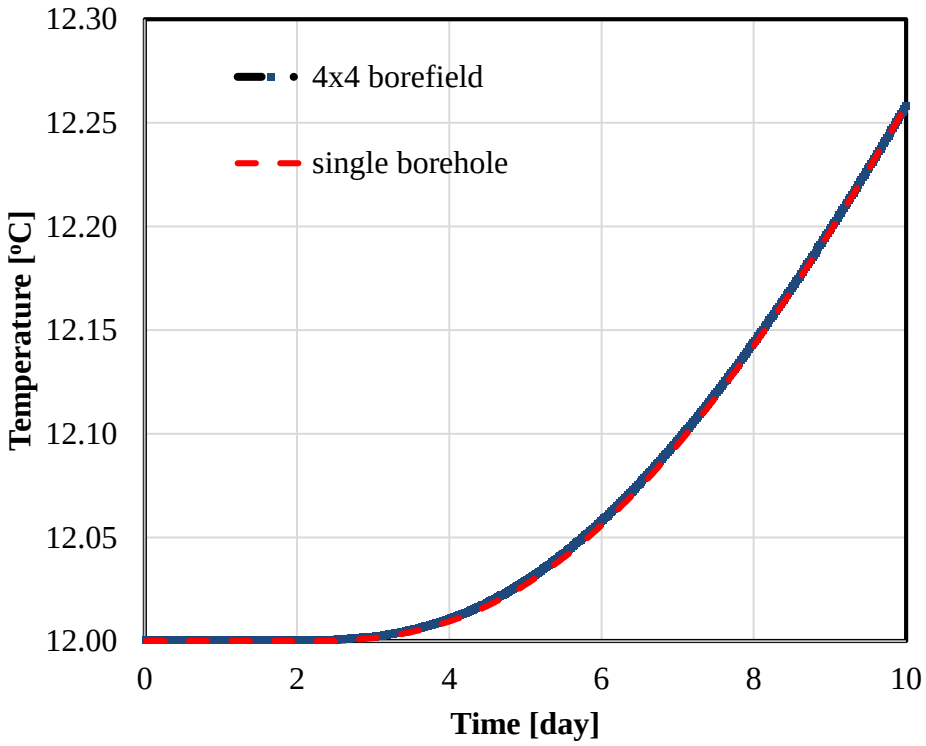

Figure A. 2 Comparison of temperature change over 10 day at the boundary line from multi-borehole model and a single borehole model.

Table A. 1 Model parameters and boundary conditions from multi-boreholes and single borehole model

Borehole Components	**Thermal C. [$W \cdot m^{-1} \cdot K^{-1}$]**	**Specific heat Cap. [$J \cdot kg^{-1} \cdot K^{-1}$]**	**Density [$kg \cdot m^{-3}$]**
fluid	0.6	4253	1000
pipe	0.42	950	2300
grout	2.5	820	1800
ground	**3**	800	2630
Boundary conditions			
Initial ground temperature, T_i		12 ^{o}C	
Fluid inlet temperature , T_{in}		32 ^{o}C	
Fluid outlet temperature, T_{out}		30 ^{o}C	
Adiabatic boundary at the side			

A.2 Development of Improved 2D Single Borehole Model

Justification for a 2D model

The objective of this section is to justify why the assumption of equal heat generation and therefore temperatures of both the hot and cold legs of the U-loop is reasonable. The properties and geometry of all materials in the model where set equal to the material properties used for the representative 2D model of Epic's Borefield 3 as presented in Chapter 3.4.

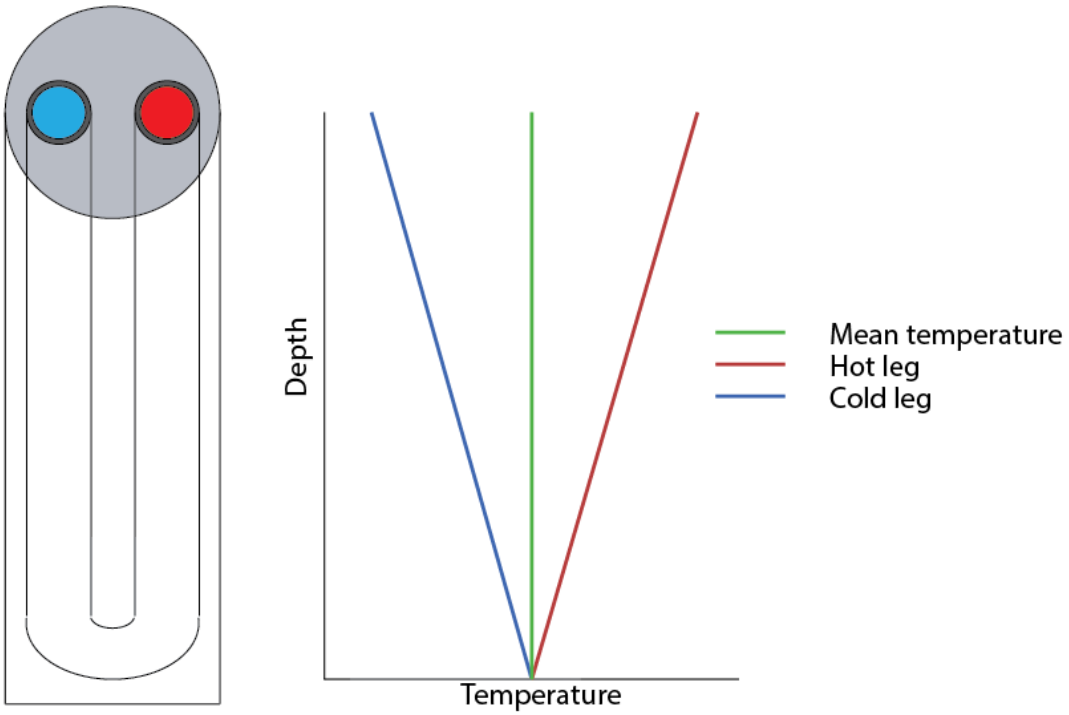

Figure A. 3 Simple representation of GHXs in the borehole and temperature profile along the U-pipe

Although the temperatures of the hot leg (red) and cold leg (blue) vary with depth, the mean temperature (shown in green) can be assumed to be relatively uniform. The constant absolute slope of the hot and cold legs is a reflection of the assumption that heat is being transferred equally at all depths along the length of the borehole.

It was demonstrated through running multiple numerical simulations that the total heat flux from the hot and cold legs of the U-loop is equal to the heat flux that would result from both legs of U-loop at the mean temperature (see Table A.2). Therefore, assuming heat transfer only occurs in the horizontal direction, the heat flux can be considered uniform along the entire length and the temperature of the hot and cold leg can be considered equal. Fluid temperature and heat fluxes following 5 h of operation are shown in Table A.1. The ground was initialized at 10 ^{o}C.

Table A. 2 Fluid temperature and heat fluxes for a 5 h of operation

T_{mean} [^{o}C]	T_{hot} [^{o}C]	T_{cold} [^{o}C]	Q_{hot} [W]	Q_{cold} [W]	Q_{total} [W]
25	30	20	66.9	16.5	83.4
25	27.5	22.5	54.3	29.1	83.4
25	25	25	41.7	41.7	83.4

Averaging of Grand Marsh Data

An operational geothermal system has been running since November, 2013, at a residential property in Grand Marsh, Wisconsin. A closed, ground-coupled heat-pump (GCHP) system in which the 0.15-m-diameter borehole contains a 6.1 cm SDR 11 HDPE fused geo-exchange (GHX) was installed. Three wells were drilled into Precambrian granite rock overlain by Cambrian sandstone, logged with geophysics, and fully instrumented with fiber-optic distributed-temperature, sensing (DTS) tools. The depth of vertical U-loop GHXs are of 90, 95, and 125 m respectively (Walker 2014). Each operating well has a fiber optic DTS that provides a real-time fluid temperature measurement at a discrete point every 1 m along the GHX pipe. The preliminary temperature measurement with DTS that motivated our model justification is shown in Fig. A.4.

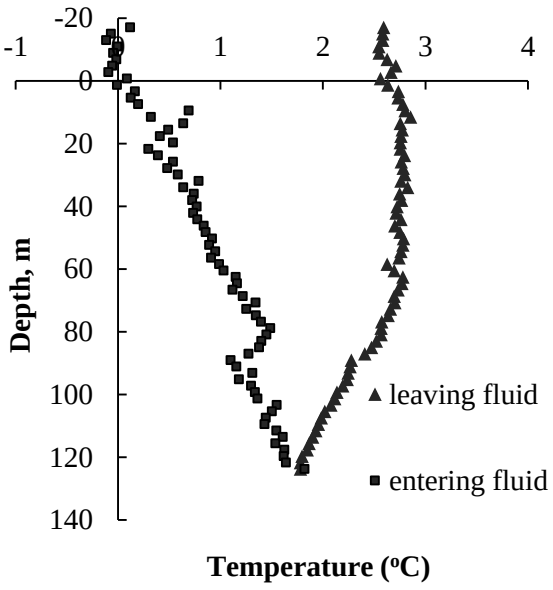

Figure A. 4 Distributed temperature measurement of GHX #3 (used three pairs of data with 120s acquisition)

From the geophysical log at Grand Marsh it was estimated that the first 58 m of the subsurface is primarily overburden sand and gravel, 58 m to 121 m is Jordan sandstone, and 121 to 126 m is Granite (see Fig. A.5). Because of the relatively low penetration of the Granitic layer by the U loops, only the properties of the first two geologic layers were considered. Making this assumption, 56.1 % of the total length of the exchangers is surrounded by overburden sand and Jordan Sandstone surrounds 43.9 % of the total length of the exchanger. The flow rate at Grand Marsh used to determine conductivity of the boundary layer was the average of the 4 months of data modeled.

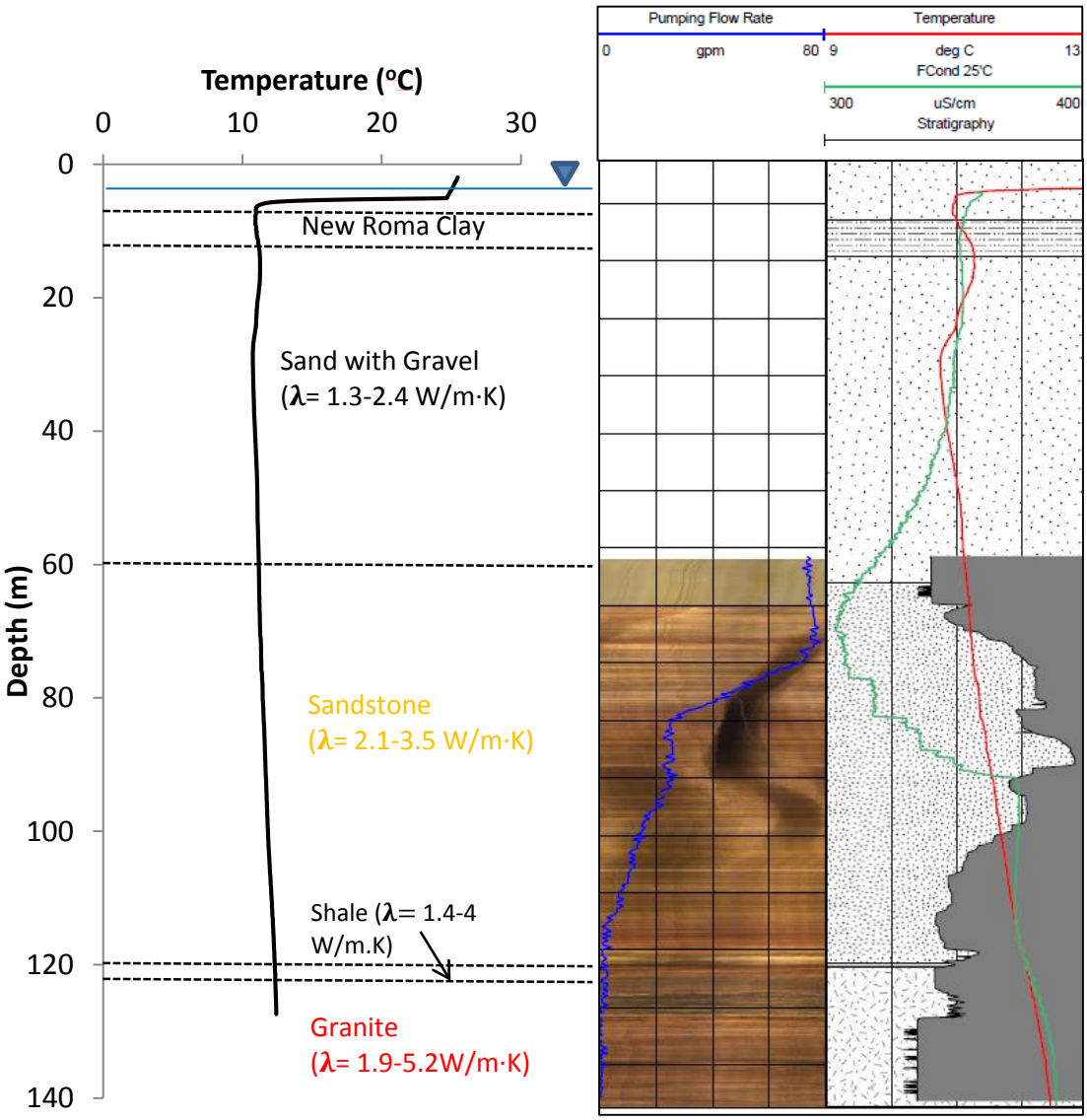

Figure A. 5 Ground temperature profile and corresponding stratigraphic ground formation based on geophysical logging collected by WNGHS on June 2013 in Grand Marsh, Wisconsin.

The dry properties of the Jordan Sandstone at the study site are known through laboratory testing by Meyer (2013) and saturated conductivity of the overburden were recorded by Hyunjun (2014). The minimum void ratio was used with the specific gravity to estimate the density for the sand. The heat capacity of saturated sand was estimated by assuming the same specific heat of the solids in the sandstone. The saturated properties for the sandstone were found using the following relationships:

$$\rho_{sat} = \rho_b + \rho_w \cdot n$$

$$\lambda_{sat} = (1 - n) \cdot \lambda_s + n \cdot \lambda_w$$

$$C_{p,sat} = (1 - n) \cdot \ C_{p,s} \cdot \rho_s + n \cdot C_{p,w} \cdot \rho_w$$

$$k_{solid} = \frac{k_{dry} - n \cdot k_{air}}{(1 - n)}$$

$$C_{p,solid} = \frac{C_{p,dry}}{(1 - n)}$$

$$\rho_{solid} = \frac{\rho_b}{(1 - n)}$$

Where ρ_{sat} is the saturated density of solid, ρ_b is the bulk density of the solid, ρ_{water} is the density of the water, λ_{sat} is the saturated thermal conductivity of the solid, λ_s is the solid thermal conductivity of the solid, λ_w is the thermal conductivity of the water, $c_{p,sat}$ is the saturated specific heat of the solid, $c_{p,s}$ is the specific heat capacity of the solid, $c_{p,w}$ is the specific heat capacity of the water. n is the total porosity. The average properties along the exchanger were then determined by multiplying the saturated properties of each formation by the percent length of that formation surrounding the boreholes as follows:

$$Avg\ property = \%_{sand} \cdot (sat\ property\ sand) + \%_{sandstone} \cdot (sat\ property\ sandstone)$$

Calculated dry and the saturated thermo-physical properties of the ground are summarized in Table A.3.

Table A. 3 Calculated thermo-physical properties of ground for model input

Dry properties					
Geologic formation	λ $[W \cdot m^{-1} \cdot K^{-1}]$	ρ $[kg \cdot m^{-3}]$	c_p $[J \cdot kg^{-1} \cdot K^{-1}]$	n	Source
Jordan Sandstone	3.86	2347	818	0.153	(Meyer 2013)
Saturated properties					
Jordan Sandstone	3.95	2500	1385	0.153	56.1 %
Sand	1.81	2185	1162	0.286	43.9 %
Weighted average	2.75	2323	1261	-	

APPENDIX B

B.1 Analogy between Solute and Heat Transport in Porous Media

B.2 Comparison of CFD and Modflow-MT3DMS

B.1 Analogy between Solute and Heat Transport in Porous Media

MODFLOW is a commercial three-dimensional finite-difference model used to simulate groundwater flow under steady and unsteady flow conditions in any flow system which aquifer layers can be confined, unconfined or a combination of confined and unconfined aquifer (Harbaugh 2005). MT3DMS is stand for a modular three-dimensional multispecies transport model for simulation of advection, dispersion and chemical reactions of contaminants in groundwater systems. Using the analogy between solute and heat transport process this program can also be applicable to simulate heat transport in porous medium. This is indicated by recent studies (Martin et al., 2001, Cathomen 2002). Hecth-Mendez et al. 2010 studied the utility of MT3DMS for shallow geothermal systems. MODFLOW and MT3DMS are coupled which MT3DMS uses flow regime predicted from MODFLOW. Hence, temperature effect on water viscosity, density, and hydraulic conductivity is not accounted. This is the main limitation of MT3DMS. However, temperature variation in the shallow subsurface is usually small and acceptable. This is proved by previous study that the total temperature differences across the model domain is less than 5 K, there is no significant difference between heat transport predictions generated with MT3DMS and heat transport predictions that account for variable density and variable viscosity flow (Hecht-Mendez et al. 2010, Ma and Zheng 2010).

In this section, the analogy between solute and heat transport equations are presented. Problems taken from MT3DMS documentation and user guide (Zheng and Wang 1999) is benchmarked to get the familiarity of MODFLOW and MT3DMS uses. For the aim of this study, results of CFD model and MT3DMS model are compared to validate the CFD groundwater-coupled heat transport process through porous media, which has not been shown by previous studies.

Governing Equations

The general governing equation for contaminant transport solved by MT3DMS for our system is as follows (see Zheng and Wang 1999):

$$R\frac{\partial(nC)}{\partial t} = \nabla.(n\boldsymbol{D}.\nabla C) - \nabla.(\boldsymbol{q}C) + q_s C_s \qquad \text{Eq. B.1}$$

Where: C= mass concentration [kgm^{-3}]

t= time [d]

$\boldsymbol{q}$ = specific discharge vector (Darcy's velocity) [md^{-1}]

q_s= volumetric flow rate per unit volume of the aquifer (fluid sources) [$m^3s^{-1}m^{-3}$]

C_s = concentration of the source and sink flux [kgm^{-3}]

R= retardation factor [dimensionless]

$$R = \left(1 + \frac{\rho_b}{n}K_d\right)$$

where n is the porosity of the subsurface medium [dimensionless], ρ_b is the bulk density of the rock matrix, $\rho_b = (1-n)\,\rho_s$ where ρ_s is the solid density.

K_d= distribution coefficient [m^3kg^{-1}],

D = hydrodynamic dispersion coefficient tensor [m^2s^{-1}]

$$D = D_{mech} + D_m$$

where D_{mech} is the mechanical dispersion coefficient tensor and D_m is the molecular diffusion coefficient.

Assuming the thermal equilibrium is maintained between the pore fluid and solid phase, the analogous heat transfer equation can be expressed as (de Marsily 1986):

$$\left(1 + \frac{1-n}{n}\frac{\rho_s}{\rho_w}\frac{c_s}{c_w}\right)\frac{\partial(nT)}{\partial t} = \nabla.\left(n\left(\frac{\lambda_{eff}}{n\rho_w c_w} + \boldsymbol{D_{mech}}\right).\nabla T\right) - \nabla.(\boldsymbol{q}T) + q_s T_s \qquad \text{Eq. B.2}$$

where: T = temperature [K]

T_s = source temperature [K]

c_s = specific heat capacity of the solid [$Jkg^{-1}K^{-1}$]

c_w = specific heat capacity of the fluid [$Jkg^{-1}K^{-1}$]

ρ_w = density of the fluid [kgm^{-3}]

q_s = volumetric heat source and sink [Wm^{-3}]

λ_{eff} = effective thermal conductivity of the rock matrix [$Wm^{-1}K^{-1}$]

$$\lambda_{eff} = n\lambda_w + (1\text{-}n)\,\lambda_s$$

where λw and λs are the thermal conductivities of the water and solid medium respectively.

The analogy between solute transport and heat transport equations is obvious from a comparison of equation (Eq. B.1) with equation (Eq. B.2). The first term on the right in solute transport equation (Eq.B.1) is diffusion and dispersion term. The diffusion term is the pure molecular diffusion D_m that denotes a process driven only by concentration gradient and equivalent to the thermal diffusivity driven by the temperature gradient in heat transfer equation as follows:

$$D_m = \frac{\lambda_{eff}}{n\rho_w c_w}$$

The dispersion term in Eq. B.1 is the hydrodynamic dispersion that denotes a process driven by velocity gradient at pole scale

$$D_{mech} = \alpha v$$

where α is the dispersivity term [m], ν is the seepage velocity [m/d]. The dispersion term is equivalent to natural convection in heat transport process, but it is neglected because MT3DMS does not account for density and velocity change due to the temperature gradient that leads to natural convection.

The second term in Eq. B.1, which represents advection term, is analogous to transport of heat by groundwater flow (Eq. B.2). The third term in Eq.B.1 represents fluid solute sinks/sources, and is analogous to thermal sinks/sources in Eq. B.2.

Comparison of Eq. B.2 to Eq. B.1 indicates that variables for the MT3DMS solute transport model can be re-interpreted for heat transport. The solute concentration becomes the temperature. The distribution coefficient (K_d) for solute transport is replaced by the thermal distribution factor which can be calculated for temperature using the following equation:

$$K_d = \frac{c_s}{\rho_w c_w}$$

Retardation factor (R) and distribution coefficient (K_d) are represented as solute sorption in solute equation (Eq. B.1.), is analogous to heat exchange between the solid and water in heat transfer equation (Eq. B.2). Details on using solute transport simulation for heat transport modeling can be found in Kim et al. (2005) and Thorn et al. (2006).

Benchmark problem: Two-Dimensional Transport in a Uniform Flow Field

Model Set-up: An analytical solution for two-dimensional transport of solute injected continuously from a point source in a steady-state uniform flow field is given by Wilson and Miller (1978). The analytical solution is applicable under these assumptions; a) the aquifer is infinite in areal extent and relatively thin in vertical extent, so that instantaneous vertical mixing can be assumed; and b) the injection rate is insignificant compared with the ambient uniform flow.

A numerical model consisting of 46 columns, 31 rows and 1 layer is constructed for comparison with the analytical solution of Wilson and Miller (1978). The model parameters used in the simulation are listed in Table B.1.

Table B. 1 Model parameters used in 2D transport of a uniform flow model

Cell width along rows (Δx) = 10 m
Cell width along columns (Δy) = 10 m
Layer thickness (Δz) = 10 m
Groundwater seepage velocity (v) = 1/3 m/day
Porosity (θ) = 0.3
Longitudinal dispersivity = 10 m
Ratio of transverse to longitudinal dispersivity = 0.3
Volumetric injection rate = 1 m^3/day
Concentration of the injected water = 1000 ppm
Simulation time (t) = 365 days
West head = 46 m
East head = 1 m
Hydraulic conductivity (K) = 1 m/day

The flow model is surrounded by constant-head boundaries on the east and west borders and no-flow boundaries on the north and south borders. The head values at the constant-head boundaries are arbitrarily chosen to establish the required hydraulic gradient. The simulation period is chosen so that the plume developed from the point source does not

reach the boundaries.

Results

To evaluate the accuracy of flow conditions in MODFLOW mass balance between inflow and outflow to/from model domain was performed. The results show less than 0.006% error that an appropriate mass balance is achieved (see Fig. B.4). The simulated results from MT3DMS are shown in Fig. B.5. It is clear that the solute is mostly transported by advection in the flow direction, some transport by

hydrodynamic dispersion is also seen in transverse direction. This numerical simulation is in good agreement with analytical solutions done by Zheng and Wang (1999).

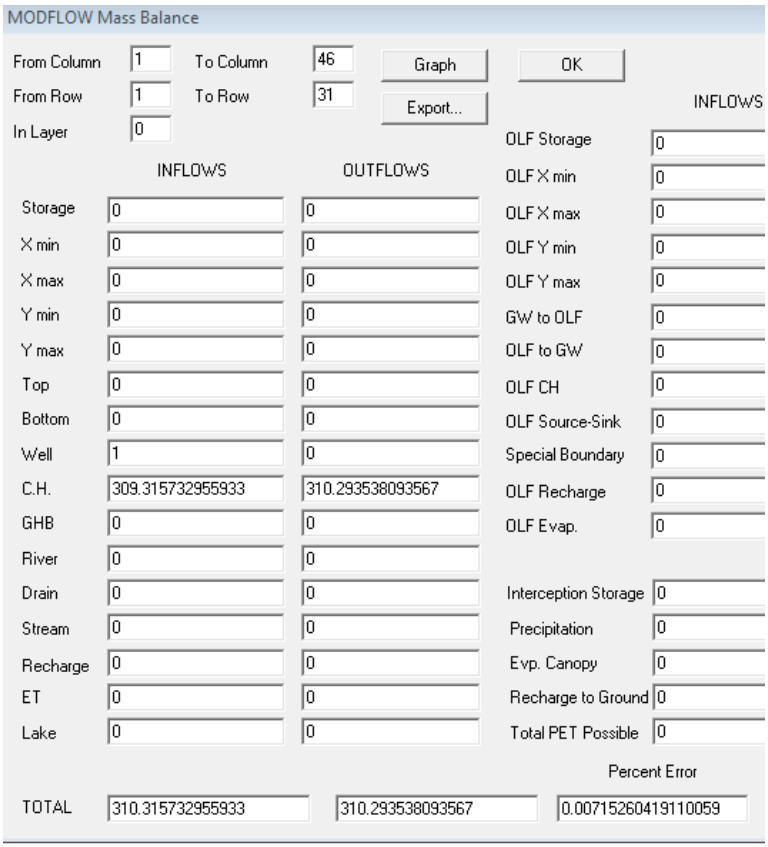

Figure B. 1 Mass balance of 2D MODFLOW model

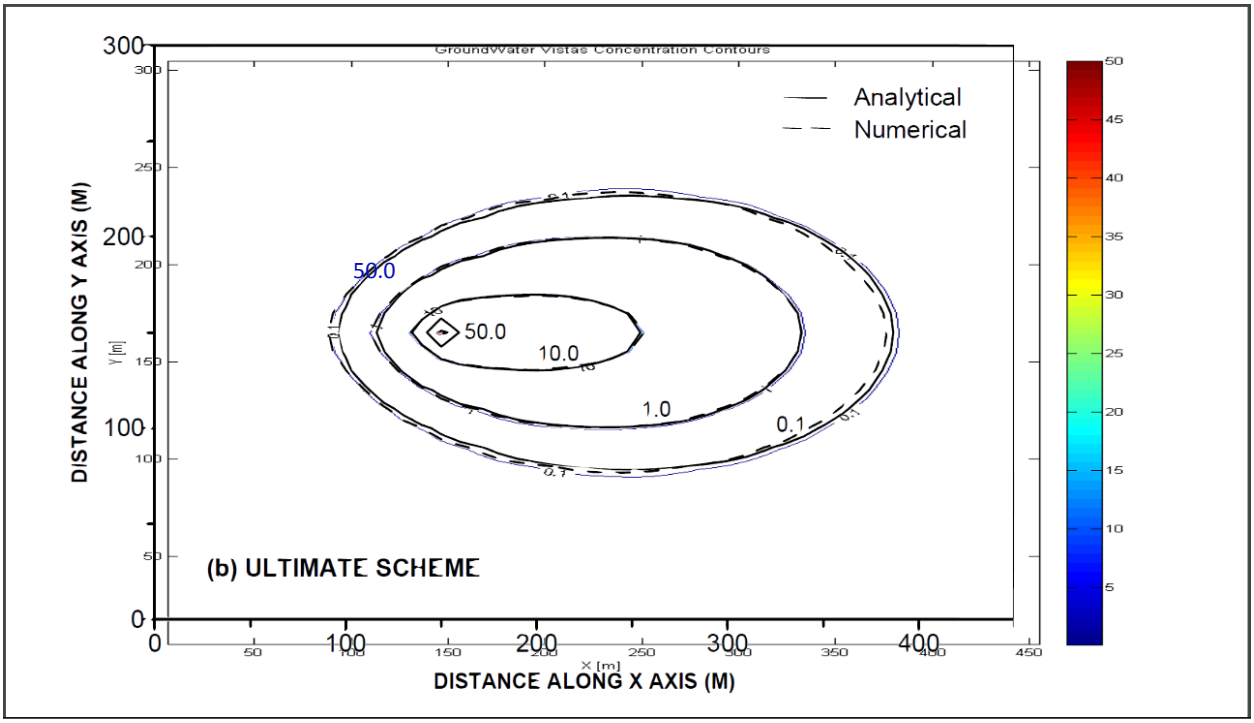

Figure B. 2 Concentrations contours from analytical solution and numerical solution (MT3DMS)

B.2 Comparison of CFD and MODFLOW-MT3DMS

Two-dimensional rectangular aquifer (490 m in horizontal and 310 m in vertical) is simulated using both CFD and MT3DMS. The simulated aquifer domain represents same dimension with one of Epic borefield size. The model domain is discretized into cells 10 m by 10 m in the x- and y-directions (see Fig. B.6). Solute/or temperature being injected to aquifer is represented as a red square with size of 10 m by 10 m as shown in Fig.B.6. The model parameters used in CFD and MT3DMS model are presented in Table B.2. Additionally, a viscous resistance [$1/m^2$] is a parameter used only in CFD simulation. This parameters is inverse of the intrinsic permeability and can be defined using

$$\kappa = K\frac{\mu}{\rho g}$$

where κ is intrinsic permeability [m^2], K is hydraulic conductivity [m/s], μ is dynamic viscosity [kg/m·s], ρ is density [kg/m] and g is the acceleration due to gravity [m/s^2].

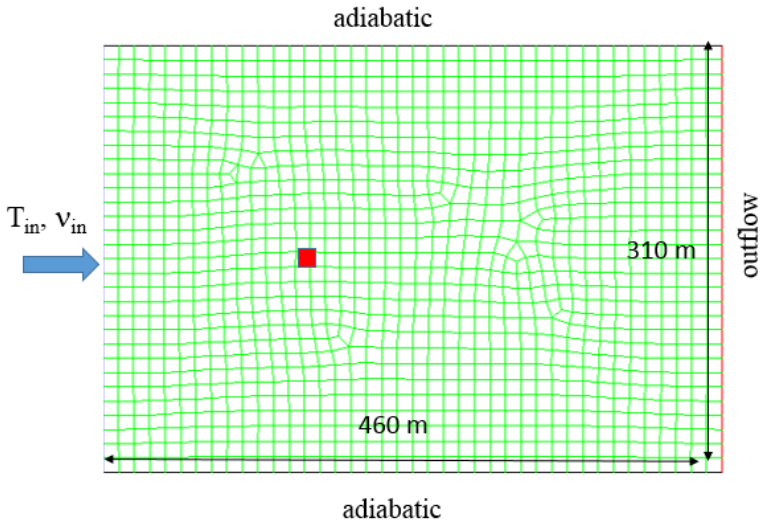

Figure B. 3 Model geometry and boundary conditions used in CFD simulation

Table B. 2 Model parameters used in CFD and MT3DMS simulations

Geologic Unit		Description	CFD	MT3DMS
n	[--]	Porosity	0.3	0.3
ρ_b	[kgm^{-3}]	Bulk density of geologic medium	[-]	157
ρ_s	[kgm^{-3}]	Density of solids in the geologic medium	224.3	[--]
c_s	[$Jkg^{-1}K^{-1}$	Specific heat capacity of the solid	7350	[--]
λ_s	[$Wm^{-1}K^{-1}$]	Thermal conductivity of the solid	3	[--]
K	[ms^{-1}]	Hydraulic conductivity of geologic medium	1.15E-05	1.15E-05
Fluid				
ρ_w	[kgm^{-3}]	Density of water	998.2	[--]
c_w	[$Jkg^{-1}K^{-1}$]	Specific heat capacity of the water	4182	[--]
λ_w	[$Wm^{-1}K^{-1}$]	Thermal conductivity of the water	0.6	[--]
μ	[$kgm^{-1}s^{-1}$]	Dynamic viscosity	0.001003	[--]
Boundary Conditions				
q	[ms^{-1}]	Inlet velocity (Darcy's)	1.04E-06	[--]
v	[ms^{-1}]	Seepage velocity	[--]	3.47E-06
T_i /C_i	[K]	Initial ground temperature/or concentration	0	0
T_{in} /C_{in}	[K]	Inlet fluid temperature/ or concentration	1000	1000
Adiabatic boundary at the top and bottom edge of the model domain				

Results

Fig. B.7 shows the temperature and concentration profile along the horizontal distance from the model simulated by CFD and MT3DMS, respectively. Heat transport by conduction was simulated and showed in Fig. B.7a. Heat transport by advection was also simulated by introducing groundwater flow using a seepage velocity of 3.47e-6 m/s in MT3D and Darcy's velocity (**q**=v x n) of 1.04e-6 m/s in CFD. Both simulations are in strong agreement. Heat taken by ground water flow is transferring about a 50 m away from the source. Contours for the temperature/or concentration around the source were also presented in Fig. B.8. MATLAB was used for post-processing the results, so due to discretization size used for surface meshing some temperature disorder in CFD can be seen.

The results from this benchmarking problem verify that both CFD and MT3DMS are applicable for solving the heat transfer problem after necessary coefficient and unit conversion are carefully done. Model set-up and post procedures are different as MT3D is built for mass and solute transport equation specifically in underground conditions while CFD is more for momentum and energy equation in complex fluid conditions. Using the analogy between mass transport and heat transport equation MT3DMS may even be more applicable in terms of computational time when a three-dimensional transient large-scale model is considered. However, MT3DMS uses a finite-difference method so it is limited to structured mesh whereas CFD is finite-volume based that can give more flexibility to model both structured/or unstructured mesh (such as circular borehole, pipe and U-pipe).

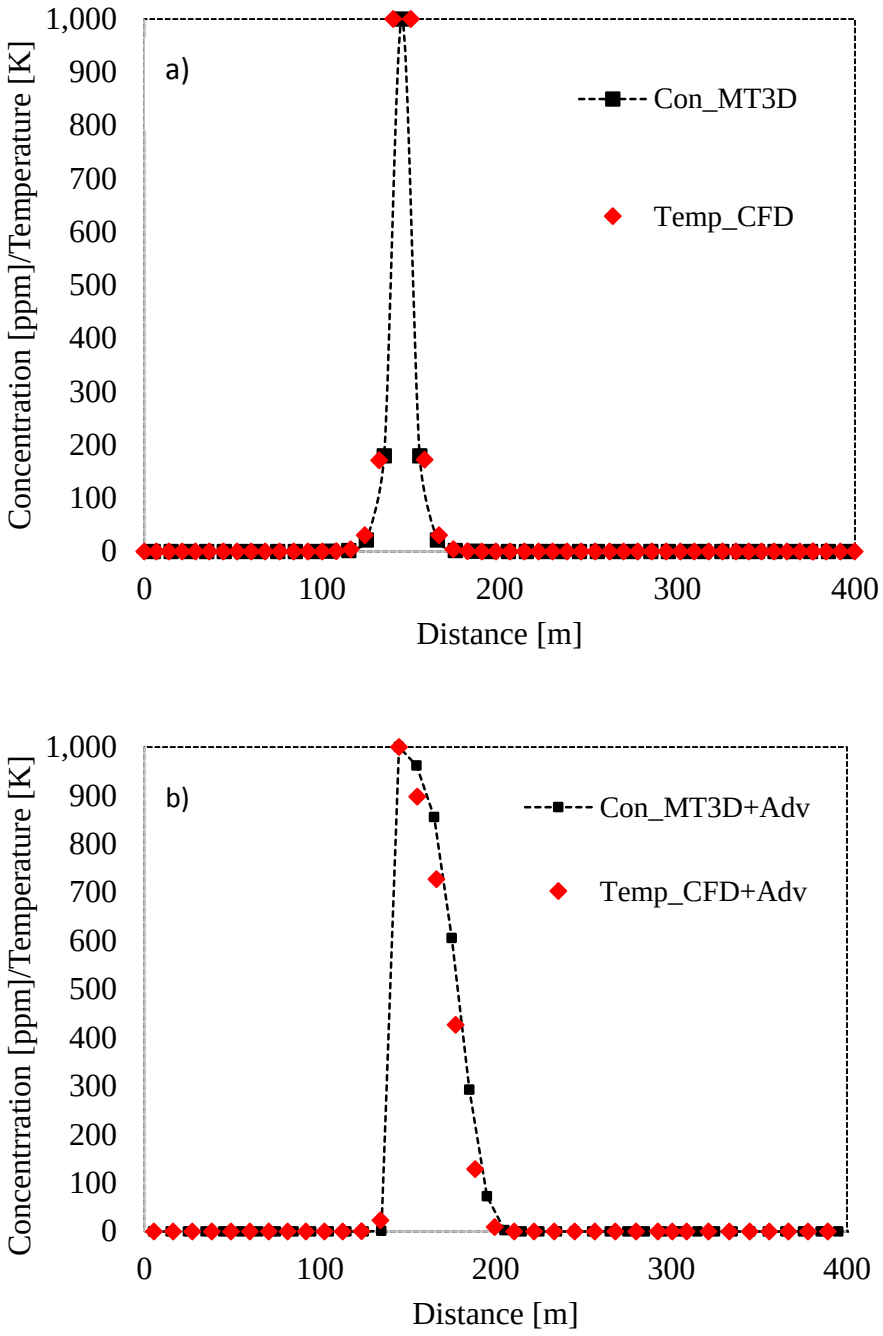

Figure B. 4 CFD validation with MT3DMS, (a) heat conduction/ diffusion, (b) heat advection by groundwater flow

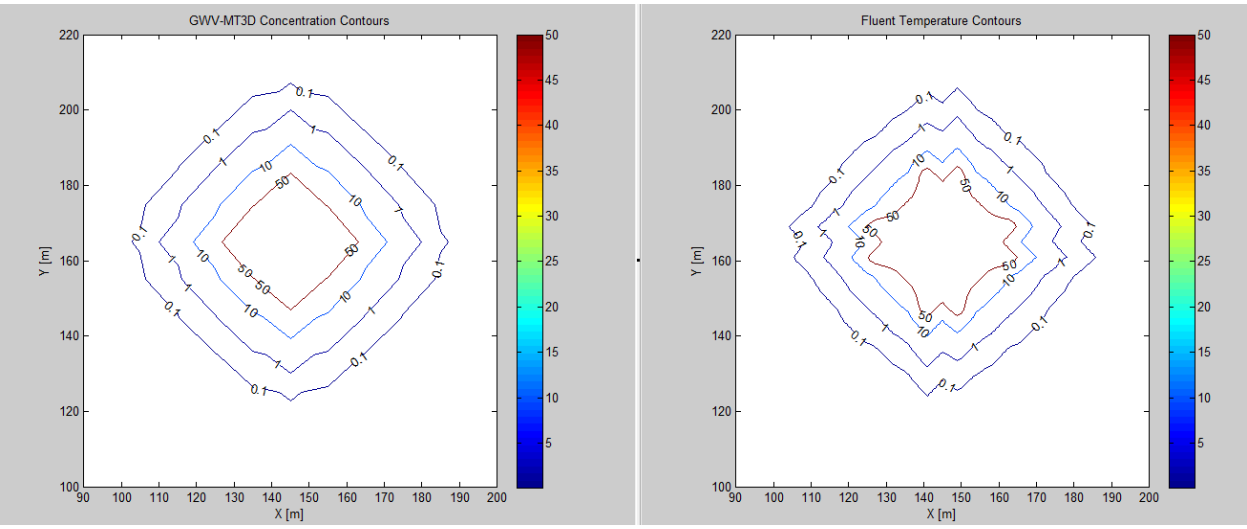

Figure B. 5 Temperature contours from CFD (on the right) and concentration contours from MT3DMS (on the left) around the borehole